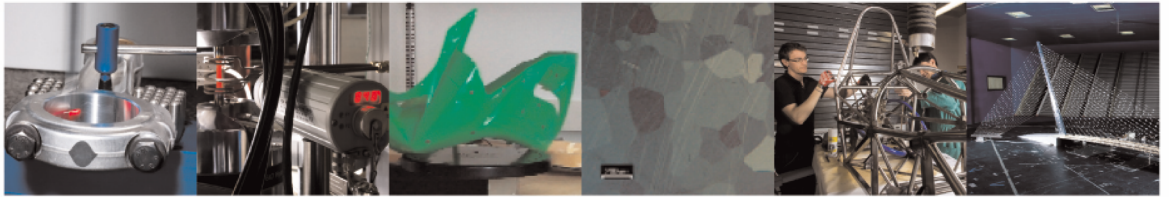




POLITECNICO
MILANO 1863

DIPARTIMENTO DI MECCANICA



Neutralization of temperature effects in damage diagnosis of MDOF systems by combinations of autoencoders and particle filters

Cadini F.; Lomazzi L.; Ferrater Roca M.; Sbarufatti C.; Giglio M.

This is a post-peer-review, pre-copyedit version of an article published in Mechanical Systems and Signal Processing. The final authenticated version is available online at:

<https://doi.org/10.1016/j.ymssp.2021.108048>

© <2021>

This content is provided under [CC BY-NC-ND 4.0](https://creativecommons.org/licenses/by-nc-nd/4.0/) license



Mechanical Systems and Signal Processing

Neutralization of temperature effects in damage diagnosis of MDOF systems by combinations of autoencoders and particle filters

--Manuscript Draft--

Manuscript Number:	MSSP20-2710R1
Article Type:	Standard Research Article
Keywords:	Structural Health Monitoring; changing environmental conditions; diagnosis; damage localization; particle filter; auto-encoder
Corresponding Author:	Francesco Cadini, Ph.D. Politecnico di Milano Milano, ITALY
First Author:	Francesco Cadini
Order of Authors:	Francesco Cadini Luca Lomazzi, M.D. Aeronautical Engineering Marc Ferrater Roca Claudio Sbarufatti Marco Giglio
Abstract:	<p>In the last years, scientific and industrial communities have put a lot of efforts into the development of a new framework for the assessment of structural integrity, generally known as Structural Health Monitoring (SHM), which should allow real-time, automatic evaluations of the state of the structures based on a network of permanently installed sensors. In the context of mechanical, aerospace and civil structures, several approaches have been proposed to address the SHM problem, yet, it remains often difficult to diagnose damages and estimate the structural health when dealing with varying operating and environmental conditions. Particle Filters have already been proposed as a time-domain-based method in the field of SHM, showing promising results as estimators of hidden, not directly observable states, such as those typically related to damages. At the same time, neural networks-based autoencoders have been proposed for structural damage detection, demonstrating to be capable of capturing damage-related features from vibration measurements. This work aims at exploiting the individual advantages offered by the two approaches by combining them in a novel algorithm for structural damage detection and localization, robust with respect to changing environmental conditions. The algorithm is further equipped with a fault indicator module stemming from the introduction of an automatic threshold and both deterministic and probabilistic fault indicators, thus offering a complete, valuable tool for supporting decision making with limited human intervention. The method is demonstrated with reference to a numerical MDOF system whose parameters are taken from a literature benchmark case study.</p>

Mechanical Systems and Signal Processing

To the Editor

Milan, November 06, 2020

Dear Editor,

I would be grateful if you could consider the submission of the manuscript *Damage detection and localization in structures subject to changing environmental conditions using a combination of particle filters and auto-encoders* for publication on *Mechanical Systems and Signal Processing*. The manuscript has never been published elsewhere and the contents are original. All the other authors have approved the submission.

The paper deals with the structural health monitoring of structural systems subject to degradation, under changing operating and environmental conditions, which severely hamper the damage identification process. In the literature some methods have already been proposed for suppressing the influence of those confounding factors, thus leading to case-specific methodologies for performing damage identification. Yet, a general approach to damage localization under varying external conditions is still missing, since those methods are often case-specific and not generalizable to different system configurations.

Both damage detection and localization tasks are performed in our study, with reference to multi degrees of freedom (MDOF) systems. In order to do so, we propose an original *time-domain* approach consisting of the combination of particle filtering (PF), for estimating some otherwise not directly observable structural parameters, and ANN-based auto-encoders, for subtracting the changing external conditions effects affecting the damage related features. The method is then successfully demonstrated on a 6-DOF mechanical system subject to temperature variations.

Finally, please note that the use of ANN-based autoencoders (a machine learning algorithm) is not new in the field of SHM of mechanical systems subject to varying environmental conditions, but, to the authors' best knowledge, it has remained restricted (i) to the case of simple novelty detection, whereas in the present work, its coupling with a Bayesian filter allows to broaden the diagnostic capabilities, including localization and, possibly, quantification (although this last task has not been directly tackled in the present work and has been left to further developments of the algorithm) and (ii) to a trivial single DOF system, whereas we here extend the methodology to the very general case of MDOF models.

In conclusion, the authors believe that this paper may be of large interest for the scientific community and that it is appropriate for publication in *Mechanical Systems and Signal Processing*.

Thank you for your cooperation

Yours Sincerely,

Francesco Cadini, Ph.D.

Politecnico di Milano - Dipartimento di Meccanica,
via La Masa 1, 20156, Milano, Italy.

Phone: +39 02.2399.6355

Email: francesco.cadini@polimi.it



**POLITECNICO
DI MILANO**

DIPARTIMENTO DI MECCANICA

To: Prof. Fassois

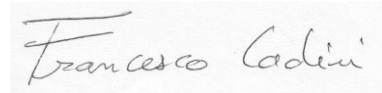
Milano, March 9, 2021

Dear Prof. Fassois,

Thank you very much for your email and for sending us the reviewers' reports. We have proceeded to a careful consideration of the comments by the reviewers and have accordingly modified the paper, adding the requested modifications (colored in blue).

Again, we appreciate your collaborative efforts,

With best regards,





REVIEWER 1

NOTE: All the references that follow are numbered according to the references list of the revised work. The references starting with the letter N (e.g., [N1]) are reported in this document as proofs for the answers, they are not included in the work.

1. *“The introduction and the second section should be shortened and focus more on the contributions than on the description of FP and Auto-encoders which are now fairly well known by the SHM community.”*

Author Reply: According to the reviewer’s advice, the introduction and the second sections have been shortened.

2. *“When using these methods for SHM two main concerns rise: the nature of the excitation to ensure the identifiability (PF) of the target parameters and the availability (or the possibility of building) a database to train the Auto-encoders. Hence, beyond discussing these points, it would have been more worthwhile to look at a real case and discuss the applicability of the approach”.*

Author Reply: As common practice in this field, applying a sinusoidal force is possible on several real structures. The topic of the feasibility of the kind of excitation considered in the work is discussed in more details in the answer to question 1a from Reviewer 2. With regards to the *identifiability* of the system, the following paragraph has been added at the end of Section 2.1:

“Indeed, in this context, the problem of the identifiability of the parameters becomes very important. Thus, identifiability assessment should always be performed before the application of the method. This activity is out of the scope of the present work, in which identifiability is heuristically assessed by trial-and-error procedure. In case more complex systems are involved, the heuristic approach should possibly consist of increasing the number of forcing terms and, in case applying more loads is hard in the specific real application (e.g., on large civil infrastructures), diversification of the type of observations could prove a good strategy, e.g., considering displacement, velocity and acceleration measurements together. The interested reader is referred to [55] for further details about the identifiability problem.”

With regards to the problem of training the autoencoders, the following paragraph has been added to the Conclusions:

“The proposed method is believed to be ready to be employed to real structures, provided that some key points are considered: (i) the autoencoders database may be built by installing sensors on the structure, acquiring the baseline in its early life, confidently assuming that the structure is healthy right after being installed or built; (ii) the baseline acquisition process should be long enough to capture the whole expected temperature variability during the operational life of the monitored structure, in order to allow the autoencoders working in the learnt space during the diagnostic phase; (iii) the temperatures may be acquired using at least one sensor per degree of freedom, to consider temperature variability in time and space and (iv) at least one accelerometer per DOF should be installed on the structure. However, more sensors may be installed on the structure both for redundancy and for collecting more information about the single DOF, which may not be a concentrated entity in the real world, in order to determine the corresponding acceleration and temperature values.”

With regards to the realistic application, please refer to the answer to question 1b from Reviewer 2.



Accordingly, the following references have been added to the references list:

[55] M.N. Chatzis, E.N. Chatzi, A.W. Smyth, On the observability and identifiability of nonlinear structural and mechanical systems, *Structural Control and Health Monitoring*, 2015, 22(3), 574-593

3. “What about the damping assumption and model in the case of complex structures (anisotropic, multilayered,...)?”.

Author Reply: The Paragraph which introduced damping (Section 2.1) has been modified as follows:

“According to common practice in this kind of SHM applications, the consolidated assumption of viscous damping is made in this work, which represents a velocity-dependent damping formulation allowing not to introduce non-linearities in the system, while still guaranteeing a quite satisfactory description of the damping effects [46]. In particular, the widely adopted proportional damping, or Rayleigh damping, assumption is made [47]. Some issues may arise adopting this model, e.g., (i) proportional damping does not allow for satisfactory representation of eventual non-linear damping behaviors or (ii) it provides not very accurate results when the structure undergoes yielding, buckling or when the local behavior around the tip of an eventual crack has to be investigated, to cite some. However, being these particular scenarios not relevant in this work, proportional damping is considered to be a valid and accurate enough damping modelling technique. Moreover, a relevant property of Rayleigh damping is that it can be applied both to structures made of homogeneous materials and to those made of non-homogeneous materials, without any difference in the specific formulation, which allows not limiting to analyze structures made of isotropic materials, but also more complex systems including non-isotropic materials [48]. In this work, damping is assumed to be proportional to stiffness only through a coefficient β , assumed identical for all the dampers in the MDOF system [49].”

Accordingly, the following references have been added to the references list:

[46] J. F. Hall, *Problems encountered from the use (or misuse) of Rayleigh damping*, *Earthquake Engng Struct. Dyn.*, 2006, 35, 525-545

[48] C. Kyriazoglou, F.J. Guild, *Finite element prediction of damping of composite GFRP and CFRP laminates – a hybrid formulation – vibration damping experiments and Rayleigh damping*, *Composites Science and Technology*, 2007, 67(11), 2643-2654

4. “Can you give more details on the relation (6) and the assumption that goes with?”.

Author Reply: The following paragraph has been added at Section 2.1, after equation (6):

“Equation (6) is obtained from [30] by rescaling the coefficients of the original equation describing the elastic modulus as a function of the temperature [50, 51] to have a stiffness value of 10^4 N/m at 0°C in correspondence of an elastic modulus of 203.07 GPa.”

Accordingly, the following references have been added to the references list:

[50] O. Hubert, X. Milhet, P. Gadaud, M. Tatat, P. Renault and C. Coupeau, *Modeling of Young's modulus variations with temperature of Ni and oxidized Ni using a magneto-mechanical approach*, *Materials Science and Engineering: A*, 2015, 633, 76-91



[51] W. Wang, B. Liu and V. Kodur, Effect of Temperature on Strength and Elastic Modulus of High-Strength Steel, *J. Mater. Civ. Eng.*, 2013, 25(2), 174-182

5. “*Quid of the performance in the case of non-uniform temperature variations?*”.

Author Reply: The following sentences have been added at Section 3.2 (below Figure 4):

“Note that, for simplicity and with no loss of generality, all the springs are subjected to the same temperature. As verified by the authors, but not reported here for the sake of brevity, the algorithm can effectively cope with the effects of a spatial temperature gradient, i.e., temperatures varying across the elements of the structure. In fact, the spring stiffness-temperature relationship is independently “encoded” spring by spring, so that a spatially non-uniform temperature variation can only affect the dynamics of the system, which is fully captured by the PF, similarly to considering different stiffness values amongst the degrees of freedom.”

6. “*The discussion of the performance of the approach (detection, false alarm, ...) depends a lot on the choice of simulation parameters' (variances, temperature, ...). How one can then extract the general guidelines for setting up the approach?*”.

Author Reply: The following *Discussion* Section has been added to the paper before the Conclusions:

“

4. Discussion

The model-based framework presented in this work offers the advantage that, in real applications, most algorithm parameters can be set up by trial-and-error procedures during a preliminary, purely numerical phase, where the dynamic behavior of the system and the associated acceleration measurements are synthetically generated using the process and the measurement equations. The calibrated parameters are probably not “optimal” for the real application, due to the model errors, but would certainly guarantee satisfactory performances of the algorithm. For instance, the performance of the whole framework significantly depends on the performance of the PF, which, in turn, is quite sensitive to both the measurement and the process noise. While the measurement noise is related to the precision of the sensors (although there might also be some calibration margin), the process noise is well-known to be mainly a filter calibration factor, not easily identifiable a-priori. The suggestion is then to calibrate the process noise by means of a trial-and-error approach, also according to common practice in the literature [64, 65]. Another example is represented by the detection thresholds, which are set according to specific percentiles of the pdfs of the squared error and the error defined by equations 15 and 16, respectively, the calibration of which is again suggested via a trial-and-error procedure, with the ultimate goal of establishing a trade-off between false alarms rate and raising time for damage alarms. The usual percentiles considered in statistics may be adopted, e.g., 95th, 99th and 99.9th percentile. The greater the percentile, the smaller the false alarms rate, albeit at the price of an increase in the raising time for damage detection.

As far as the autoencoders are concerned, the healthy baseline acquisition should be performed over a temperature range sufficiently wide to cover most of the temperatures the structure will experience during its operational life. Since this may be a lengthy process, it is suggested to start acquiring the baseline right after the structure installation, i.e., when the structure is reasonably still healthy, start using the diagnostic tool and keep re-training the autoencoders as new temperature ranges are experienced. Another possible strategy may be that of numerically generating the missing examples of the relationship between temperature and stiffness



DIPARTIMENTO DI MECCANICA

by using some sufficiently accurate material model, which would provide a hybrid experimental-numeric baseline for training the autoencoders. This procedure has the advantage of potentially covering any temperature range, at the risk of introducing modelling errors that would certainly affect the diagnostic performances.”

Accordingly, the following references have been added to the references list:

- [64] M. Corbetta, C. Sbarufatti, M. Giglio, M.D. Todd, *Optimization of nonlinear, non-Gaussian Bayesian filtering for diagnosis and prognosis of monotonic degradation processes*, Mechanical Systems and Signal Processing, 2018, 104, 305-322
- [65] M. Corbetta, C. Sbarufatti, M. Giglio, *Optimal tuning of particle filtering random noise for monotonic degradation processes*, 3rd European Conference of the PHM Society, PHME16, Bilbao, Spain, 2016

7. “*In the conclusion you rightly raise several developments to overcome several points necessary for a real application of the method. Can you give some theoretical and methodological guidelines to overcome them?*”.

Author Reply: In the Conclusions the authors wrote that a potential significant improvement of the framework would be the extension to changing environmental/operating conditions other than temperature. No significant differences are expected in case, for example, wind or traffic induced loads are considered as additional external conditions to deal with. The authors believe the framework would still work the same way as presented in the paper. Hence, the two identified phases would not change, i.e., the autoencoders may be trained with a baseline acquired on the healthy structure and the online functioning would be preserved. More specifically, the authors believe traffic and wind loads may be dealt with as different forcing terms, since (as a first approximation) they do not affect the stiffness properties of the structure. Hence, the PF should still be able to estimate the state-space vector evolution in time relying on acceleration measurements, while the autoencoders should still process temperature measurements and estimated stiffness values to drive the damage identification procedure. Yet, the task would probably be more challenging, mainly due to the random nature of this kind of excitations.

Accordingly, the following sentences have been added to the Conclusions:

“For instance, in case of structures significantly affected by traffic and/or wind loads, a typical SHM problem in large infrastructures, these could be considered as different/additional forcing terms, as they do not directly influence the stiffness properties of the structure. In this regard, performing the diagnostic task only on the basis of vibration signals induced by environmental/operative loads (wind, traffic, etc.) would be more practical in realistic scenarios, yet more challenging, mainly due to the random nature of this kind of excitations.”

On the other hand, the authors are quite confident that the performances will not be significantly influenced by the different nature of those excitation loads, as already stated above, since several trials have been carried out to assess the robustness of the algorithm with respect to the number, positions and intensities of the forcing terms, with robust results, not reported in the present paper for the sake of brevity, but partially used in another forthcoming publication dealing with non-linear components (also see below).

Finally, with regards to the effects of a non-linear behavior of the system, the authors have already performed some analyses considering a degrading hysteretic behaviour described by the Bouc-Wen’s model, with satisfactory results. Those results will soon be provided to the scientific community.



REVIEWER 2

NOTE: All the references that follow are numbered according to the references list of the revised work. The references starting with the letter N (e.g., [N1]) are reported in this document as proofs for the answers, they are not included in the work.

1. “The one-dimensional MDOF system can only represent periodic structures, and is extremely simplified in the way that the effect of damage on the whole dynamical response of the structure is modelled. For this application the authors have chosen a 6-DOF model (following K. Worden's work published in 1997). Since then, a lot more developments have been published in terms of vibration analysis and its application in structural health monitoring. What is the reason behind choosing such a simplistic model?”

Author Reply: First, it is worth noting that the combined PF-Autoencoders algorithm is generic and not bounded to the specific model employed for simulating the structure under monitoring. Hence, any other modelling technique different from the MDOF system can in principle be considered, with no compatibility issues with the proposed framework, as long as a model of the structure is provided. For example, Particle Filter was employed as dynamic state estimation tool in combination with the Finite Element model of different types of structures, e.g., rubber sheet with a hole, single span beam and multi-span masonry arch bridge, with satisfactory performances [44]. Similarly, nonlinear Finite Element method and extended Kalman filter were successfully combined in a unique framework to estimate some non-linear material parameters of a structural system [45]. As a matter of fact, the authors are currently investigating the possibility to apply the PF-Autoencoders framework to Finite Element-discretized structures, which may open up the chance to deal with non-periodic systems as well.

The reason behind choosing the one-dimensional MDOF system to show the performances of the developed framework lies in the fact that (i) the model is widely accepted as a tool for representing those structures that are considered discrete systems with a finite number of degrees of freedom, mainly experiencing one-dimensional motions (to highlight this, reference 43 has been added) and (ii) it is simple enough to allow for the quick and repeated analyses and computer runs typically required when devising and testing new algorithms, while still guaranteeing reasonable representation performances. Its use is common in static and dynamic applications in the aeronautical, civil and mechanical fields [40- 42].

Accordingly, the first paragraph of Section 2 has been extended as follows:

“The methodology is proposed with reference to a modeling strategy commonly used to represent the dynamic behavior of many mechanical, aeronautical and civil structural systems, such as rotary machines, multi-storey buildings and multi-span bridges, i.e., the one-dimensional MDOF systems [40- 42]. MDOF structural systems are also known as periodic structures, which basically consist of several structural components of the same type, i.e., springs, masses, dampers, joined together [41, 43]. These models are particularly useful for describing the vibration of a structure when it experiences significant motions in one preferential direction. However, the proposed methodology is generic and not bounded to the specific model employed for simulating the structure under monitoring. Hence, any other modelling technique different from the MDOF system can in principle be considered, with no compatibility issues with the proposed framework, as long as a model of the structure is provided. For instance, the Finite Element modelling strategy may represent a promising alternative to the MDOF technique, yet more complicated, which would also open up the chance to deal with non-periodic structures. In fact, a combination of Particle Filter as dynamic state estimation tool and Finite Element model of different types of structures, e.g., rubber sheet with a hole, single span beam and multi-span masonry arch bridge, was employed in the work in [44] with satisfactory performances. Similarly, nonlinear Finite Element



method and extended Kalman filter were successfully combined in a unique framework to estimate some non-linear material parameters of a structural system [45].”

Then, the following references have been added to the references list:

[44] H.A. Nasrellah, C.S. Manohar, *Finite element method based Monte Carlo filters for structural system identification*, Probabilistic Engineering Mechanics, 2011, 26(2), 294-307

[45] H. Ebrahimian, R. Astroza, J.P. Conte, *Extended Kalman filter for material parameter estimation in nonlinear structural finite element models using direct differentiation method*, Earthquake Engng Struct. Dyn., 2015, 44(10), 1495-1522

[43] G.P. Cimellaro, S. Marasco, *MDOF Systems*, In: Introduction to Dynamics of Structures and Earthquake Engineering. Geotechnical, Geological and Earthquake Engineering, vol 45, 2018, Springer, Cham.

1a. (i) “Frist of all, what type of structures and damage scenarios do the authors have in mind for the application of their methodology? Is it a bridge structure? A truss? (ii) What type of damage is representative of real damage in the structure? How severe the damage has to be to affect the acceleration of the structure? (iii) How many accelerometers are expected to be mounted on the structure to measure noticeable changes in the acceleration of the structure? (iv) Depending on the chosen application, is it realistic or even possible to excite the structure with a prescribed force?”.

Author Reply: (i) In general, the proposed methodology can be applied to any kind of structure as long as it can be modelled as a one-dimensional MDOF system. Indeed, the problem of the effects of temperature variations on the SHM system performances has historically affected large infrastructures, such as bridges. However, we preferred not to explicitly restrict the applicability of the method to such structures to underline the generality of the approach.

(ii) The choice of simulating damages by reducing the stiffness of the damaged elements is common in the SHM field [30, 37, 39]. Although this modelling technique seems simple, it is often chosen when it is not necessary to consider an a priori model for the damage description, as in the present case. Moreover, the purpose of the authors is to simulate a change in the structural properties due to a generic damage that may arise, not to identify a specific damaged state of the system. Regarding the relationship between damage severity and acceleration variations, note that, when using a numerical model to describe the behavior of the structure, any stiffness reduction produces acceleration variations. However, the latter can be interpreted as a true variation only when it overcomes the measurement noise, which is assumed to be described by a normal distribution with zero mean and variance $20\text{m}^2/\text{s}^4$ in this work. That said, as it can be seen from the results presented in the paper, the identification task performed using the PF successfully tracks the 10% sudden reduction in the stiffness of an element of the system, which implies the measured accelerations are already significantly affected. Moreover, the Particle Filter has also been shown to be effective in tracking gradually decreasing stiffness values, down to the 43% of the corresponding healthy value at the same temperature, i.e., a 57% of stiffness reduction, allowing reconstructing the progressive degradation even in the earliest phases right after the damage onset. However, a detailed sensitivity analysis of the PF performances with respect to the stiffness degradation value has not been systematically performed in this work, since it is considered out of the scope.

There are some works which investigate stiffness degradation in real scenarios by post-processing acceleration measurements acquired on the structure. For instance, in the work in [49], a notch was cut in a beam in order to experimentally represent a change in the stiffness value of the structure around the damage location. By processing acceleration measurements the authors were able to detect the damage, which validates the possibility of using acceleration measurements to identify local stiffness variations. However, no information about the amount of stiffness reduction was reported in that work. A different framework based on the use of



convolutional neural networks (CNNs) for post-processing transmissibility functions, which were computed from acceleration measurements, was presented in the work in [62] with the purpose of identifying damages in structures. Two experimental validations of that framework were reported there, i.e., the assessment of a MDOF system and that of a structural beam. Damage was introduced in the former system by means of changing one spring with a softer one (55% damage), while in the latter structure saw cutting was employed for reducing the beam local stiffness, thus not leading to known stiffness reduction values. The results showed that the CNN-based method was able to predict damages of at least 10% stiffness reduction. These values are comparable to those considered by the authors in the present work, where two damages have been considered: (i) a 10% instantaneous reduction of the stiffness of one spring and (ii) a progressive, linear decrease of the stiffness value of one spring up to the 43% of the corresponding healthy value at the same temperature, i.e., 57% damage. Moreover, a numerical work by Deraemaeker et. al [63] was published which deals with stiffness reduction down to 1.25%.

Accordingly, the following paragraph has been modified in Section 3.2:

“We consider the cases of (i) a sudden damage consisting of a 10% reduction of the stiffness value associated to spring 7 (the most critical one), occurring at time $t=10.0s$, and (ii) a progressive, linear decrease of the stiffness value associated to spring 4, occurring at time $t = 13.3s$ and leading to a final stiffness value (at T_{hor}) equal to the 43% of the corresponding healthy one at the same temperature, i.e., at $10^{\circ}C$. Those damage values are typical in the SHM field and are different enough to allow testing the proposed methodology both with minor stiffness degradations, i.e., 10%, and with more significant ones, i.e., the 57% stiffness reduction modelled on spring 4 [62, 63].”

Accordingly, the following references have also been added to the references list:

[62] S. Cofre-Martel, P. Kobrich, E. Lopez Droguett and V. Meruane, *Deep Convolutional Neural Network-Based Structural Damage Localization and Quantification Using Transmissibility Data*, Shock Vib., 2019

[63] A. Deraemaeker, E. Reynders, G. De Roeck and J. Kullaa, *Vibration-based structural health monitoring using output-only measurements under changing environment*, Mechanical Systems and Signal Processing, 2008, 22(1), 34-56

(iii) Please, also refer to the answer to question 2 by Reviewer 1 for what concerns the identifiability problem. In any case, the number of accelerometers to be used is indeed strictly structure-related in a real scenario. In principle, if the main degrees of freedom with respect to some type of motion can be identified in a structure, then one accelerometer per DOF should work fine, as it was proposed in this work and already employed, for example, in the work in [63]. Note that in many practical applications, accelerations can be accompanied also by position and velocity observations: the PF framework here proposed would be perfectly suited to include also those kinds of measurements to increase parameter identifiability. Moreover, one temperature sensor per degree of freedom may also be installed, with the purpose of capturing both the spatial and the temporal variation of the temperature. However, in a practical scenario, it may be decided to place more sensors per DOF, both for redundancy and for capturing more information about the single DOF, which may not be a concentrated entity in the real world, in order to determine the corresponding mean-value acceleration and temperature.

Accordingly, the two Paragraphs already reported in the answer to question 2 from Reviewer 1 (in the autoencoders-related answer) have been added to the Conclusions.



(iv) With regards to the possibility to excite the structure with a prescribed force, the following paragraph has been added to Section 3 with the purpose of clarifying that aspect:

“Note that applying external forces for monitoring the health state of structures is typical in the SHM field. For instance, bridges may be excited by means of servo-hydraulic vibration generators [60] or electrodynamic shakers [61], to cite some, which are tools that can excite structures with prescribed force patterns, such as sinusoidal forces or random vibrations.”

Accordingly, the following references have been added to the references list:

- [60] Y. Deger, R. Cantieni and S. Pietrzko, *Modal analysis of an arch bridge: experiment, finite element analysis and link*, Proceedings of the 12th International Modal Analysis Conference (IMAC), 1994, 425-432
[61] P. Fanning, P. Healy, A. Pavic, P. Reynolds and J. Brownjohn, *Sean O’Casey Bridge: comparison of operational and traditional modal analysis test results*, Proceedings of the 2nd International Operational Modal Analysis Conference, 2007, 293-298

Ib. “The main weakness of the paper is that the results are not supported or validated by experiments. Nor the chosen model is representative of a realistic scenario in which the shortcomings of the validation results could be overlooked since during this pandemic access to lab might be restricted. However, the proposed example is too simplistic and does not represent a realistic application. The reviewer kindly asked the authors whether they can present a more realistic example or validate their results experimentally”.

Author Reply: As already mentioned in the answer to question 1 by the same Reviewer, the MDOF system model is generic and representative of a wide class of realistic structures. Provided that it is not completely clear what the reviewer refers to when writing about more realistic models, we attempt anyway to provide three considerations:

1. First, in case “more realistic” means with more DOFs, the authors believe that a 6DOF system is a sufficiently good choice for testing the performances of the proposed framework, as similarly done in many other works in the SHM field [see for example 14, 30, 31, 34, 39, N1, N2]. In these works, compact MDOF systems were considered with the aim of testing the proposed methodology by means of easily manageable case studies, often fully numerically without presenting results based on experimental data. Moreover, it is conceptually straightforward to consider more degrees of freedom, only affecting the state-space definition in the PF framework. Indeed, the more degrees of freedom are considered, (i) the less identifiable can be the parameters in the state space (see in this regard the answer to question 2 by Reviewer 1), (ii) the more computational and time resources are needed by the PF to generate and propagate the particles and (iii) the more particles are usually required for larger state-space models. This motivated the choice of the benchmark 6DOF model to assess the robustness of the method and, consequently, to present the results.
2. In case more realistic model means a more complex modelling technique, then, for example, a FEM model would indeed provide a more accurate representation of the dynamics of the structure. As demonstrated in [44, 45] the framework is in principle suitable to integrate FEM models, which is in some way similar to a MDOF modelling technique improved with the introduction of proper shape functions. Given the number of degrees of freedom of a FEM model, the state-space vector would significantly increase in size, thus tending to require high-performance hardware even for simple analyses. Anyway, we are currently working towards this direction, in an effort to find the right compromise between model accuracy and computational times.



3. Finally, in case more realistic means non-linear, as already stated above the authors have performed some analyses considering a degrading hysteretic behaviour described by the Bouc-Wen's model, with satisfactory results. Those results will soon be provided to the scientific community.

As it comes to experimental applications, the authors are currently looking for experimental datasets available in the literature, since it is common practise to prove the performances of a framework on such benchmark data. However, it is hard to identify datasets which include both measurements under structural properties degradation and temperature information. Thus, ad hoc experimental tests, not straightforward due to the temperature control requirements, should be conducted which the authors believe would deserve an independent, future publications.

[N1] Z.Q. Lang, G. Park, C.R. Farrar, M.D. Todd, Z. Mao, L. Zhao and K. Worden, *Transmissibility of non-linear output frequency response functions with application in detection and location of damage in MDOF structural systems*, International Journal of Non-Linear Mechanics, 2011, 46(6), 841-853

[N2] F. Wang, X. Ling, X. Xu, F. Zhang, *Structural Stiffness Identification Based on the Extended Kalman Filter Research*, Abstr. Appl. Anal., 2014, 2014, 1-8

2. *“What the reviewer has understood is that the baseline pristine state which is used for training, covers temperatures between -30 to 100 degrees and the current state where some of the springs have damage is simulated at 40 degrees. Is this correct? For the training what temperature steps have been taken between -30 and 100 degrees? Was the 40 degrees indeed part of the trained temperature? If yes, can the authors show the reliability of the diagnosis with a temperature that has not been used in the training? Usually for machine learning applications it is customary to separate the data for training and validation so perhaps the authors can comments on this and use a validation scenario which is not used in the training phase.”*

Author Reply: We agree with the Reviewer about the testing scenarios for machine learning-based algorithms. That the training baseline for the autoencoder has been generated at temperatures ranging from -30°C to 100°C, with a step of 0.1°C (this information was missing in the paper and has been added), while the simulation of the damaged system considers an initial temperature of 40°C, which linearly decreases to 10°C. Of course, the temperature **range** experienced by the damaged system was included within the temperature range used for training the autoencoders. The temperature **step** considered for building the training database is such that the training set can be considered dense enough to have satisfactory interpolation performances by the neural networks, provided (as said above) the experienced temperatures lie within the training space. The autoencoder training procedure has indeed involved the partition of the database into the training, validation and test sets, according to the common good practice and the generalization capabilities have then been successfully verified. We believe there is no need to report the results of these standard procedure steps in the paper. Please, note only that no substantial differences are expected in case the algorithm is applied to a real scenario: refer to the answer to question 2 by Reviewer 1 for further details about the possible procedure.

3. *“Also the noise that has been included for the temperature observation noise is 0.1 degrees. Is this correct? If yes, this is extremely low as even in a single day, within a single acquisition the temperature could vary +- 1 or 2 degrees. Moreover, there must be very accurate temperature sensors distributed over the whole structure to measure this temperature with 0.1 degree accuracy. How would the results change if you include a more realistic temperature noise?”*



Author Reply: The comments by the Reviewer are not fully clear to the authors, especially when stating “even in a single day, within a single acquisition the temperature could vary ± 1 or 2 degrees”. Anyway, a possible answer to the question is here provided. The observation noise standard deviation (assuming a Gaussian error distribution) for the temperature is 0.1 degrees, which is typical of some commercially available sensors [N3, N4]. Indeed, as expected whenever the measurements are affected by larger noises, increasing the temperature noise magnitude would affect the results, possibly leading to a higher false alarm rate and a longer time between the onset of damage and the triggering of the alarm.

[N3] MMS Electronics, (2021, February 16), *SMT172 Calibrated digital temperature Sensor*, <http://www.mmselectronics.co.uk/smt172.htm>

[N4] J. L. Tan, J. N. Wang, *Error analysis and measurement uncertainty for a fiber grating strain-temperature sensor*, *Sensors*, 2010, 10(7), 6582-6593

4. “Why only the springs 2, 4 6 and 7 chosen to show the results? Was this just random? It would be good to show all of them for one single plot for the comparison.”

Author Reply: Those springs have been chosen to show the results because they are representative of the damaged and the undamaged conditions. Springs 4 and 7 have been chosen because those are the damaged springs. The healthy springs 2 and 6 have been selected since they turned out to be the most critical, as it can be seen from Figure 10(a), which shows they are characterized by higher values of the probabilistic damage indicator. The authors believe reporting a plot superposing all the deterministic damage indicators and the PF estimates would negatively affect the clarity, since many of the curves overlap (see for instance Figures 3 and 4). Instead, Figure 10 already shows the probabilistic indicators performance for all the springs.

4a. “Also, how realistic is to apply the proposed sinusoidal input load F in a real application?”

Author Reply: Please, see the answer to question 1a from the same Reviewer.

5. “What is the computational cost of the 10k particle vs 30k particle PF estimates presented in Table 1?”

Author Reply: The following Paragraph has been added to Section 3.1:

“The simulations are performed using a laptop with 16GB RAM and six physical Intel Core i7-9750H CPUs. The mean time required by the PF for estimating the 8s time history with $3 \cdot 10^4$ particles is approximately four times the mean time required using 10^4 particles. The computational times are slightly higher than the expected linear increase with the number of particles. That is due to the fact that some background processes always run in the computer and that the code is not completely computationally efficient, since the main goal of this work is to test a new SHM algorithm.”

6. “It would be beneficial to the reader to add a summary of the results at the end of section 3.2. stating what DI indicator works and what not. it is difficult to follow this section with so many different indices, and all the figures are located 5 pages away from this section so it is hard to follow by keep changing between pages and a clear summary would be appreciated.”



Author Reply: Following the reviewer's advice, a summary table of the damage indicators has been reported at the end of Section 3.2.

7. *"Is there any experimental validation that the proposed damages (change in stiffness in %) indeed can be recorded by changes in the acceleration?"*

Author Reply: Please, see the answer (ii) to question 1a from the same Reviewer.

8. *"It indeed would have been more realistic as the authors themselves commented in the conclusion section that the vibration signals induce by operation and environmental causes would have been a more realistic scenario however more challenging."*

Author Reply: Please, see the answer to question 7 from Reviewer 1.

9. *"The title of the paper and the abstract suggests something much more substantial than what it contains so it could be misleading to the readers. It does not reflect the simplified formulations and the computational nature of the work, and it is not validated by experimental results, neither for the effect of temperature change on the recorded accelerations nor for the effect of damage on the acceleration."*

Author Reply: The title has been changed to:

"Neutralization of temperature effects in damage diagnosis of MDOF systems by combinations of autoencoders and particle filters"

Moreover, the following sentence has been added to the abstract:

"The method is demonstrated with reference to a numerical MDOF system whose parameters are taken from a literature benchmark case study."

10. *"Some typos: line 258 should be expressions, line 595 should it be ANN?"*

Author Reply: Line 258 has been fixed, while line 595 has been changed to autoencoders. It should be AANN, which stands for Auto-Associative Neural Networks, but unfortunately the acronym was not introduced in the paper.

Highlights

- Structural Health Monitoring in changing temperature conditions is here addressed
- We propound a time domain method for damage identification and localization
- An integrated framework combining Particle Filter and Auto-encoders is investigated
- Auto-encoders are exploited for neutralizing temperature effects on SHM outcomes
- A benchmark 6-DOF case-study demonstrates the capabilities of the proposed method

1
2
3
4
5
6
7
8
9
10
11
12
13
14
15
16
17
18
19
20
21
22
23
24
25
26
27
28
29
30
31
32
33
34
35
36
37
38
39
40
41
42
43
44
45
46
47
48
49
50
51
52
53
54
55

Neutralization of temperature effects in damage diagnosis of MDOF systems by combinations of autoencoders and particle filters

16
17
18
19
20
21
22
23
24
25
26
27
28
29
30
31
32
33
34
35
36
37
38
39
40
41
42
43
44
45
46
47
48
49
50
51
52
53
54
55

Francesco Cadini^{*1}; Luca Lomazzi¹; Marc Ferrater Roca¹; Claudio Sbarufatti¹; Marco Giglio¹

20
21
22
23
24
25
26
27
28
29
30
31
32
33
34
35
36
37
38
39
40
41
42
43
44
45
46
47
48
49
50
51
52
53
54
55

March 9, 2021

23
24
25
26
27
28
29
30
31
32
33
34
35
36
37
38
39
40
41
42
43
44
45
46
47
48
49
50
51
52
53
54
55

¹Politecnico di Milano, Dipartimento di Meccanica, Via La Masa 1, I-20156 Milano, Italy

25
26
27
28
29
30
31
32
33
34
35
36
37
38
39
40
41
42
43
44
45
46
47
48
49
50
51
52
53
54
55

**Corresponding author: francesco.cadini@polimi.it*

Abstract

27
28
29
30
31
32
33
34
35
36
37
38
39
40
41
42
43
44
45
46
47
48
49
50
51
52
53
54
55

In the last years, scientific and industrial communities have put a lot of efforts into the development of a new framework for the assessment of structural integrity, generally known as Structural Health Monitoring (SHM), which should allow real-time, automatic evaluations of the state of the structures based on a network of permanently installed sensors. In the context of mechanical, aerospace and civil structures, several approaches have been proposed to address the SHM problem, yet, it remains often difficult to diagnose damages and estimate the structural health when dealing with varying operating and environmental conditions. Particle Filters have already been proposed as a time-domain-based method in the field of SHM, showing promising results as estimators of hidden, not directly observable states, such as those typically related to damages. At the same time, neural networks-based autoencoders have been proposed for structural damage detection, demonstrating to be capable of capturing damage-related features from vibration measurements. This work aims at exploiting the individual advantages offered by the two approaches by combining them in a novel algorithm for structural damage detection and localization, robust with respect to changing environmental conditions. The algorithm is further equipped with a fault indicator module stemming from the introduction of an automatic threshold and both deterministic and probabilistic fault indicators, thus offering a complete, valuable tool for supporting decision making with limited human intervention. The method is demonstrated with reference to a numerical MDOF system whose parameters are taken from a literature benchmark case study.

56
57
58
59
60
61
62
63
64
65

Keywords: Structural health monitoring; changing environmental conditions; diagnosis; damage localization; particle filter; autoencoder.

1 Introduction

Structural systems exposed to long service times, changing environmental and operating conditions and occasional loads may suffer from damage within their lifespan. For example, civil infrastructures, including buildings and bridges, crucial for a well-functioning society, face serious safety problems due to ageing [1]. In general, increasing the expected lifetime of a structure would be appealing, especially in case of very large infrastructures, because it can significantly increase the return on investment of the existing assets [2]. In this context, updating of maintenance policies plays a fundamental role for the economic and safe management of mechanical and structural systems. In fact, corrective and preventive maintenance strategies are gradually being replaced by condition-based and predictive maintenance techniques, relying on automatic evaluations of the state of the structures based on a network of permanently installed sensors, so-called Structural Health Monitoring (SHM), leading to large operative cost reductions and to the improvement of safety margins.

Several approaches have been proposed in the literature to correlate any deviation of suitably defined damage sensitive features (extracted from measured data) with the presence of a damage, possibly also identifying damage parameters, such as position, type, extent, and finally enabling damage prognosis. A typical categorization is made according to whether they operate in the frequency or time domain. As for the frequency domain feature extraction methods, it is worth mentioning the envelope spectrum [3], cepstrum [4], high-order spectrum and coherence function [5]. In particular, it has been thoroughly shown that damage detection may be successfully performed in the frequency domain by means of the transmissibility functions (TFs) [6–13], defined as the ratio of two response spectra of like-variables at two different locations (or nodes of the structural model) for a given excitation [14]. Among time domain features, time-waveform indices, orbits, probability density functions and probability density moments are commonly used. Applying time domain methods, little to no data is lost before processing the signal, allowing for detailed analyses, yet with the possibility of incurring into the risk of making diagnosis more burdensome due to the often required accumulation of available data [5]. For the sake of completeness, it is worth mentioning that mixed time-frequency analysis may also be adopted. These hybrid approaches are particularly useful for revealing the inherent information of non-stationary signals, which may be contained in the measures taken from the damaged structure [15]. For a thorough discussion of such a class of analysis techniques, the reader is referred to [15], where the benefits and limitations of these methods are discussed.

However, a general problem of any feature extraction method is that they are sensitive to any change in the environmental and operating conditions, including temperature, pressure, humidity and operative loads, which act as confounding influences, thus hampering the damage identification process potentially increasing the false alarm rate, as widely discussed in [16], [17], [18] and [19]. In this context, several approaches have been proposed to magnify the effect of damage over the monitored features and suppress the influence of confounding factors, usually referred to as data

1
2
3
4
5
6
7
8
9
10
11
12
13
14
15
16
17
18
19
20
21
22
23
24
25
26
27
39 normalization [16]. Some methods rely on regression and interpolation techniques to “learn” the
40 dependence of any measured feature from the varying boundary condition [20–23]. Other methods
41 leverage on a feature’s shift, induced by damage, “orthogonal” with respect to the reference normal
42 condition space. These include, for example, singular-value decomposition [24], principal component
43 analysis [25], factor analysis [26], cointegration [27, 28] and auto-associative neural networks [29].
44 However, most of these approaches can often only detect the presence of damages in structures,
45 not being able to locate and quantify them. So far, no general method provides fault isolation for
46 a wide range of systems while accounting for possible variations of operational and environmental
47 conditions. In most cases, these methods appear to be, in fact, case-specific, hence no extension of
48 such algorithms to generic problems seems to be able to provide reliable results. An exception seems
49 the work in [30], where an approach is proposed based on the quantification of stiffness variation
50 of all the elements in a structure due to temperature and damage effects, followed by suppression
51 of temperature effects to estimate the actual damage location and extent. That method works in
52 the frequency-domain, in fact the procedure needs a harmonic force to be applied to the structure
53 under examination, in order to determine the actual frequency response function, which is further
54 processed for detecting, localizing and quantifying the damage.

55
56
57
58
59
60
61
62
63
64
65
66
67
68
69
70
71
72
73
74
75
76
77
78
79
80
81
82
83
84
85
86
87
88
89
90
91
92
93
94
95
96
97
98
99
100
101
102
103
104
105
106
107
108
109
110
111
112
113
114
115
116
117
118
119
120
121
122
123
124
125
126
127
128
129
130
131
132
133
134
135
136
137
138
139
140
141
142
143
144
145
146
147
148
149
150
151
152
153
154
155
156
157
158
159
160
161
162
163
164
165
166
167
168
169
170
171
172
173
174
175
176
177
178
179
180
181
182
183
184
185
186
187
188
189
190
191
192
193
194
195
196
197
198
199
200
201
202
203
204
205
206
207
208
209
210
211
212
213
214
215
216
217
218
219
220
221
222
223
224
225
226
227
228
229
230
231
232
233
234
235
236
237
238
239
240
241
242
243
244
245
246
247
248
249
250
251
252
253
254
255
256
257
258
259
260
261
262
263
264
265
266
267
268
269
270
271
272
273
274
275
276
277
278
279
280
281
282
283
284
285
286
287
288
289
290
291
292
293
294
295
296
297
298
299
300
301
302
303
304
305
306
307
308
309
310
311
312
313
314
315
316
317
318
319
320
321
322
323
324
325
326
327
328
329
330
331
332
333
334
335
336
337
338
339
340
341
342
343
344
345
346
347
348
349
350
351
352
353
354
355
356
357
358
359
360
361
362
363
364
365
366
367
368
369
370
371
372
373
374
375
376
377
378
379
380
381
382
383
384
385
386
387
388
389
390
391
392
393
394
395
396
397
398
399
400
401
402
403
404
405
406
407
408
409
410
411
412
413
414
415
416
417
418
419
420
421
422
423
424
425
426
427
428
429
430
431
432
433
434
435
436
437
438
439
440
441
442
443
444
445
446
447
448
449
450
451
452
453
454
455
456
457
458
459
460
461
462
463
464
465
466
467
468
469
470
471
472
473
474
475
476
477
478
479
480
481
482
483
484
485
486
487
488
489
490
491
492
493
494
495
496
497
498
499
500
501
502
503
504
505
506
507
508
509
510
511
512
513
514
515
516
517
518
519
520
521
522
523
524
525
526
527
528
529
530
531
532
533
534
535
536
537
538
539
540
541
542
543
544
545
546
547
548
549
550
551
552
553
554
555
556
557
558
559
560
561
562
563
564
565
566
567
568
569
570
571
572
573
574
575
576
577
578
579
580
581
582
583
584
585
586
587
588
589
590
591
592
593
594
595
596
597
598
599
600
601
602
603
604
605
606
607
608
609
610
611
612
613
614
615
616
617
618
619
620
621
622
623
624
625
626
627
628
629
630
631
632
633
634
635
636
637
638
639
640
641
642
643
644
645
646
647
648
649
650
651
652
653
654
655
656
657
658
659
660
661
662
663
664
665
666
667
668
669
670
671
672
673
674
675
676
677
678
679
680
681
682
683
684
685
686
687
688
689
690
691
692
693
694
695
696
697
698
699
700
701
702
703
704
705
706
707
708
709
710
711
712
713
714
715
716
717
718
719
720
721
722
723
724
725
726
727
728
729
730
731
732
733
734
735
736
737
738
739
740
741
742
743
744
745
746
747
748
749
750
751
752
753
754
755
756
757
758
759
760
761
762
763
764
765
766
767
768
769
770
771
772
773
774
775
776
777
778
779
780
781
782
783
784
785
786
787
788
789
790
791
792
793
794
795
796
797
798
799
800
801
802
803
804
805
806
807
808
809
810
811
812
813
814
815
816
817
818
819
820
821
822
823
824
825
826
827
828
829
830
831
832
833
834
835
836
837
838
839
840
841
842
843
844
845
846
847
848
849
850
851
852
853
854
855
856
857
858
859
860
861
862
863
864
865
866
867
868
869
870
871
872
873
874
875
876
877
878
879
880
881
882
883
884
885
886
887
888
889
890
891
892
893
894
895
896
897
898
899
900
901
902
903
904
905
906
907
908
909
910
911
912
913
914
915
916
917
918
919
920
921
922
923
924
925
926
927
928
929
930
931
932
933
934
935
936
937
938
939
940
941
942
943
944
945
946
947
948
949
950
951
952
953
954
955
956
957
958
959
960
961
962
963
964
965
966
967
968
969
970
971
972
973
974
975
976
977
978
979
980
981
982
983
984
985
986
987
988
989
990
991
992
993
994
995
996
997
998
999
1000

Recently, particle filters (PFs) and other Bayesian methods have been used as time-domain tools for structural parameters identification [31] and fault diagnosis [32, 33]. For example, some works used PFs for identifying the stiffnesses of a multiple-degree of freedom (MDOF) system subject to a seismic-like acceleration forcing function [34]. Moreover, the PF estimation capabilities in presence of non-linear dynamics for the spring components have also been investigated, albeit restricting the attention to the problem of system identification, without delving into the potentiality of the method as a damage diagnosis tool. To the best of the authors knowledge, the effects of environmental conditions have not been taken into account yet in damage diagnosis methods based on the use of PFs in the time domain.

Furthermore, machine learning approaches, specifically neural networks, have been widely implemented for damage diagnosis [35, 36], due to their performance in capturing the behavior of relevant damage features even in presence of very complex dynamics, whose detailed physics-based modeling would often require extraordinary computational efforts. In particular, neural network-based autoencoders have been quite extensively used for performing damage detection [35, 37, 38]. For example, some early work [39] proposed the use of autoencoders for extracting damage-related features from vibration measurements in the frequency domain, thus being able to perform novelty detection in MDOF-modeled systems. However, that procedure relied on the information extracted from the transmissibility function, which, as already mentioned, may not always provide reliable results in damage localization [14].

In this work, we propose an original time-domain approach to perform fault identification in structural components subject to degradation, under changing operating and environmental conditions. Exploiting the complementarity of PFs and autoencoders outlined above, in this paper

1
2
3
4 77 it is proposed to combine them to derive a robust and flexible algorithm, offering the possibility
5
6 78 to automatically perform damage detection and identification in a unique, coherent and simple
7
8 79 framework. More specifically, the PF estimates some not directly observable structural parameters
9
10 80 on the basis of commonly available vibration measurements (e.g., accelerations, positions, etc.). PF
11
12 81 posterior estimation is then combined with temperature measurements using autoencoders, which
13
14 82 suppress confounding influences over the estimated structural parameters. Finally, for an effective
15
16 83 use of the algorithm as a decision support, a novel detection strategy is also proposed, based on
17
18 84 the introduction of automatic thresholds, thus delivering a result less dependent from external,
19
20 85 i.e., human, interpretation. The method is demonstrated with reference to a MDOF system whose
21
22 86 parameters are taken from a literature benchmark case study [39].

23
24 87 The paper is organized as follows. In Section 2 the generic methodological approach is presented,
25
26 88 focusing on the specific design of the PF and of the autoencoder, tailored to the specific application
27
28 89 to the MDOF system model. Section 3 introduces a case study, which consists of a 6-DOF system
29
30 90 affected by temperature variations. The Section first presents a brief sensitivity analysis aimed
31
32 91 at tuning the performances of the PF algorithm, and then demonstrates the performances of the
33
34 92 proposed methodology. In Section 4 the conclusions of this work are provided, along with a critical
35
36 93 discussion of the main results achieved and possible future work.

31 94 **2 Methodology**

37
38 95 The methodology is proposed with reference to a modeling strategy commonly used to represent
39
40 96 the dynamic behavior of many mechanical, aeronautical and civil structural systems, such as rotary
41
42 97 machines, multi-storey buildings and multi-span bridges, i.e., the one-dimensional MDOF systems
43
44 98 [40–42]. MDOF structural systems are also known as periodic structures, which basically consist
45
46 99 of several structural components of the same type, i.e., springs, masses, dampers, joined together
47
48 100 [41, 43]. These models are particularly useful for describing the vibration of a structure when it
49
50 101 experiences significant motions in one preferential direction. However, the proposed methodology
51
52 102 is generic and not bounded to the specific model employed for simulating the structure under mon-
53
54 103 itoring. Hence, any other modelling technique different from the MDOF system can in principle
55
56 104 be considered, with no compatibility issues with the proposed framework, as long as a model of
57
58 105 the structure is provided. For instance, the Finite Element modelling strategy may represent a
59
60 106 promising alternative to the MDOF technique, yet more complicated, which would also open up
61
62 107 the chance to deal with non-periodic structures. In fact, a combination of Particle Filter as dynamic
63
64 108 state estimation tool and Finite Element model of different types of structures, e.g., rubber sheet
65
66 109 with a hole, single span beam and multi-span masonry arch bridge, was employed in the work in [44]
67
68 110 with satisfactory performances. Similarly, nonlinear Finite Element method and extended Kalman
69
70 111 filter were successfully combined in a unique framework to estimate some non-linear material pa-
71
72 112 rameters of a structural system [45]. In this context, according to the common practice in the SHM
73
74 113 field, structural damage is modeled as a stiffness reduction of one or more springs in the system



Figure 1: MDOF mass-spring-damper system.

[30, 37, 39]. Since the stiffness values are not directly observable parameters, a PF algorithm is derived for the estimation of the hidden stiffnesses on the basis of the most commonly available vibration measurements, i.e., the accelerations of the MDOF system masses, although the filter could in principle be generalized to process also other types of possible measurements (positions and velocities).

Then, within the PF framework, the differential equations describing the dynamic evolution of each degree of freedom of the MDOF system are discretized in time and used to create the state-space for the PF-based state estimation process. At each time step, the acceleration of each degree of freedom of the system is measured. Simultaneously, a sufficiently large number of possible system dynamic evolutions (particles) are sampled and are assigned some importance weights based on the observation likelihood. The weights are then used to provide an estimate of the MDOF model structural stiffnesses within an augmented state parameter estimation framework. This process allows to obtain temporal estimates of the system stiffnesses, which can be used to evaluate the structure health state.

As shown in previous works of literature (e.g., [32]) and also later in this paper, if no external operating and/or environmental conditions are modifying the values of the system stiffnesses, in principle PF would allow not only to detect the presence of damage, but, at the same time, to locate and, somehow, quantify it. When, on the other hand, the effects of external conditions on the stiffnesses are superposed to those of damages, then even the simple damage detection task by PF is severely hampered. We here propose to address this issue by processing the PF estimates of the stiffnesses through a neural network autoencoder, previously trained with a healthy, but temperature-dependent baseline, so as to be able to capture the physical relationship between the external conditions and the stiffnesses. During the operational phase, the error between the input and the reconstructed data serves, upon the introduction of an automatic threshold, for the damage diagnosis purpose. By so doing, the autoencoder will be able to generate signals sensitive to the presence of damages only, which will be further processed to obtain an automatic alarm system.

In what follows, some details of PF algorithms and of autoencoders are provided, with a focus on how they are combined to perform damage diagnosis. For further mathematical details on the individual methods, the interested reader is referred to the vast literature available.

2.1 State-space model and particle filter

Consider a generic MDOF mass-spring-damper system as the one shown in Figure 1. According to common practice in this kind of SHM applications, the consolidated assumption of viscous damping is made in this work, which represents a velocity-dependent damping formulation allowing not to introduce non-linearities in the system, while still guaranteeing a quite satisfactory description of the damping effects [46]. In particular, the widely adopted proportional damping, or Rayleigh damping, assumption is made [47]. Some issues may arise adopting this model, e.g., (i) proportional damping does not allow for satisfactory representation of eventual non-linear damping behaviors or (ii) it provides not very accurate results when the structure undergoes yielding, buckling or when the local behavior around the tip of an eventual crack has to be investigated, to cite some. However, being these particular scenarios not relevant in this work, proportional damping is considered to be a valid and accurate enough damping modelling technique. Moreover, a relevant property of Rayleigh damping is that it can be applied both to structures made of homogeneous materials and to those made of non-homogeneous materials, without any difference in the specific formulation, which allows not limiting to analyze structures made of isotropic materials, but also more complex systems including non-isotropic materials [48]. In this work, damping is assumed to be proportional to stiffness only through a coefficient β , assumed identical for all the dampers in the MDOF system [49]. In order to be able to perform stiffness parameters estimation, an augmented state space representation of the system is introduced, which includes four types of variables: position and speed of each mass of the system, stiffness value of the springs of the structure and proportionality constant of damping. Hence, the state vector for n degrees of freedom becomes:

$$\mathbf{x}^\tau = \left[x_1^\tau \quad \dots \quad x_n^\tau \quad y_1^\tau \quad \dots \quad y_n^\tau \quad k_1^\tau \quad \dots \quad k_{n+1}^\tau \quad \beta \right]^\top \quad (1)$$

where x_i^τ is the position of mass i at time step τ , y_i^τ is the speed of mass i at the generic, discrete time step τ , k_i^τ is the i -th spring stiffness at time step τ and β is the proportionality constant of damping, according to the relationship $c_i^\tau = \beta k_i^\tau$. Within the PF framework, the state-space model describing the system evolution at the discrete time step τ must be a hidden Markov process of the form:

$$\mathbf{x}^\tau = g(\mathbf{x}^{\tau-1}, \mathbf{w}^{\tau-1}) \quad (2)$$

where $g(\cdot)$ represents a generic function, which may be non-linear, and $\mathbf{w}^{\tau-1}$ is the process noise vector value at time step $\tau - 1$, here assumed to be distributed according to a Gaussian multivariate distribution $N(0, \Sigma_w)$, $\Sigma_w = \text{diag}(\sigma_{x_1}, \dots, \sigma_\beta)$. In the specific system considered in this study, i.e., a MDOF mass-spring-damper system, four state evolution equations are considered, one for each type of state included in the state vector of equation 1. The dynamic evolution of each individual mass position is then governed by:

$$x_i^{\tau+1} = y_i^\tau dt + x_i^\tau + w_{\text{position}}^\tau; \quad \forall i = 1, \dots, n \quad (3)$$

1
2
3
4
5
6
7
8
9
10
11
12
13
14
15
16
17
18
19
20
21
22
23
24
25
26
27
28
29
30
31
32
33
34
35
36
37
38
39
40
41
42
43
44
45
46
47
48
49
50
51
52
53
54
55
56
57
58
59
60
61
62
63
64
65

175 which is obtained from the discretization of the system of differential equations of motion with the
176 addition of the position process noise $w_{position}^\tau$. The state-space equation for the velocity of each
177 degree of freedom (mass) is given by:

$$y_i^{\tau+1} = \frac{F_i^\tau}{m_i} dt + y_i^\tau \left(1 - \frac{dt}{m_i} (c_i + c_{i+1})\right) + y_{i-1}^\tau \frac{dt}{m_i} c_i + y_{i+1}^\tau \frac{dt}{m_i} c_{i+1} - x_i^\tau \frac{dt}{m_i} (k_i^\tau + k_{i+1}^\tau) + x_{i-1}^\tau \frac{dt}{m_i} k_i^\tau + x_{i+1}^\tau \frac{dt}{m_i} k_{i+1}^\tau + w_{speed}^\tau; \quad \forall i = 1, \dots, n \quad (4)$$

178 where F_i^τ represents the forcing load applied to mass m_i , c_i is the damping coefficient value of
179 the i -th damper and w_{speed}^τ is the speed process noise. Equation 4 is again obtained from the
180 discretization of the system of differential equations of motion with the addition of the speed process
181 noise w_{speed}^τ . Note that for the side masses equation 4 must be updated deleting some terms, in
182 particular those including x_{i-1}^τ and y_{i-1}^τ for $i = 1$, and those with x_{i+1}^τ and y_{i+1}^τ for $i = n$. Spring
183 stiffness values are assumed to be invariant over time in a healthy structure without any variations
184 of operating and/or environmental conditions, such as temperature. Therefore, in agreement with
185 the common parameter identification practice, each parameter k_i is modeled as an augmented state
186 characterized by a value constant in time, only slightly perturbed by some unmodeled dynamics,
187 here represented by the process noise w_{spring}^τ :

$$k_i^{\tau+1} = k_i^\tau + w_{spring}^\tau; \quad \forall i = 1, \dots, n + 1 \quad (5)$$

188 In case temperature variations occur, we assume that the stiffness values evolve according to the
189 following relationship:

$$k_i(T) = 0.1 (T)^2 - 18T + k_i(0^\circ C); \quad \forall i = 1, \dots, n + 1 \quad (6)$$

190 where T identifies the external temperature measured in $^\circ C$. Equation 6 is obtained from [30] by
191 rescaling the coefficients of the original equation describing the elastic modulus as a function of
192 the temperature [50, 51] to have a stiffness value of $10^4 \frac{N}{m}$ at $0^\circ C$ in correspondence of an elastic
193 modulus of $203.07 GPa$. The proportionality constant of damping is assumed to be invariant over
194 time. Therefore, as typically done in the parameter identification practice, the parameter β is
195 modeled as an augmented state characterized by a value constant in time, only slightly perturbed
196 by some unmodeled dynamics, here represented by the process noise $w_{damping}^\tau$:

$$\beta^{\tau+1} = \beta^\tau + w_{damping}^\tau \quad (7)$$

197 hence, in case temperature variations occur, the i -th damping value changes accordingly to the
198 change of the related stiffness value, i.e., k_i , according to the equation $c_i^\tau = \beta^\tau k_i^\tau$.

199 In the PF framework, the hidden Markov states whose evolution is described in equations 3, 4,
200 5 and 7 are assumed to be indirectly observed by collecting some measurements z . The relationship

201 between the hidden states and the measurement \mathbf{z}^τ is assumed to be known and to take the following
 202 form:

$$\mathbf{z}^\tau = h(\mathbf{x}^\tau, \mathbf{v}^\tau) \quad (8)$$

203 where $h(\cdot)$ is a generic function, which may be non-linear, and \mathbf{v}^τ is the measurement noise vector
 204 at time step τ , here assumed to be distributed according to a Gaussian multivariate distribution
 205 $N(0, \Sigma_v)$, $\Sigma_v = \text{diag}(\sigma_{z_1} \dots \sigma_{z_n})$. In this study, without any loss of generality, we restrict our
 206 attention to the case in which only acceleration measurements are available for each degree of
 207 freedom (mass). The measurement equation relating the acceleration value of mass m_i to the state
 208 vector at time step τ is:

$$z_i^\tau = \frac{F_i^\tau}{m_i} - \frac{y_i^\tau}{m_i}(c_i + c_{i+1}) + \frac{y_{i-1}^\tau}{m_i}c_i + \frac{y_{i+1}^\tau}{m_i}c_{i+1} - \frac{x_i^\tau}{m_i}(k_i^\tau + k_{i+1}^\tau) + \frac{x_{i-1}^\tau}{m_i}k_i^\tau + \frac{x_{i+1}^\tau}{m_i}k_{i+1}^\tau + v_i^\tau; \quad \forall i = 1, \dots, n \quad (9)$$

209 where v_i^τ represents the acceleration measurement noise at time step τ . Note that for the side
 210 masses equation 9 must be updated deleting some terms, in particular those including x_{i-1}^τ and
 211 y_{i-1}^τ for $i = 1$, and those with x_{i+1}^τ and y_{i+1}^τ for $i = n$.

212 Then, in the PF framework it is possible to divide the filtering process in two stages, whose
 213 final objective is the on-line, recursive estimation of the posterior probability density function (pdf)
 214 $p(\mathbf{x}^\tau | \mathbf{z}^{1:\tau})$ of the hidden state vector \mathbf{x}^τ conditioned on the sequence of data observed up to time
 215 step τ , i.e., $\mathbf{z}^{1:\tau}$.

216 In the first step (also called transition or prediction stage), the pdf of the hidden states \mathbf{x}^τ at
 217 time step τ , i.e., $p(\mathbf{x}^\tau | \mathbf{z}^{1:\tau})$, is predicted based on prior information available at time step $\tau - 1$.
 218 Operatively, the process equations 3, 4, 5 and 7 are used for the random generation of N_s possible
 219 state trajectories (particles) \mathbf{x}_s^τ , $s = 1, \dots, N_s$, at time step τ , which is equivalent to sampling the
 220 importance density function (the prior) $p(\mathbf{x}^\tau | \mathbf{x}^{\tau-1})$.

221 Then, in the second stage (also called update stage), as soon as a new observation \mathbf{z}^τ is acquired
 222 at time step τ , according to the Bayes' theorem, the measurement equation 9 is used to assign a
 223 weight w_s^τ to each of the N_s particles, recursively calculated as:

$$w_s^\tau = w_s^{\tau-1} \cdot \prod_{i=1}^n \frac{1}{\sqrt{2\pi}\sigma_{z_i}} e^{-0.5 \left(\frac{z_{s,i}^\tau - a_i^\tau}{\sigma_{z_i}} \right)^2} \quad (10)$$

224 where $z_{s,i}^\tau = h(\mathbf{x}_s^\tau, \sigma_{z_i})$ is the acceleration virtual measurement of mass m_i , associated to the
 225 particle \mathbf{x}_s^τ at time τ and computed according to measurement equation 9, $\sigma_{z_i}^2$ the variance of the
 226 i -th measurement and $z_i^\tau = a_i^\tau$ is the acceleration observation of the i -th DOF at time step
 227 τ . Equation 10 is formulated under the hypothesis of Gaussian measurement noise \mathbf{v}^τ equal for all
 228 the acceleration measurements available.

1
2
3
4
5
6
7
8
9
10
11
12
13
14
15
16
17
18
19
20
21
22
23
24
25
26
27
28
29
30
31
32
33
34
35
36
37
38
39
40
41
42
43
44
45
46
47
48
49
50
51
52
53
54
55
56
57
58
59
60
61
62
63
64
65

229 Upon the normalization of the importance weights, the posterior pdf can then be approximated
230 by the ordered set $\{\mathbf{x}_s^\tau, \tilde{w}_s^\tau\}_{s=1}^{N_s}$ [52, 53], or, using the Monte Carlo formalism:

$$p(\mathbf{x}^\tau | \mathbf{z}^{1:\tau}) \approx \sum_{s=1}^{N_s} \tilde{w}_s^\tau \delta_{\mathbf{x}_s^\tau, \mathbf{x}^\tau} \tag{11}$$

231 where \tilde{w}_s^τ represents the normalized weight assigned to the s -th particle. Note that, to avoid the
232 problem of degeneracy, bootstrap resampling is applied at each time step τ , which implies re-setting
233 the importance weights of the particles to $w_j^\tau = \frac{1}{N_s}$. Hence, the state estimate $\hat{\mathbf{x}}^\tau$ is computed as
234 the mean value of the posterior distribution of the state vector \mathbf{x}^τ estimated by the particle filter.
235 For a more detailed discussion on particle filtering and Monte Carlo methods, the reader is referred
236 to the seminal works [54] and [52].

237 Indeed, in this context, the problem of the identifiability of the parameters becomes very im-
238 portant. Thus, identifiability assessment should always be performed before the application of the
239 method. This activity is out of the scope of the present work, in which identifiability is heuristically
240 assessed by trial-and-error procedure. In case more complex systems are involved, the heuristic ap-
241 proach should possibly consist of increasing the number of forcing terms and, in case applying more
242 loads is hard in the specific real application (e.g., on large civil infrastructures), diversification of
243 the type of observations could prove a good strategy, e.g., considering displacement, velocity and
244 acceleration measurements together. The interested reader is referred to [55] for further details
245 about the identifiability problem.

246 **2.2 Combination of PF with neural network-based auto-encoders**

247 Neural networks are computational models aimed at fitting any linear and/or non-linear relationship
248 $\mathbf{y} = f(\mathbf{x})$ between some input and output vectors \mathbf{x} and \mathbf{y} . A network is a collection of connected
249 elements, called *nodes* or *neurons*, arranged in layers. In general, the architecture of a neural
250 network includes one input layer, some hidden layers and the output layer. Considering a simplified
251 case with one hidden layer only, each node $i = 1, \dots, N_i$ of the input layer receives one input signal
252 x_i and is fully connected to each node $j = 1, \dots, N_h$ of the hidden layer through a path to which
253 a weight w_{ij} is associated. All the input signals x_i feeding a node j and a bias parameter b_j are
254 summed up to give the excitation $\sum_{i=1}^{N_i} (w_{ij} \cdot x_i) + b_j$ of that specific hidden neuron. The excitation
255 signal is further processed by a generally non-linear *activation function*, thus giving rise to the
256 j -th hidden node output $z_j = g(\sum_{i=1}^{N_i} (w_{ij} \cdot x_i) + b_j)$. Note that the activation function $g(\cdot)$ is a
257 monotonically increasing, continuous function with output range $(0, 1)$, and that the bias has the
258 purpose of giving a constant offset to the excitation level of the hidden nodes, or, equivalently,
259 to set different activation thresholds. Each node $j = 1, \dots, N_h$ of the hidden layer is then fully
260 connected to each output node $k = 1, \dots, N_o$ through a weight w_{jk} . All the signals z_j feeding an
261 output node k are summed up to give the excitation $\sum_{j=1}^{N_h} (w_{jk} \cdot z_j)$ of that specific output neuron.
262 The excitation signal is further processed by a usually linear activation function $h(\cdot)$, thus giving

rise to the k -th node output $y_k = h(\sum_{j=1}^{N_h}(w_{jk} \cdot z_j))$. The equation describing the input-output relationship can then be written in a compact form:

$$y_k = h\left(\sum_{j=1}^{N_h}(w_{jk} \cdot (g(\sum_{i=1}^{N_i}(w_{ij} \cdot x_i) + b_j)))\right) \quad (12)$$

Under some assumptions, the Cybenko theorem [56] guarantees that expressions as that in equation 12 are universal approximators, provided the proper architecture and suitable values of the weights are used. However, the theorem does not provide any strategy to build an effective network. While the architecture is often left to the designer experience, several methods have been proposed to identify optimal sets of weights, through procedures generally known as “training” or “learning”, the most popular of which is probably the error back-propagation algorithm with gradient descent. The training algorithm requires that a set of input-output examples be available from the observed process to be approximated. The inputs are fed to the network, which produces some outputs. The outputs are then compared with the actual ones and the error is then used to back-updating the weights by a weight gradient-descent approach. The procedure ends when satisfactory generalization capabilities and reconstruction errors are achieved (see [57]).

In this framework, the *autoencoders* (or *auto-associative neural networks*), are deep neural models (i.e., containing more than three layers, including input and output) including a dimensionality reduction side and a reconstructing side, exploited for learning data properties in an unsupervised manner [58]. In particular, the dimensionality reduction side reduces the dimensionality of the input data fed to the network, while the reconstructing side is aimed at reconstructing in the output layer the same values fed in input to the network. In this work, the auto-associative neural network architecture considered is described by a symmetric structure, consisting of two mirrored multilayer perceptrons (MLPs), with one input layer, three hidden layers (typically called mapping, bottleneck and demapping layers) and an output layer (Figure 2). Indeed, the input and output vectors have the same dimension, which is typically larger than the bottleneck size. The mapping and demapping layers usually have the same number of nodes, which is greater than that of the input vector. During the mapping phase, which involves input, mapping and bottleneck layers, if the bottleneck has less nodes than input and output layers, then the autoencoder reduces the input dimensionality through the following general relationship:

$$\mathbf{y} = H_{map}(\mathbf{x}) \quad (13)$$

where $H_{map}(\cdot)$ is the vector of generic models implemented by the first MLP of the autoencoder (see equation 12). The subsequent demapping phase aims at reconstructing the input variables in the output nodes via the demapping layer, which is an “inverted” version of the first MLP, according

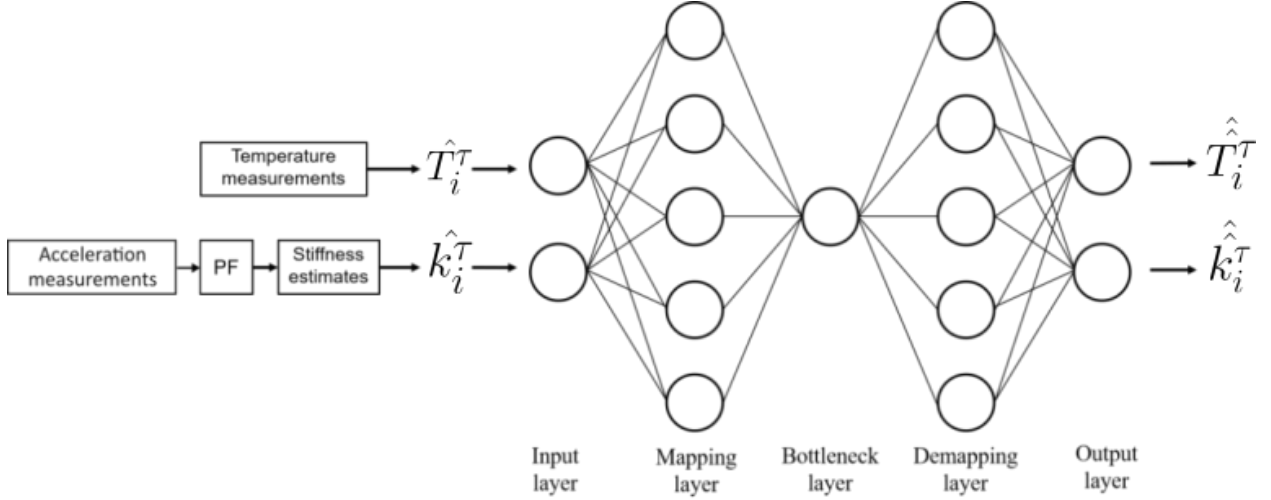


Figure 2: Proposed autoencoder structure.

to the following relationship:

$$\hat{\mathbf{x}} = H_{demap}(\mathbf{y}) \quad (14)$$

where $H_{demap}(\cdot)$ is the vector of generic models implemented by the second MLP of the autoencoder and $\hat{\mathbf{x}}$ is the reconstructed input vector in the output layer.

In this work, different autoencoders are associated to each spring of the MDOF model. Each autoencoder is then structured with two input nodes, characterized by linear functions, one receiving the temperature observed at the location of the associated spring and one receiving the PF-based estimate of the stiffness for each spring, i.e., as illustrated above, the mean of the PF-based sample posterior pdfs of the stiffnesses. The two input values are then processed by the autoencoder mapping layer, combined into a single signal within the single bottleneck node and then further reconstructed in the output vector of size two. The choice of one single node in the bottleneck layer (activated by a sigmoid function) is inspired by a similar strategy followed in the work in [37] and, at the same time, it is also intuitively sound. In fact, only one variable, i.e., the temperature, can give rise to variations in the structural stiffnesses in healthy conditions. The mapping and demapping layers are made up of 5 nodes, identified upon a trial and error procedure, each characterized by a sigmoid activation function. This architecture allows the autoencoder to extract relevant information about the nature of the spring stiffness change during the operational phase, eventually leading to the detection and the localization of the structural damage, as it will be shown in Section 3. In fact, autoencoders are able to reconstruct the input variables in the output layer according to the baseline they have been trained with. Thus, if any change occurs in the correlation between the input parameters (i.e., in our case temperatures and estimated stiffnesses), since the autoencoder tends to provide in output the correlations it has been trained to recognize, it should give rise to some discrepancies between the input and the output data. Then, by processing some properly defined reconstruction error (or distance) between the input and the output signals, it is possible, in

1
2
3
4
5
6
7
8
9
10
11
12
13
14
15
16
17
18
19
20
21
22
23
24
25
26
27
28
29
30
31
32
33
34
35
36
37
38
39
40
41
42
43
44
45
46
47
48
49
50
51
52
53
54
55
56
57
58
59
60
61
62
63
64
65

principle, to detect any anomaly in the input signals which disrupt their healthy baseline correlation. In order to further localize the anomalies, as anticipated above, for the general case of a n -degrees of freedom MDOF model, $n + 1$ autoencoders must be associated to the $n + 1$ spring stiffnesses in the system. Indeed, only the outputs of the autoencoders associated to a damaged spring would then be affected by the presence of the anomaly, thus consequently allowing for their localization.

Here, according to several works of literature [37, 58, 59], the squared error is used to measure the differences between the inputs and the reconstructed outputs of the autoencoders, upon proper normalization of their values:

$$SE_i^\tau = (\hat{T}_i^\tau - \hat{\hat{T}}_i^\tau)^2 + (\hat{k}_i^\tau - \hat{\hat{k}}_i^\tau)^2 \tag{15}$$

where SE_i^τ is the squared error between the input variables (\hat{T}_i^τ and \hat{k}_i^τ) and the output variables ($\hat{\hat{T}}_i^\tau$ and $\hat{\hat{k}}_i^\tau$) recorded at time step τ on the i -th spring of the system. Additionally, it is here proposed to also use the simple error:

$$E_i^\tau = (\hat{T}_i^\tau - \hat{\hat{T}}_i^\tau) + (\hat{k}_i^\tau - \hat{\hat{k}}_i^\tau) \tag{16}$$

Note that, for a proper functioning of neural networks, the normalization of all the training data is a common practice, which becomes basically mandatory when the inputs are quantities characterized by different units of measures (as it is the case in the present work). Here, the input data are normalized according to the following linear transformations:

$$\frac{\hat{T}_i^\tau - (-50^\circ C)}{120^\circ C - (-50^\circ C)} \tag{17}$$

$$\frac{\hat{k}_i^\tau}{1.1 \cdot 10^4 \frac{N}{m}} \tag{18}$$

so that the errors defined above can vary in the ranges $E_i^\tau \in [-2, 2]$ and $SE_i^\tau \in [0, 2]$. From here on, the values \hat{T}_i^τ and \hat{k}_i^τ directly refer to the already normalized input data.

In practical applications, the healthy baseline to be used for training the $n + 1$ autoencoders can be acquired during the early life of the system, when it is reasonable to assume that no damages are present. Then, upon proper excitation of the structure, the PF algorithm described above can be turned on, so as to provide estimates of the model stiffnesses. At the same time, the temperature at each spring location must be recorded. Indeed, for a correct functioning of the algorithm, a rather wide range of temperatures should be explored, either artificially applied or, for certain types of structures, only expected to occur in the environment, during the recording of the baseline.

2.3 Definition of the diagnostic indicators

For the definition of suitable diagnostic indicators, to be used for timely triggering diagnostic alarms, in principle one could set proper thresholds for the errors described in the previous Section, as also suggested in [39] for SE_i^τ . Unfortunately, as it shall be shown in the next Section, the choice of the proper threshold values is somewhat arbitrary and, if not properly set, may easily lead to unreliable results, either too conservative (too many false alarms) or too risky (too many missed alarms). The problem is further exacerbated by the fact that both the autoencoder inputs are affected by noises, the temperature measurement noise and the whole uncertainty affecting the PF-based stiffness estimates, due to a combination of acceleration measurement noise, process noises (unmodeled dynamics) and Monte Carlo errors. Indeed, this is one of those “eternal” dilemmas ever characterizing any diagnostic task, for which no definitive answers exist. Nevertheless, in this work an attempt is made to address this issue, which will be proven to be effective at least within the scope of the application presented here. The proposed approach consists of combining an automatic threshold definition module with the construction of both a deterministic and a probabilistic indicator. More specifically, two automatic thresholds for each spring $i = 1, \dots, n + 1$ are introduced as:

$$ATE_i^1 = p1(E_i^{1:\tau_0}) \quad (19a)$$

$$ATE_i^{99} = p99(E_i^{1:\tau_0}) \quad (19b)$$

where $p1(E_i^{1:\tau_0})$ and $p99(E_i^{1:\tau_0})$ are the 1th and the 99th percentiles of the probability density function of the error defined in equation 16, respectively, computed over a fixed time window of width τ_0 time steps taken at the beginning of the operational life of the structure, when the system is assumed to be in healthy conditions. In a similar fashion, an automatic threshold for each spring i can also be defined for the squared error as:

$$ATSE_i^{99} = p99(SE_i^{1:\tau_0}) \quad (20)$$

where $p99(SE_i^{1:\tau_0})$ is the 99th percentile of the probability density function of the squared error defined in equation 15 taken over the same time window of width τ_0 time steps defined above.

Then, in order to operatively trigger the diagnostic alarm, a binary, deterministic fault indicator is introduced for each spring i , which compares the threshold value with the error value computed as the moving average of the errors for each spring i . The moving average is computed over a sliding window of width τ_0 time steps, equal to that used for the definition of the automatic threshold:

$$Id_{E,i}^{\tau-\tau_0+1,\tau} = \begin{cases} 1 & \text{if } \mu_{E_i^{\tau-\tau_0+1,\tau}} < ATE_i^1 \vee \mu_{E_i^{\tau-\tau_0+1,\tau}} > ATE_i^{99} \\ 0 & \text{otherwise} \end{cases} \quad (21)$$

1
2
3
4
5
6
7
8
9
10
11
12
13
14
15
16
17
18
19
20
21
22
23
24
25
26
27
28
29
30
31
32
33
34
35
36
37
38
39
40
41
42
43
44
45
46
47
48
49
50
51
52
53
54
55
56
57
58
59
60
61
62
63
64
65

369 where $\mu_{E_i^{\tau-\tau_0+1,\tau}}$ indicates the moving average of the errors for each spring i computed over the
370 sliding window $[\tau - \tau_0 + 1, \tau]$. Thus, when the error value E_i^τ at time step τ , for spring i , exits
371 the healthy region defined by the thresholds ATE_i^1 and ATE_i^{99} , the fault indicator value is set to
372 1, indicating a possible damage is occurring in spring i . By so doing, alarms should be triggered
373 only in presence of persistent variations of the signal $\mu_{E_i^{\tau-\tau_0+1,\tau}}$, as those induced by damages,
374 filtering out random fluctuations due to noises and disturbances. Indeed, the choice of the width
375 of the window of the moving average-based filter is again another of those long-standing diagnostic
376 problems: here, in order to reduce the number of parameters to be tuned and to make the algorithm
377 as automatic as possible, the width of the window is taken equal to that used for the definition of
378 the error thresholds, i.e., τ_0 . Besides the convenience associated to the reduction of the tunable
379 algorithm parameters, the choice also intuitively makes sense, in that the use of different widths
380 for the definition of the automatic thresholds and for its operative use might, perhaps, introduce
381 biases caused by different samples size considered in each window, thus leading to a less robust
382 monitoring performance. Note that, due to the well-known properties of a moving average, the
383 wider the window is, the more robust the algorithm is with respect to false alarms due to spurious
384 fluctuations of the error, at the price though of being slower in detecting anomalies. On the other
385 hand, the narrower the window is, the faster the algorithm is, at the price of a potentially high
386 false alarm rate.

387 Following the same procedure described above, a binary, deterministic fault indicator for each
388 spring i is defined also with respect to the squared error:

$$Id_{SE,i}^{\tau-\tau_0+1,\tau} = \begin{cases} 1 & \text{if } \mu_{SE_i^{\tau-\tau_0+1,\tau}} > ATSE_i^{99} \\ 0 & \text{otherwise} \end{cases} \quad (22)$$

389 The introduction of the moving average-based filter renders the algorithm less sensitive to
390 random fluctuations. However, as it will be shown in Section 3, false alarms might still be present
391 and even missed alarms, if the algorithm is too slow and no detection is achieved within a reasonable
392 time horizon, before the damage evolves to catastrophic levels. Thus, an alternative indicator based
393 on a different perspective is here proposed to further support any decision making process based
394 on this algorithm. In particular, in order to be able to account for the uncertainties arising from
395 the employment of the deterministic indicators, two probabilistic fault indicators are introduced:

$$Ip_{E,i}^{\tau-\tau_0+1,\tau} = \frac{\sum_{j=\tau-\tau_0+1}^{\tau} Id_{E,i}^j}{\tau_0} \quad (23)$$

$$Ip_{SE,i}^{\tau-\tau_0+1,\tau} = \frac{\sum_{j=\tau-\tau_0+1}^{\tau} Id_{SE,i}^j}{\tau_0} \quad (24)$$

1
2
3
4
5
6
7
8
9
10
11
12
13
14
15
16
17
18
19
20
21
22
23
24
25
26
27
28
29
30
31
32
33
34
35
36
37
38
39
40
41
42
43
44
45
46
47
48
49
50
51
52
53
54
55
56
57
58
59
60
61
62
63
64
65

396 where the fault indicators $Id_{E,i}^\tau$ and $Id_{SE,i}^\tau$ are the instantaneous counterparts of the previously
397 introduced $Id_{E,i}^{\tau-\tau_0+1,\tau}$ and $Id_{SE,i}^{\tau-\tau_0+1,\tau}$, evaluated at time step τ :

$$Id_{E,i}^\tau = \begin{cases} 1 & \text{if } E_i^\tau < ATE_i^1 \vee E_i^\tau > ATE_i^{99} \\ 0 & \text{otherwise} \end{cases} \quad (25)$$

$$Id_{SE,i}^\tau = \begin{cases} 1 & \text{if } SE_i^\tau > ATSE_i^{99} \\ 0 & \text{otherwise} \end{cases} \quad (26)$$

399 At a first sight, the definition of the indicators $Ip_{E,i}^{\tau-\tau_0+1,\tau}$ and $Ip_{SE,i}^{\tau-\tau_0+1,\tau}$ apparently just shifts
400 the application of the moving average from the instantaneous errors $E_i^{1:\tau_0}$ and $SE_i^{1:\tau_0}$ to the de-
401 terministic instantaneous indicators $Id_{E,i}^\tau$ and $Id_{SE,i}^\tau$, respectively. However, this simple operation
402 allows a probabilistic interpretation of the results, which, as it shall be shown in the next Section,
403 enriches the information conveyed by the diagnostic module, since it accounts for the uncertainties
404 involved in the estimation process.

405 3 Case Study

406 The structure considered in this case study is modelled on the basis of the MDOF system shown
407 in Figure 1, considering six degrees of freedom. The structural parameter values characterizing
408 the 6-DOF model are taken from the work in [39], i.e., $m_i = 1kg \forall i = 1, \dots, n$, $k_j = 10^4 \frac{N}{m}$ and
409 $c_j = 20 \frac{N \cdot s}{m}$ (i.e., $\beta = 2 \cdot 10^{-3}$) $\forall j = 1, \dots, n + 1$. The process noises are described by normal
410 distributions with zero mean and variances $\sigma_{w,position}^2 = 10^{-16}m^2$, $\sigma_{w,speed}^2 = 10^{-16} \frac{m^2}{s^2}$, $\sigma_{w,spring}^2 =$
411 $20 \frac{N^2}{m^2}$ and $\sigma_{w,damping}^2 = 8 \cdot 10^{-13}$ for position, velocity, stiffness and damping proportionality constant
412 states, respectively, whereas the acceleration measurement noise variance is taken $\sigma_v^2 = 20 \frac{m^2}{s^4}$. Note
413 that the variance of the process noise related to the damping proportionality constant is set so that
414 the same standard deviation to nominal value ratio is achieved for damping and stiffness values.

415 First, the performances of the PF algorithm will be analyzed for the case the 6-DOF system
416 is not affected by damages and it operates with all the elements at a constant temperature. The
417 reference state evolution x_{ref}^τ is syntetically generated according to equations 3 and 4, using the
418 stiffness values of the healthy baseline (i.e., $k_j = 10^4 \frac{N}{m} \forall j = 1, \dots, n + 1$) and the related damping
419 values obtained through the proportionality constant β . The synthetic acceleration measurements
420 a_i^τ of each mass m_i are then calculated on the basis of the reference state evolution x_{ref}^τ by using
421 equation 9. Then, damages will be artificially introduced and, at the same time, the temperature
422 will be varied in time. A new reference state evolution x_{ref}^τ will be generated and, accordingly, a
423 new set of synthetic acceleration measurements will be computed.

3.1 Undamaged structure with constant temperature

The structural elements are assumed to be in equilibrium with the external temperature, constant and equal to $T = 0^\circ C$. The time horizon of the analysis is $T_{hor} = 8s$, discretized in $N_t = 1.2 \cdot 10^4$ time intervals of width $dt = 0.667ms$ each. The 6-DOF system is excited by an external sinusoidal load $F_1 = 40 \sin(25 \cdot 2\pi t) N$ applied to mass m_1 . Note that applying external forces for monitoring the health state of structures is typical in the SHM field. For instance, bridges may be excited by means of servo-hydraulic vibration generators [60] or electrodynamic shakers [61], to cite some, which are tools that can excite structures with prescribed force patterns, such as sinusoidal forces or random vibrations. The sampling frequency is $f_s = 1/dt = 1500Hz$, which turns out to be sufficiently larger than the forcing function frequency $f_{force} = 25Hz$, thus satisfying the Shannon sampling theorem. The particles values are initialized as follows:

- the position and velocity states estimates are initialized according to a normal distribution with zero mean and variance $\sigma_{w,position}^2 = 10^{-16}m^2$ and $\sigma_{w,speed}^2 = 10^{-16}\frac{m^2}{s^2}$, respectively;
- the stiffnesses and damping coefficient values are initialized to a random number between the 90% and the 110% of the actual state value to be estimated.

The objective of this first case study is that of testing the behavior of the PF in estimating the model stiffnesses. It is worth reminding that the state estimator proposed here is the mean of the posterior pdf of equation 11. To this aim, a particle filter with 10^4 particles is used for estimating the whole state vector \mathbf{x}^τ at each time step τ , according to the procedure outlined in Section 2.1. Figure 3 shows the state estimates (coloured lines) for only the spring stiffnesses k_2 , k_4 , k_6 and k_7 , i.e., the mean value of the respective marginal state posterior pdf. The estimates of the other stiffnesses (k_1 , k_3 and k_5) show very similar behaviors, so they are not shown here for brevity's sake. It can be seen that all the stiffnesses are satisfactorily estimated, after a fast transient needed to pass from the initial value to the actual one. It is however important to further delve into the performance of the PF, since the estimated stiffnesses will then be fed to the autoencoders, so that any estimation error will propagate and affect the diagnostic module outputs.

Thus, in order to quantify the quality of the stiffness estimates, the root mean square error (RMSE) is calculated over T_{hor} for all the stiffness estimates. The results are compared in Table 1, column 2. Spring 1 is the one characterized by the maximum RMSE value, followed by springs 6 and 7. No increasing trend seems to characterize the RMSE as the springs move away from the point of application of the excitation. In order to improve the statistics of the estimates, a new simulation with $3 \cdot 10^4$ particles is then run. Figure 4 shows the PF-based estimates, which, on a first visual inspection, seems to be better than before, as confirmed by the RMSEs reported in Table 1, column 3. Moreover, the RMSE values obtained with $3 \cdot 10^4$ particles seem not to exhibit the same trend observed before among the different springs, with spring 1 still being the one characterized by the maximum RMSE, followed now by spring 2. Unfortunately, due to the non-linearity of the state space in equations 3 and 4, it is not an easy task to draw any conclusions on this analysis,

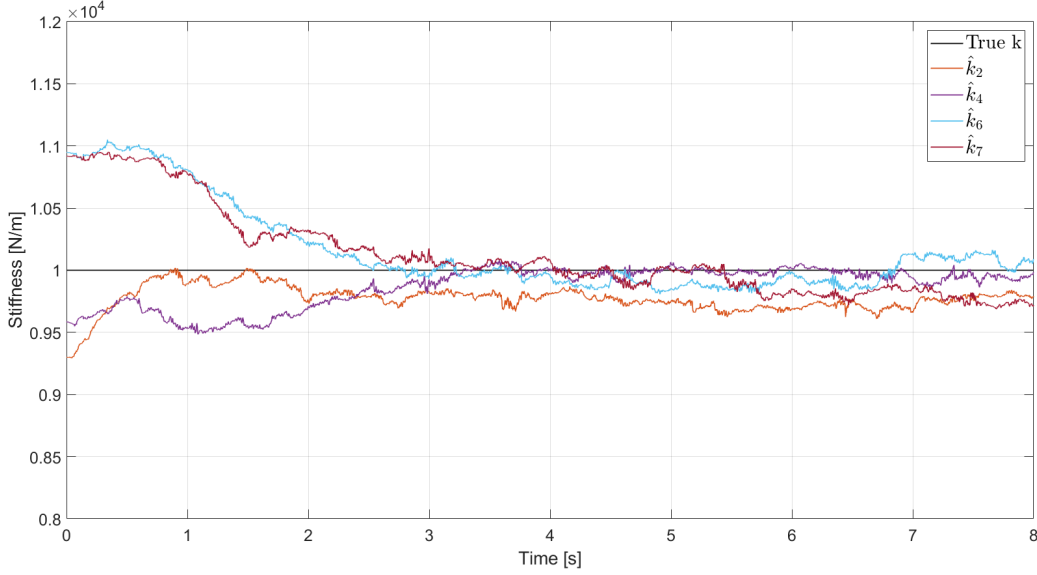


Figure 3: Temporal evolution of the particle filter stiffness estimates and reference stiffness values (black) of springs $i = 2$, $i = 4$, $i = 6$ and $i = 7$ - undamaged scenario with excitation force applied at mass m_1 and 10^4 particles.

Component	RMSE @ 10k particles $\left[\frac{N}{m}\right]$	RMSE @ 30k particles $\left[\frac{N}{m}\right]$
Spring 1	450.0	452.0
Spring 2	250.0	228.0
Spring 3	143.2	90.1
Spring 4	211.2	62.5
Spring 5	201.8	132.9
Spring 6	388.2	102.2
Spring 7	373.7	153.8

Table 1: PF estimates of k_2 , k_4 , k_6 and k_7 in the undamaged scenario, with excitation applied at mass m_1 .

which is also out of the scope of this work. In any case, it has been verified that an increase in the number of particles used in the PF improves the performances.

The simulations are performed using a laptop with 16GB RAM and six physical Intel Core i7-9750H CPUs. The mean time required by the PF for estimating the 8s time history with $3 \cdot 10^4$ particles is approximately four times the mean time required using 10^4 particles. The computational times are slightly higher than the expected linear increase with the number of particles. That is due to the fact that some background processes always run in the computer and that the code is not completely computationally efficient, since the main goal of this work is to test a new SHM algorithm.

For completeness, some simulations have been carried out where the position and also the

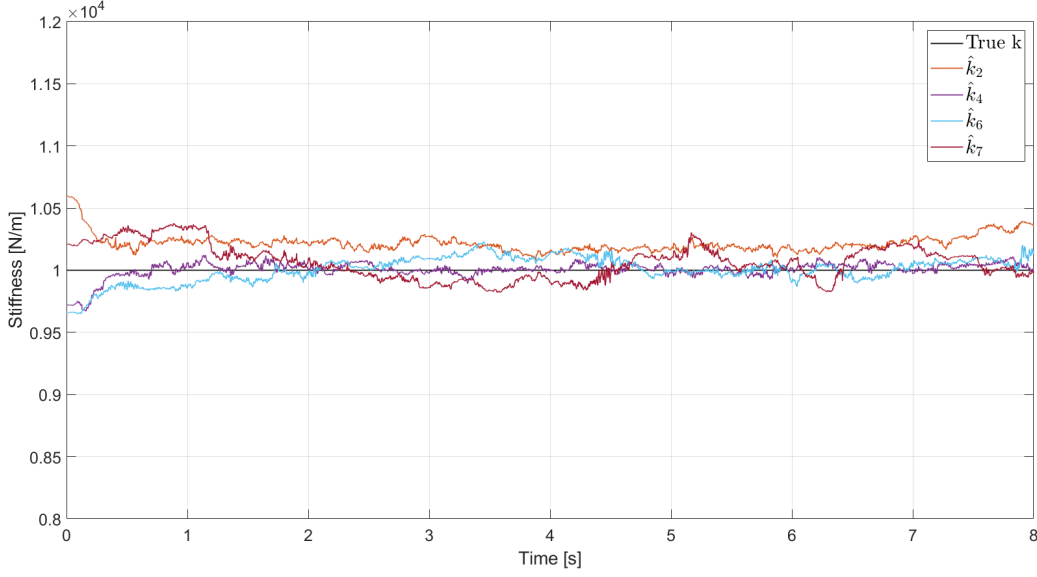


Figure 4: Temporal evolution of the particle filter stiffness estimates and reference stiffness values (black) of springs $i = 2$, $i = 4$, $i = 6$ and $i = 7$ - undamaged scenario with excitation force applied at mass m_1 and $3 \cdot 10^4$ particles.

number of exciting loads was varied, obtaining different behaviors, but it was not possible to identify any clear scheme, so they are not reported here for brevity's sake. In what follows, the algorithm will be always demonstrated with respect to the springs 2, 4, 6 and 7, keeping in mind that an increase in the number of particles can always reduce the fluctuations and, consequently, improve the results, provided enough computational resources are available.

3.2 Damaged structure with temperature variation in time

The same model of Section 3.1 is here considered. Before running the estimation simulation, the healthy baseline for the autoencoders training is acquired by simulating the system with no damages and by simultaneously running the PF for estimating the model stiffnesses over $N_t = 1.2 \cdot 10^4$ time steps of width $dt = 0.667ms$ each, corresponding to a baseline time horizon of $T_{hor}^{baseline} = 8s$, during which the temperatures of all the structural elements are assumed to be in equilibrium with an external temperature linearly varying from $-30^\circ C$ to $100^\circ C$ with step $0.1^\circ C$. The range of temperature variation has been chosen wide enough to guarantee the autoencoders are trained over an input space which almost surely contains examples of temperatures that will be encountered during operation. Indeed, this is possible only in artificially generated case studies, as in the present work, or in all those applications where a temperature-controlled environment can be created; in real applications this is not generally possible, and a long baseline should be acquired in order to ensure the temperature range is sufficiently represented.

Note that, for simplicity and with no loss of generality, all the springs are subjected to the

490 same temperature. As verified by the authors, but not reported here for the sake of brevity, the
491 algorithm can effectively cope with the effects of a spatial temperature gradient, i.e., temperatures
492 varying across the elements of the structure. In fact, the spring stiffness-temperature relationship
493 is independently “encoded” spring by spring, so that a spatially non-uniform temperature varia-
494 tion can only affect the dynamics of the system, which is fully captured by the PF, similarly to
495 considering different stiffness values amongst the degrees of freedom.

496 The baseline is then constructed by associating the temperature observations, either generated
497 at time step τ using $\hat{T}^\tau = T^\tau + w_T^\tau$, where w_T^τ is the temperature observation noise, which in the
498 present work is $w_T^\tau \sim N(0, 0.1)^\circ C$, or directly acquired in the field, to the PF-based estimates of the
499 model stiffnesses. A total of $N_t = 1.2 \cdot 10^4$ examples per spring are thus generated, which are used for
500 training seven autoencoders, each associated to a different spring of the model and characterized by
501 the architecture described in Section 2.2. The construction of the autoencoders and their training
502 have been performed resorting to the MATLAB Deep Learning ToolboxTM. Once the autoencoders
503 are properly trained, it is possible to put them on-line according to the scheme illustrated in Section
504 2.2. In order to test the diagnostic module over a time span larger than in the undamaged case,
505 the time horizon of the analysis is now extended to $T_{hor} = 40s$, discretized into $N_t = 6 \cdot 10^4$
506 time steps of $0.667ms$ each. By so doing, we let the algorithm settle after damages are artificially
507 introduced in the system. Again, the structural elements are assumed to be in equilibrium with
508 the external temperature, which is let decrease linearly from $40^\circ C$ to $10^\circ C$ within the time horizon
509 T_{hor} . Two different damages are assumed that can occur in the structure, i.e., a sudden drop in
510 the structural stiffness value of a spring and a progressive degradation. We consider the cases of
511 (i) a sudden damage consisting of a 10% reduction of the stiffness value associated to spring 7 (the
512 most critical one), occurring at time $t = 10.0s$, and (ii) a progressive, linear decrease of the stiffness
513 value associated to spring 4, occurring at time $t = 13.3s$ and leading to a final stiffness value (at
514 T_{hor}) equal to the 43% of the corresponding healthy one at the same temperature, i.e., at $10^\circ C$.
515 Those damage values are typical in the SHM field and are different enough to allow testing the
516 proposed methodology both with minor stiffness degradations, i.e., 10%, and with more significant
517 ones, i.e., the 57% stiffness reduction modelled on spring 4 [62, 63].

518 The system dynamics is simulated, according to the equations presented in Section 2.1, starting
519 from the following initial state vector values:

$$x_i^0 = 0 \text{ m} \quad \forall i = 1, \dots, n \quad (27a)$$

$$y_i^0 = 0 \frac{\text{m}}{\text{s}} \quad \forall i = 1, \dots, n \quad (27b)$$

$$k_j^0 = 9440 \frac{\text{N}}{\text{m}} \quad \forall j = 1, \dots, n + 1 \quad (27c)$$

$$\beta^0 = 2 \cdot 10^{-3} \quad (27d)$$

523 where k_j^0 represents the j -th spring stiffness at the initial temperature $T^0 = 40^\circ C$. A PF with

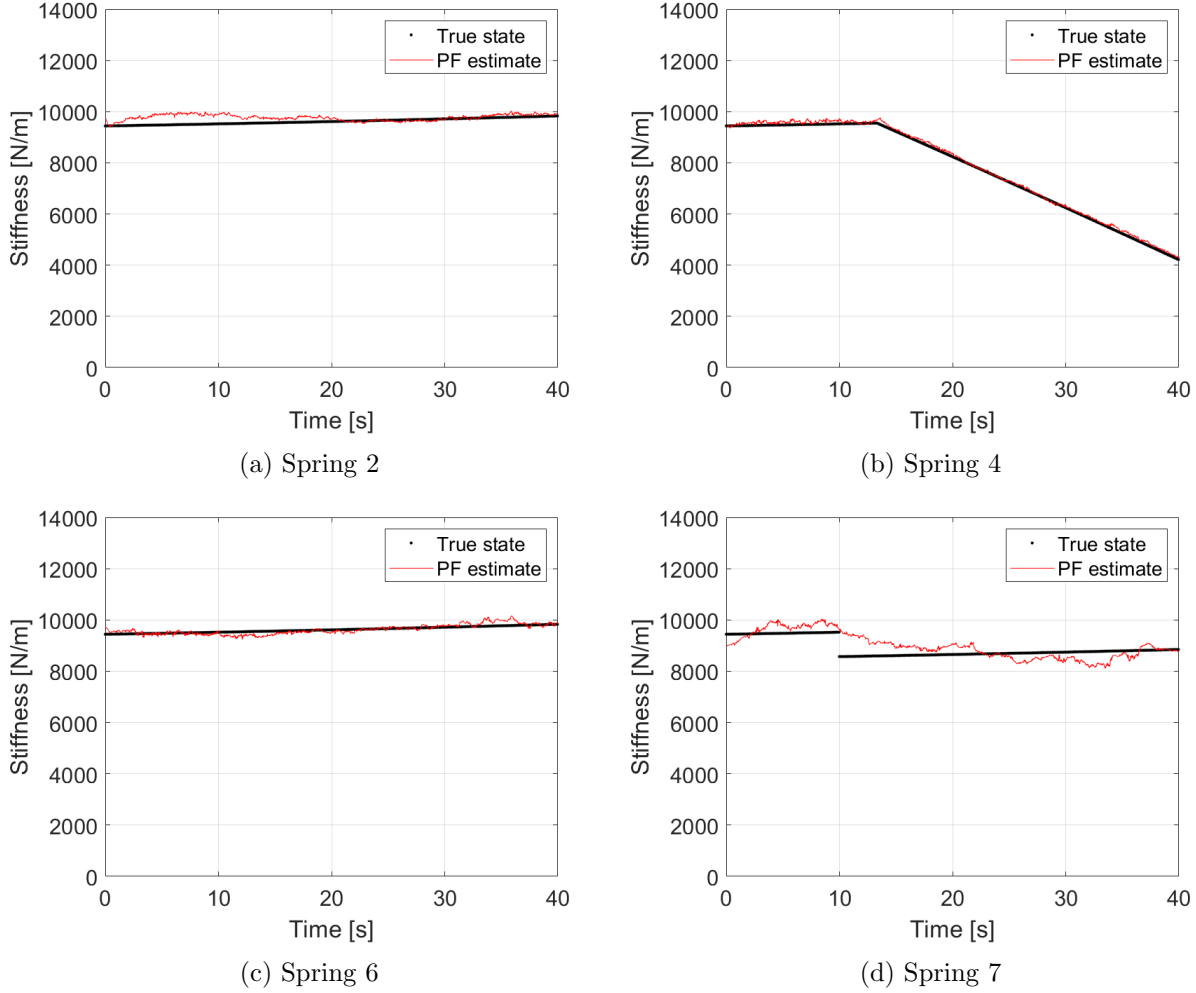


Figure 5: Temporal evolution of the particle filter stiffness estimates (red) and true stiffness values (black) of spring $i = 2$ (a), $i = 4$ (b), $i = 6$ (c) and $i = 7$ (d).

$3 \cdot 10^4$ particles is used for estimating the whole state vector \mathbf{x}^τ at each time step τ , according to the procedure outlined in Section 2.1. Figure 5 shows the state estimates (red lines) and the corresponding reference values (black) of the spring stiffnesses $k = 2$ (a), $k = 4$ (b), $k = 6$ (c) and $k = 7$ (d). As expected, the PF performances appear to be satisfactory, even in presence of the damages, with quite fast settling times. Indeed, while sudden changes might probably be detected just by processing the PF estimates, the slower, progressive damages may not easily be distinguished from the temperature effects. That is the case of slow progressive degradations, with characteristic time close to the one driving the stiffness change due to temperature effects. However, that is not the case of the present study, in which the progressive degradation damage is clearly visible just by looking at the PF estimate (Figure 5b).

The PF-estimated stiffness values and the temperature measurements, corrupted with noise according to the same procedure aimed at building the healthy baseline illustrated in this Section,

1
2
3
4
5
6
7
8
9
10
11
12
13
14
15
16
17
18
19
20
21
22
23
24
25
26
27
28
29
30
31
32
33
34
35
36
37
38
39
40
41
42
43
44
45
46
47
48
49
50
51
52
53
54
55
56
57
58
59
60
61
62
63
64
65

are then fed, in real time at each time step τ , to the seven autoencoders. Figure 6 shows the time evolution of the error E_i^τ between the input and output values of the autoencoder (solid lines), calculated according to equation 16, its average over the time window of width τ_0 time steps, i.e., $\mu_{E_i^{\tau-\tau_0+1,\tau}}$ (black, dashed lines), and the corresponding automatic thresholds ATE_i^1 and ATE_i^{99} (red, dashed and dotted lines), for the stiffnesses k_2 , k_4 , k_6 and k_7 . The first τ_0 time steps of the analysis are used to automatically set the error thresholds for each stiffness in the system, implicitly assuming the system is in its healthy state at early times. Accordingly, the thresholds are reported in the Figure only after the healthy baseline processing is completed. At the same time, Figure 7 is built following the same procedure, but using the squared error SE_i^τ between the input and output values of the autoencoder (see equation 15), its average over the time window of width τ_0 time steps, i.e., $\mu_{SE_i^{\tau-\tau_0+1,\tau}}$, and the associated automatic threshold $ATSE_i^{99}$, for the stiffnesses k_2 , k_4 , k_6 and k_7 . Note that different scales have been used for each sub-Figure due to the fact that, at the end of the simulation, the error E_4^τ and squared error SE_4^τ related to spring number 4 are much greater than those associated to k_2 , k_6 and k_7 . The corresponding deterministic fault indicators $Id_{E,i}^{\tau-\tau_0+1,\tau}$ and $Id_{SE,i}^{\tau-\tau_0+1,\tau}$ are shown in Figures 8 and 9, respectively, whereas their probabilistic counterparts $Ip_{E,i}^{\tau-\tau_0+1,\tau}$ and $Ip_{SE,i}^{\tau-\tau_0+1,\tau}$ are shown in Figures 10a and 10b, respectively, for the stiffnesses k_2 , k_4 , k_6 and k_7 . Although no damages are introduced on spring $i = 2$, the mean error associated to stiffness k_2 (Figure 6a) exits the healthy region in a brief time window centred at $t = 30s$, re-entering it by the end of the simulation. Differently, the mean squared error associated to stiffness k_2 never exceeds the automatic threshold $ATSE_2^{99}$ (Figure 7a). Accordingly, the deterministic damage indicator $Id_{E,2}^{\tau-\tau_0+1,\tau}$ is triggered at time $t = 26.1s$ and deactivated after 8.6s (Figure 8a), while $Id_{SE,2}^{\tau-\tau_0+1,\tau}$ is always equal to zero (Figure 9a), not triggering any diagnostic alarm. The probabilistic indicator, or probability of damage occurrence, $Ip_{E,2}^{\tau-\tau_0+1,\tau}$ reaches a peak value of 85% within the mission time, while $Ip_{SE,2}^{\tau-\tau_0+1,\tau}$ always remains null. Instead, both the mean error and the mean squared error associated to stiffness k_4 exceed the automatic thresholds $\{ATE_4^1, ATE_4^{99}\}$ and $ATSE_4^{99}$ (Figures 6b and 7b, respectively). That is coherent with the fact that a progressive degradation damage is introduced in that spring starting from time $t = 13.3s$. In particular, the error mean value $\mu_{E_4^{\tau-\tau_0+1,\tau}}$ exceeds the one of the related threshold with a time delay from the time instant in which the damage is introduced evaluated in $T_{4,E} = 3.0s$. Similarly, the squared error mean value $\mu_{SE_4^{\tau-\tau_0+1,\tau}}$ exceeds the one of the related threshold with a time delay evaluated in $T_{4,SE} = 3.0s$. Accordingly, the deterministic damage indicators $Id_{E,4}^{\tau-\tau_0+1,\tau}$ and $Id_{SE,4}^{\tau-\tau_0+1,\tau}$ (Figures 8b and 9b, respectively) are raised at the time the related mean error and mean squared error values exit the healthy region. The probabilistic indicators $Ip_{E,4}^{\tau-\tau_0+1,\tau}$ and $Ip_{SE,4}^{\tau-\tau_0+1,\tau}$ clearly identify the damage on spring $i = 4$, reaching, after a brief transient phase, the unit value, which is kept constant until the end of the analysis. Coherently with the fact that no damages are introduced on spring $i = 6$, the mean squared error associated to stiffness k_6 (Figure 7c) never exceeds the automatic threshold $ATSE_6^{99}$. However, the same consideration is not true for the mean error value. In fact, according to Figure 6c, the $\mu_{E_6^{\tau-\tau_0+1,\tau}}$ value exits the healthy region at time $t = 14.0s$, re-entering it after 4.6s. That behaviour is reflected on the deterministic fault indicators. In fact, while the

575 indicator $Id_{SE,6}^{\tau-\tau_0+1,\tau}$ (Figure 9c) is always equal to zero, not triggering any diagnostic alarm, the
 576 one related to the non-squared error (Figure 8c) is raised at time $t = 14.0s$, and is turned off at time
 577 $t = 18.6s$. Accordingly, also the probabilistic indicators $Ip_{E,6}^{\tau-\tau_0+1,\tau}$ and $Ip_{SE,6}^{\tau-\tau_0+1,\tau}$ have a slightly
 578 different behaviour. In fact, the squared error based probability of damage occurrence outperforms
 579 the error based one, determining a maximum value $max(Ip_{SE,6}^{\tau-\tau_0+1,\tau}) = 6\%$, while according to
 580 $Ip_{E,6}^{\tau-\tau_0+1,\tau}$ a maximum damage probability of 71% is estimated. Finally, both the mean error
 581 and the mean squared error associated to stiffness k_7 exceed the respective automatic thresholds
 582 (Figures 6d and 7d, respectively). That is coherent with the fact that a step damage is introduced
 583 in that spring starting from time $t = 10s$. In particular, the error mean value $\mu_{E_7}^{\tau-\tau_0+1,\tau}$ exceeds
 584 the one of the related threshold with a time delay from the time instant in which the damage is
 585 introduced evaluated in $T_{7,E} = 7.2s$. Similarly, the squared error mean value $\mu_{SE_7}^{\tau-\tau_0+1,\tau}$ exceeds
 586 the one of the related threshold with a time delay evaluated in $T_{7,SE} = 7.3s$. Accordingly, the
 587 deterministic damage indicators $Id_{E,7}^{\tau-\tau_0+1,\tau}$ and $Id_{SE,7}^{\tau-\tau_0+1,\tau}$ (Figures 8d and 9d, respectively) are
 588 raised at the time the related mean error and mean squared error values exit the healthy region.
 589 The probabilistic indicators $Ip_{E,7}^{\tau-\tau_0+1,\tau}$ and $Ip_{SE,7}^{\tau-\tau_0+1,\tau}$ clearly identify the damage on spring $i = 7$,
 590 reaching, after a brief transient phase, the unit value, which is kept constant until the end of the
 591 analysis. All the results presented above are summarized in table 2.

Damage indicator	Performace
$Id_{E,2}$	X - Short false alarm
$Id_{E,4}$	✓ - Damage identified
$Id_{E,6}$	X - Short false alarm
$Id_{E,7}$	✓ - Damage identified
$Id_{SE,2}$	✓ - Correctly classified as healthy
$Id_{SE,4}$	✓ - Damage identified
$Id_{SE,6}$	✓ - Correctly classified as healthy
$Id_{SE,7}$	✓ - Damage identified
$Ip_{E,2}$	X - False damage probability > 50%
$Ip_{E,4}$	✓ - Damage identified
$Ip_{E,6}$	X - False damage probability > 50%
$Ip_{E,7}$	✓ - Damage identified
$Ip_{SE,2}$	✓ - Damage identified
$Ip_{SE,4}$	✓ - Correctly classified as healthy
$Ip_{SE,6}$	✓ - Correctly classified as healthy
$Ip_{SE,7}$	✓ - Damage identified

Table 2: Summary table of the damage indicators for springs 2, 4, 6 and 7.

4 Discussion

The model-based framework presented in this work offers the advantage that, in real applications, most algorithm parameters can be set up by trial-and-error procedures during a preliminary, purely numerical phase, where the dynamic behavior of the system and the associated acceleration measurements are synthetically generated using the process and the measurement equations. The calibrated parameters are probably not “optimal” for the real application, due to the model errors, but would certainly guarantee satisfactory performances of the algorithm. For instance, the performance of the whole framework significantly depends on the performance of the PF, which, in turn, is quite sensitive to both the measurement and the process noise. While the measurement noise is related to the precision of the sensors (although there might also be some calibration margin), the process noise is well-known to be mainly a filter calibration factor, not easily identifiable a-priori. The suggestion is then to calibrate the process noise by means of a trial-and-error approach, also according to common practice in the literature [64, 65]. Another example is represented by the detection thresholds, which are set according to specific percentiles of the pdfs of the squared error and the error defined by equations 15 and 16, respectively, the calibration of which is again suggested via a trial-and-error procedure, with the ultimate goal of establishing a trade-off between false alarms rate and raising time for damage alarms. The usual percentiles considered in statistics may be adopted, e.g., 95th, 99th and 99.9th percentile. The greater the percentile, the smaller the false alarms rate, albeit at the price of an increase in the raising time for damage detection. As far as the autoencoders are concerned, the healthy baseline acquisition should be performed over a temperature range sufficiently wide to cover most of the temperatures the structure will experience during its operational life. Since this may be a lengthy process, it is suggested to start acquiring the baseline right after the structure installation, i.e., when the structure is reasonably still healthy, start using the diagnostic tool and keep re-training the autoencoders as new temperature ranges are experienced. Another possible strategy may be that of numerically generating the missing examples of the relationship between temperature and stiffness by using some sufficiently accurate material model, which would provide a hybrid experimental-numeric baseline for training the autoencoders. This procedure has the advantage of potentially covering any temperature range, at the risk of introducing modelling errors that would certainly affect the diagnostic performances.

5 Conclusions

This study proposes a novel combination of particle filter and neural network-based autoencoder to identify the structural parameters of mechanical and/or civil structures modelled as mono-dimensional MDOF systems, and to perform damage diagnosis (both detection and localization) in presence of changing environmental conditions. The case study reported in Section 3 demonstrates that the developed framework is capable of providing a real-time temporal estimation of the stiffness of each spring in the MDOF system, by means of accelerations measurements only, and of assessing the health status of the structure under analysis, successfully detecting and localizing eventual

1
2
3
4
5 630 damages.

6
7 631 The particle filter stiffness estimation process is able to detect any change in the stiffness value
8 632 of the components of the system, however it cannot provide by itself any information about the
9 633 cause of that variation. In fact, structural properties may vary both in case of damage and in
10 634 presence of changing external conditions. Note that, in this study, only temperature is considered
11 635 amongst the external conditions capable of changing the stiffness properties in the healthy condi-
12 636 tion of the system. Thus, a properly trained auto-associative neural network has to be coupled
13
14 637 with the PF in order to offset the effects of temperature variations on structural dynamics. A
15 638 healthy baseline covering the whole range of operating conditions is first acquired with the purpose
16 639 of performing the learning phase of the autoencoder. In the operational phase, the mean values
17 640 of the error and of the squared error between input and output variables of the neural networks,
18 641 determined over a moving time window which considers the last τ_0 time steps before the actual
19 642 one, are compared to the respective automatic thresholds, thus eventually triggering the related
20 643 automatic fault indicator, $Id_{E,i}^{\tau-\tau_0+1,\tau}$ and $Id_{SE,i}^{\tau-\tau_0+1,\tau}$, respectively, for the detection and localization
21 644 of structural damages. However, occasional false alarms are also triggered due to oscillations in the
22 645 particle filter estimates, hence a probabilistic, more robust fault indicator is introduced with the
23 646 purpose of mitigating this problem, i.e., $Ip_{E,i}^{\tau-\tau_0+1,\tau}$ and $Ip_{SE,i}^{\tau-\tau_0+1,\tau}$, respectively for the error and
24 647 the squared error between the input and the output of the autoencoder. The probabilistic fault
25 648 indicators provide satisfactory results in terms of detection and localization of structural damages,
26 649 however their robustness should be further investigated testing more complex systems. Moreover,
27 650 the failure probability of undamaged springs may be further decreased by better estimating the
28 651 structural characteristics, thus damping out the eventual oscillations of the particle filter estimates.
29 652 Indeed, as discussed in Section 3.1, increasing the number of particles may be beneficial to that
30 653 purpose. However, since the computational time required is more than proportional to the num-
31 654 ber of particles considered in the analysis, this strategy may severely compromise the algorithm
32 655 real-time capabilities. Overall, the squared error-based deterministic fault indicator outperforms
33 656 the error-based one, in that the former does not present any false alarm, while the latter may
34 657 erroneously identify damage in healthy springs, as already discussed in Section 3.2. The same
35 658 consideration also holds for the probabilistic indicators, with the squared error-based one providing
36 659 lower damage probability of the healthy springs with respect to the error-based one. Moreover,
37 660 the fault indicators relying on the error value and the ones relying on the squared error value raise
38 661 alarms with comparable time delays from the actual damage instants.

39
40
41
42
43
44
45
46
47
48
49
50
51
52 662 The proposed method is believed to be ready to be employed to real structures, provided that
53 663 some key points are considered: (i) the autoencoders database may be built by installing sensors
54 664 on the structure, acquiring the baseline in its early life, confidently assuming that the structure is
55 665 healthy right after being installed or built; (ii) the baseline acquisition process should be long enough
56 666 to capture the whole expected temperature variability during the operational life of the monitored
57 667 structure, in order to allow the autoencoders working in the learnt space during the diagnostic

1
2
3
4
5 668 phase; (iii) the temperatures may be acquired using at least one sensor per degree of freedom, to
6 669 consider temperature variability in time and space and (iv) at least one accelerometer per DOF
7 670 should be installed on the structure. However, more sensors may be installed on the structure
8
9 671 both for redundancy and for collecting more information about the single DOF, which may not be
10 672 a concentrated entity in the real world, in order to determine the corresponding acceleration and
11
12 673 temperature values.

13
14 674 Not all the open issues have been properly addressed. Further work is required to test the ro-
15 675 bustness of the damage detection and localization procedure with respect to different environmen-
16 676 tal/operating conditions (other than temperature). For instance, in case of structures significantly
17
18 677 affected by traffic and/or wind loads, a typical SHM problem in large infrastructures, these could
19 678 be considered as different/additional forcing terms, as they do not directly influence the stiffness
20
21 679 properties of the structure. In this regard, performing the diagnostic task only on the basis of
22 680 vibration signals induced by environmental/operative loads (wind, traffic, etc.) would be more
23
24 681 practical in realistic scenarios, yet more challenging, mainly due to the random nature of this kind
25 682 of excitations. Finally, the effectiveness of the proposed methodology with non-linear behaviours
26
27 683 and non-Gaussian noise could be also investigated, with the aim of increasing its generality.

30 684 **References**

- 31
32 685 [1] Dan M. Frangopol and Min Liu. Maintenance and management of civil infrastructure based on
33 686 condition, safety, optimization, and life-cycle cost. *Structure and Infrastructure Engineering*,
34 687 3(1):29–41, 2007.
- 35
36
37 688 [2] Lisa Ziegler, Elena Gonzalez, Tim Rubert, Ursula Smolka, and Julio J. Melero. Lifetime
38 689 extension of onshore wind turbines: A review covering germany, spain, denmark, and the uk.
39 690 *Renewable and Sustainable Energy Reviews*, 82:1261 – 1271, 2018.
- 40
41
42 691 [3] J. Courrech and M. Gaudet. Envelope analysis - the key to rolling-element
43 692 bearing diagnosis. *Bruel & Kjaer internal document*. available online at
44 693 <https://www.bksv.com/media/doc/BO0187.pdf>.
- 45
46
47 694 [4] U. Dackermann, W. A. Smith, R. B. Randall. Damage identification based on response-
48 695 only measurements using cepstrum analysis and artificial neural networks. *Structural Health*
49 696 *Monitoring*, 13(4):430–444, 2014.
- 50
51
52 697 [5] Chris Mechefske. Machine condition monitoring and fault diagnostics. In Clarence W. de Silva,
53 698 editor, *Vibration and Shock Handbook*, chapter 25. CRC Press, Taylor and Francis Group, Boca
54 699 Raton, FL, 2005.
- 55
56
57 700 [6] Timothy J. Johnson and Douglas E. Adams. Transmissibility as a differential indicator of
58 701 structural damage. *Journal of Vibration and Acoustics*, 124, 10 2002.

1
2
3
4
5
6
7
8
9
10
11
12
13
14
15
16
17
18
19
20
21
22
23
24
25
26
27
28
29
30
31
32
33
34
35
36
37
38
39
40
41
42
43
44
45
46
47
48
49
50
51
52
53
54
55
56
57
58
59
60
61
62
63
64
65

[7] Nuno M.M. Maia, Raquel A.B. Almeida, Antonio P.V. Urgueira, and Rui P.C. Sampaio. Damage detection and quantification using transmissibility. *Mechanical Systems and Signal Processing*, 25(7):2475–2483, 2011.

[8] G. Manson and K. Worden. Experimental validation of a structural health monitoring methodology: Part iii. damage location on an aircraft wing. *Journal of Sound and Vibration*, 259(2):365–385, 2003.

[9] M.J. Schulz, A.S. Abdelnaser, P.F. Pai, M.S. Linville and J. Chung. Detecting structural damage using transmittance functions. In *International Modal Analysis Conference, Orlando, Florida*, pages 638–644, 1997.

[10] M.J. Schulz, P.F. Pai and D.J. Inman. Health monitoring and active control of composite structures using piezoceramic patches. *Compos.: Part B*, 30(7):713–725, 1999.

[11] H. Zhang, M.J. Schulz, F. Ferguson and P.F. Pai. Structural health monitoring using transmittance functions. *Mech. Syst. Signal Process.*, 13(5):765–787, 1999.

[12] A. Ghoshal, M.J. Sundaresan, M.J. Schulz and P.F. Pai. Structural health monitoring techniques for wind turbine blades. *J. Wind Eng. Ind. Aerodyn.*, 85(3):309–324, 2000.

[13] V. Caccese. Detection of bolt load loss in hybrid composite/metal bolted connections. *Eng. Struct.*, 26(7):895–906, 2004.

[14] Simon Chesne and Arnaud Deraemaeker. Damage localization using transmissibility functions: A critical review. *Mechanical Systems and Signal Processing*, 38(2):569 – 584, 2013.

[15] Z.K. Peng and F.L. Chu. Application of the wavelet transform in machine condition monitoring and fault diagnostics: a review with bibliography. *Mechanical Systems and Signal Processing*, 18(2):199 – 221, 2004.

[16] H. Sohn. Effects of environmental and operational variability on structural health monitoring. *Philos. Trans. R. Soc. London A Math. Phys. Eng. Sci.*, 365(1851):539–560, 2007.

[17] C.R. Farrar, W.E. Baker, T.M. Bell, K.M. Cone, T.W. Darling, T.A. Duffey, A. Eklund, and A. Migliori. Dynamic characterization and damage detection in the i-40 bridge over the rio grande. *Technical Report*, 6 1994.

[18] M.P. Limongelli. Frequency response function interpolation for damage detection under changing environment. *Mechanical Systems and Signal Processing*, 24(8):2898 – 2913, 2010.

[19] Charles Farrar, S. W. Doebling, Phillip Cornwell, and Erik Straser. Variability of modal parameters measured on the alamosa canyon bridge. *Proceedings of International Modal Analysis Conference*, 1, 01 1997.

1
2
3
4
5
6
7
8
9
10
11
12
13
14
15
16
17
18
19
20
21
22
23
24
25
26
27
28
29
30
31
32
33
34
35
36
37
38
39
40
41
42
43
44
45
46
47
48
49
50
51
52
53
54
55
56
57
58
59
60
61
62
63
64
65

734 [20] B. Peeters and G. De Roeck. One-year monitoring of the z24-bridge: environmental effects
735 versus damage events. *Earthq. Eng. Struct. Dyn.*, 30(2):149–171, 2001.

736 [21] K. Worden, H. Sohn, and C. R. Farrar. Novelty detection in a changing environment: regression
737 and interpolation approaches. *J. Sound Vib.*, 258(4):741–761, 2002.

738 [22] C. P. Fritzen, G. Mengelkamp, and A. Guemes. Elimination of temperature effects on damage
739 detection within a smart structure concept. *Struct. Heal. Monit.*, 10:15–17, 2003.

740 [23] K. Worden and E. J. Cross. On switching response surface models, with applications to the
741 structural health monitoring of bridges. *Mech. Syst. Signal Process.*, 98:139–156, 2018.

742 [24] R. Ruotolo and C. Surace. Damage detection using singular value decomposition. *DAMAS*
743 *97*, 1997.

744 [25] A. M. Yan, G. Kerschen, P. De Boe, and J. C. Golinval. Structural damage diagnosis under
745 varying environmental conditions - part ii: Local pca for non-linear cases. *Mech. Syst. Signal*
746 *Process.*, 19(4):865–880, 2005.

747 [26] J. Kullaa. Is temperature measurement essential in structural health monitoring? *Proc. 4th*
748 *Int. Workshop on Structural Health Monitoring*, pages 717–724, 2003.

749 [27] E. J. Cross, K. Worden, and Q. Chen. Cointegration: a novel approach for the removal of
750 environmental trends in structural health monitoring data. *Proceedings of the Royal Society*
751 *of London A: Mathematical, Physical and Engineering Sciences*, 467(2133):2712–2732, 2011.

752 [28] H. Shi, K. Worden, and E. J. Cross. A regime-switching cointegration approach for removing
753 environmental and operational variations in structural health monitoring. *Mech. Syst. Signal*
754 *Process.*, 103:381–397, 2018.

755 [29] H. Sohn, K. Worden, and C. R. Farrar. Statistical damage classification under changing
756 environmental and operational conditions. *J. Intell. Mater. Syst. Struct.*, 13(9):561–574, 2002.

757 [30] William Soo Lon Wah, Yung-Tsang Chen. A new approach toward damage localization and
758 quantification of structures under changing temperature condition. *Journal of Low Frequency*
759 *Noise, Vibration and Active Control*, 2018.

760 [31] Anis Ben Abdesslem, Nikolaos Dervilis, David Wagg, and Keith Worden. Model selection
761 and parameter estimation in structural dynamics using approximate bayesian computation.
762 *Mechanical Systems and Signal Processing*, 99:306 – 325, 2018.

763 [32] Chunfeng Wan, Rui Huang, Liyuan Huang, Bo Wen, and Tadanobu Sato. Damage identi-
764 fication using particle filters. *Procedia Engineering*, 188:41 – 47, 2017. Structural Health
765 Monitoring - From Sensing to Diagnosis and Prognosis.

1
2
3
4
5
6
7
8
9
10
11
12
13
14
15
16
17
18
19
20
21
22
23
24
25
26
27
28
29
30
31
32
33
34
35
36
37
38
39
40
41
42
43
44
45
46
47
48
49
50
51
52
53
54
55
56
57
58
59
60
61
62
63
64
65

[33] F. Cadini, E. Zio and G. Pelsoni. Particle filtering for the detection of fault onset time in hybrid dynamic systems with autonomous transitions. *IEEE Transactions on Reliability*, 61(1):130–139, 2012.

[34] Eleni Chatzi and Andrew Smyth. The unscented kalman filter and particle filter methods for nonlinear structural system identification with non-located heterogeneous sensing. *Structural Control and Health Monitoring*, 16:99 – 123, 02 2009.

[35] Chathurdara Sri Nadith Pathirage, Jun Li, Ling Li, Hong Hao, Wanquan Liu, and Pinghe Ni. Structural damage identification based on autoencoder neural networks and deep learning. *Engineering Structures*, 172:13 – 28, 2018.

[36] L.H. Yam, Y.J. Yan, and J.S. Jiang. Vibration-based damage detection for composite structures using wavelet transform and neural network identification. *Composite Structures*, 60(4):403 – 412, 2003.

[37] H. Sohn, K. Worden, and C. R. Farrar. Novelty detection using auto-associative neural network. *ASME International Mechanical Engineering Congress and Exposition, Proceedings*, 2:1525–1532, 2001.

[38] Chia-Ming Chang, Tzu-Kang Lin, and Chih-Wei Chang. Applications of neural network models for structural health monitoring based on derived modal properties. *Measurement*, 129:457 – 470, 2018.

[39] K. Worden. Structural fault detection using a novelty measure. *Journal of Sound and Vibration*, 201(1):85 – 101, 1997.

[40] I. S. Cade, P. S. Keogh, and M. N. Sahinkaya. Fault identification in rotor/magnetic bearing systems using discrete time wavelet coefficients. *IEEE/ASME Transactions on Mechatronics*, 10(6):648–657, Dec 2005.

[41] J.S. Sakellariou and S.D. Fassois. Stochastic output error vibration-based damage detection and assessment in structures under earthquake excitation. *Journal of Sound and Vibration*, 297(3):1048 – 1067, 2006.

[42] S. Marchesiello, A. Fasana, L. Garibaldi, and B.A.D. Piombo. Dynamics of multi-span continuous straight bridges subject to multi-degrees of freedom moving vehicle excitation. *Journal of Sound and Vibration*, 224(3):541 – 561, 1999.

[43] G.P. Cimellaro, S. Marasco. M dof systems. In *Introduction to Dynamics of Structures and Earthquake Engineering. Geotechnical, Geological and Earthquake Engineering, vol 45*. Springer, Cham, 2018.

[44] H.A. Nasrellah and C.S. Manohar. Finite element method based monte carlo filters for structural system identification. *Probabilistic Engineering Mechanics*, 26(2):294–307, 2011.

1
2
3
4
5
6
7
8
9
10
11
12
13
14
15
16
17
18
19
20
21
22
23
24
25
26
27
28
29
30
31
32
33
34
35
36
37
38
39
40
41
42
43
44
45
46
47
48
49
50
51
52
53
54
55
56
57
58
59
60
61
62
63
64
65

[45] H. Ebrahimian, R. Astroza and J.P. Conte. Extended kalman filter for material parameter estimation in nonlinear structural finite element models using direct differentiation method. *Earthquake Engineering & Structural Dynamics*, 44(10):1495–1522, 2015.

[46] J. F. Hall. Problems encountered from the use (or misuse) of rayleigh damping. *Earthquake Engng Struct. Dyn.*, 35:525–545, 2006.

[47] John William Strutt Baron Rayleigh. *The theory of sound*. Macmillan, 1896.

[48] C. Kyriazoglou, F.J. Guild. Finite element prediction of damping of composite gfrp and cfrp laminates – a hybrid formulation – vibration damping experiments and rayleigh damping. *Composites Science and Technology*, 67(11):2643–2654, 2007.

[49] Liangliang Cheng and Alfredo Cigada. An analytical perspective about structural damage identification based on transmissibility function. *Structural Health Monitoring*, 19(1):142–155, 2020.

[50] O. Hubert, X. Milhet, P. Gadaud, M. Tatat, P. Renault and C. Coupeau. Modeling of young’s modulus variations with temperature of ni and oxidized ni using a magneto-mechanical approach. *Materials Science and Engineering: A*, 633:76–91, 2015.

[51] W. Wang, B. Liu and V. Kodur. Effect of temperature on strength and elastic modulus of high-strength steel. *J. Mater. Civ. Eng.*, 25(2):174–182, 2013.

[52] Arnaud Doucet, Simon Godsill, and Christophe Andrieu. On sequential monte carlo sampling methods for bayesian filtering. *Statistics and Computing*, 10(3):197–208, Jul 2000.

[53] Joao FG de Freitas, Mahesan Niranjana, Andrew H. Gee, and Arnaud Doucet. Sequential monte carlo methods to train neural network models. *Neural computation*, 12(4):955 – 993, 2000.

[54] M. S. Arulampalam, S. Maskell, N. Gordon, and T. Clapp. A tutorial on particle filters for online nonlinear/non-gaussian bayesian tracking. *IEEE Transactions on Signal Processing*, 50(2):174–188, Feb 2002.

[55] M.N. Chatzis, E.N. Chatzi and A.W. Smyth. On the observability and identifiability of nonlinear structural and mechanical systems. *Structural Control and Health Monitoring*, 22(3):574–593, 2015.

[56] G. Cybenko. Approximation by superpositions of a sigmoidal function. *Mathematics of Control, Signals and Systems*, 2:303 – 314, 1989.

[57] Christopher M. Bishop. *Neural Networks for Pattern Recognition*. Oxford university press, 1995.

1
2
3
4
5
6
7
8
9
10
11
12
13
14
15
16
17
18
19
20
21
22
23
24
25
26
27
28
29
30
31
32
33
34
35
36
37
38
39
40
41
42
43
44
45
46
47
48
49
50
51
52
53
54
55
56
57
58
59
60
61
62
63
64
65

832 [58] Mark A Kramer. Nonlinear principal component analysis using autoassociative neural net-
833 works. *AIChE journal*, 37(2):233–243, 1991.

834 [59] Mohamed-Faouzi Harkat, Salah Djelal, Nouredine Doghmane, and Mohamed Benouaret. Sen-
835 sor fault detection, isolation and reconstruction using nonlinear principal component analysis.
836 *International Journal of Automation and Computing*, 4(2):149–155, 2007.

837 [60] Y. Deger, R. Cantieni and S. Pietrzko. Modal analysis of an arch bridge: experiment, finite
838 element analysis and link. *Proceedings of the 12th International Modal Analysis Conference*
839 (*IMAC*), pages 425–432, 1994.

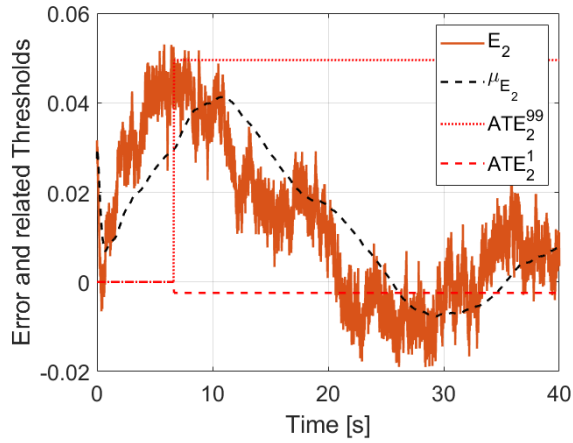
840 [61] P. Fanning, P. Healy, A. Pavic, P. Reynolds and J. Brownjohn. Sean o’casey bridge: comparison
841 of operational and traditional modal analysis test results. *Proceedings of the 2nd International*
842 *Operational Modal Analysis Conference*, pages 293–298, 2007.

843 [62] S. Cofre-Martel, P. Kobrich, E. Lopez Droguett and V. Meruane. Deep convolutional neural
844 network-based structural damage localization and quantification using transmissibility data.
845 *Shock Vib.*, 2019.

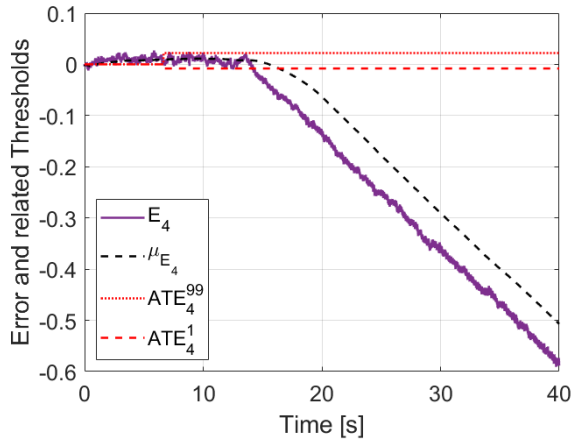
846 [63] A. Deraemaeker, E. Reynders, G. De Roeck and J. Kullaa. Vibration-based structural health
847 monitoring using output-only measurements under changing environment. *Mechanical Systems*
848 *and Signal Processing*, 22(1):34–56, 2008.

849 [64] M. Corbetta, C. Sbarufatti, M. Giglio and M.D. Todd. Optimization of nonlinear, non-gaussian
850 bayesian filtering for diagnosis and prognosis of monotonic degradation processes. *Mechanical*
851 *Systems and Signal Processing*, 142:305–322, 2018.

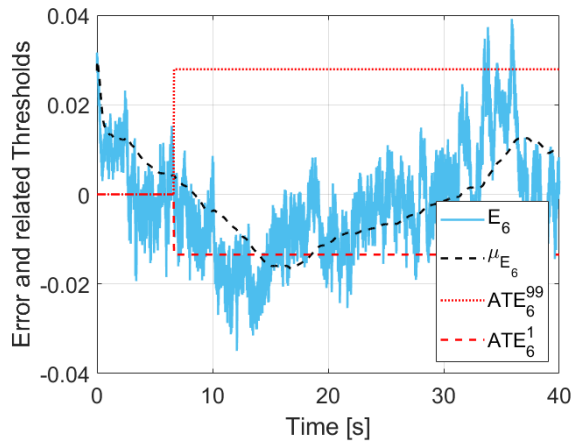
852 [65] M. Corbetta, C. Sbarufatti and M. Giglio. Optimal tuning of particle filtering random noise for
853 monotonic degradation processes. *European Conference of the PHM Society 2016 Proceedings*,
854 2016.



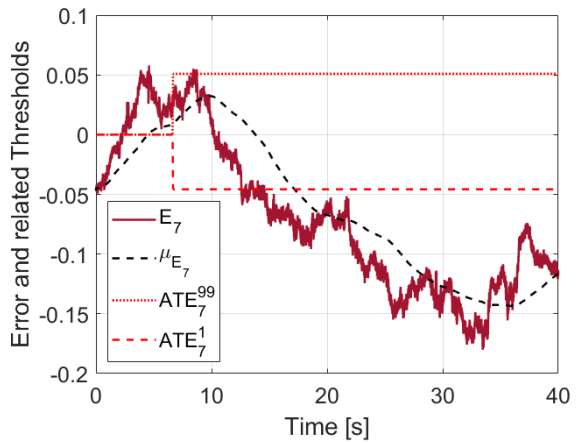
(a) Spring 2



(b) Spring 4



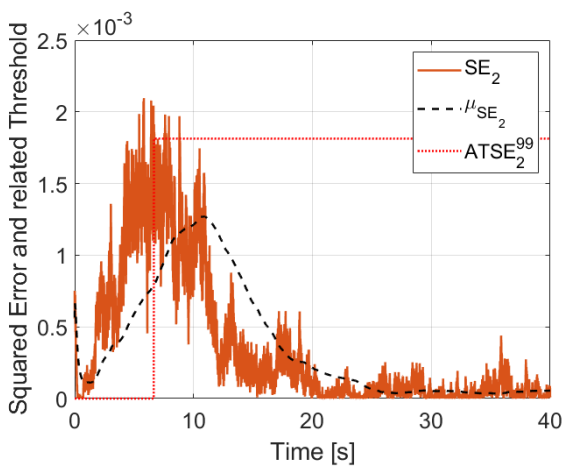
(c) Spring 6



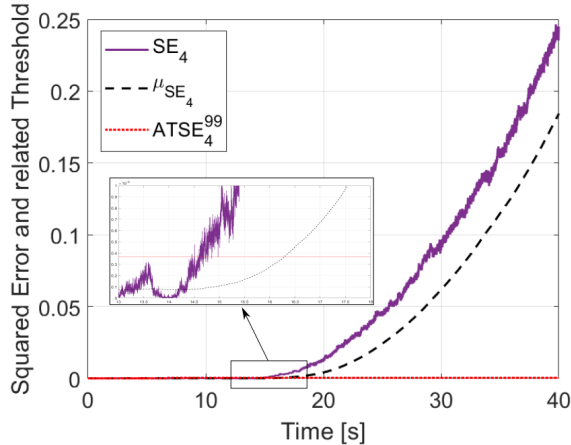
(d) Spring 7

Figure 6: Temporal evolution of the error E_i^T between the input and the output layers of the autoencoder (solid lines) for k_2 , k_4 , k_6 and k_7 , the colored dashed and dotted lines indicate the corresponding automatic thresholds and the black dashed ones the moving average.

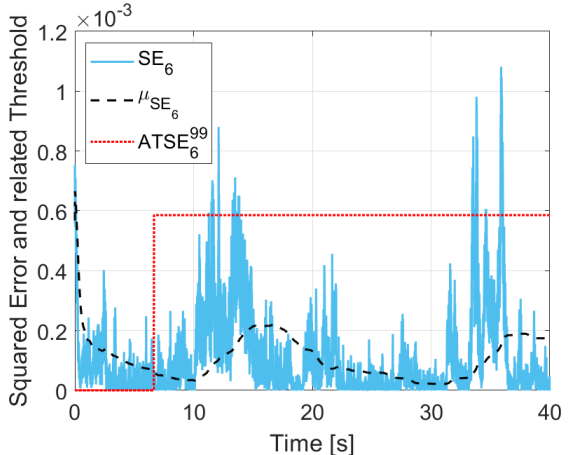
1
2
3
4
5
6
7
8
9
10
11
12
13
14
15
16
17
18
19
20
21
22
23
24
25
26
27
28
29
30
31
32
33
34
35
36
37
38
39
40
41
42
43
44
45
46
47
48
49
50
51
52
53
54
55
56
57
58
59
60
61
62
63
64
65



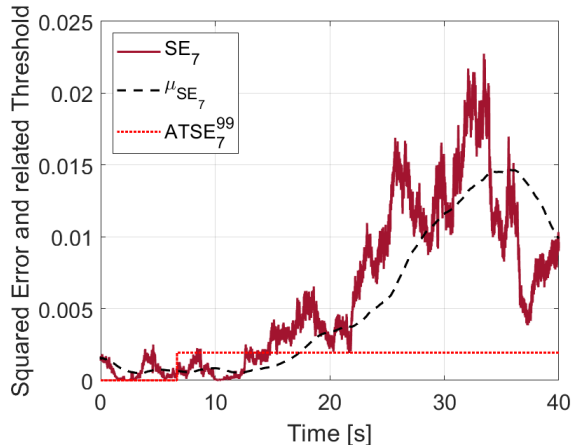
(a) Spring 2



(b) Spring 4



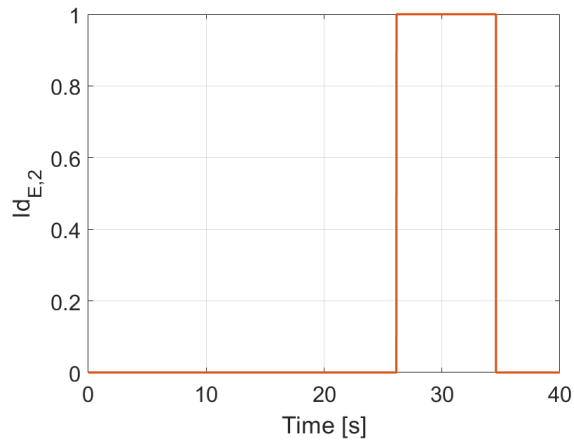
(c) Spring 6



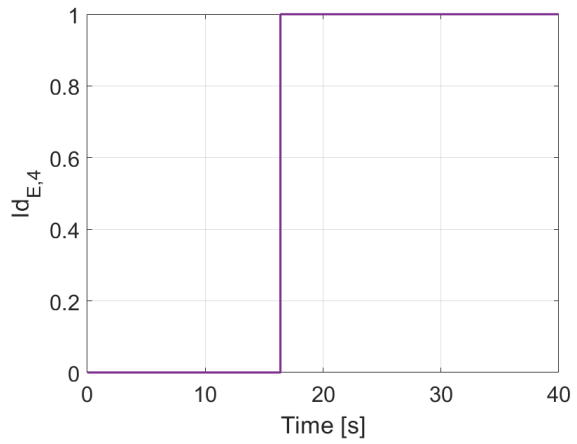
(d) Spring 7

Figure 7: Temporal evolution of the squared error SE_i^T between the input and the output layers of the autoencoder (solid lines) for k_2 , k_4 , k_6 and k_7 , the colored dotted lines indicate the corresponding automatic thresholds and the black dashed ones the moving average.

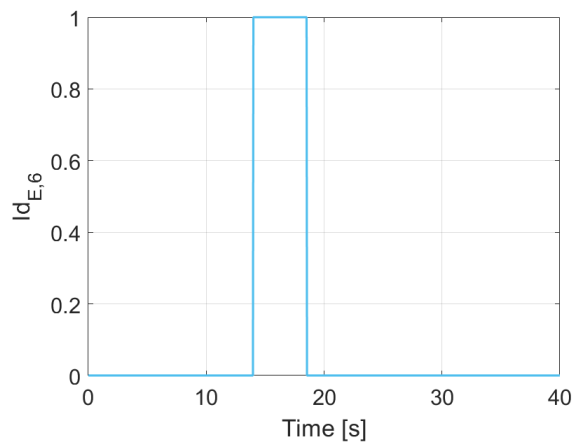
1
2
3
4
5
6
7
8
9
10
11
12
13
14
15
16
17
18
19
20
21
22
23
24
25
26
27
28
29
30
31
32
33
34
35
36
37
38
39
40
41
42
43
44
45
46
47
48
49
50
51
52
53
54
55
56
57
58
59
60
61
62
63
64
65



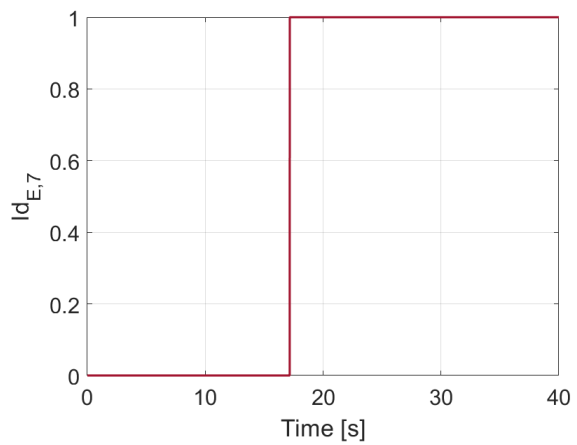
(a) Spring 2



(b) Spring 4

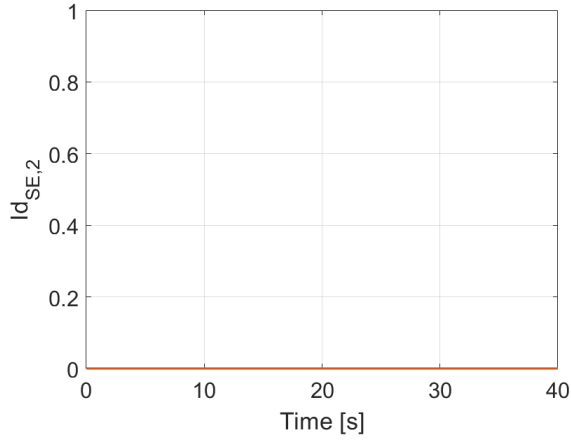


(c) Spring 6

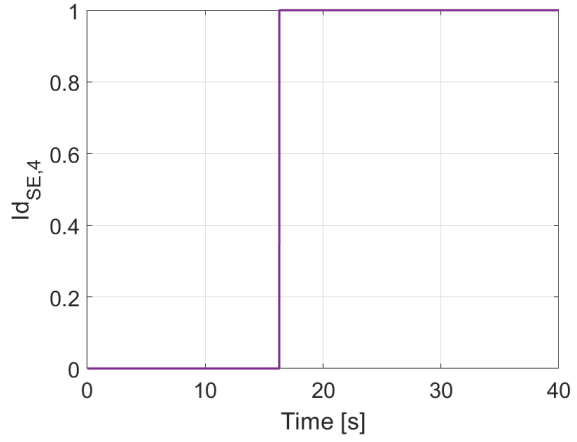


(d) Spring 7

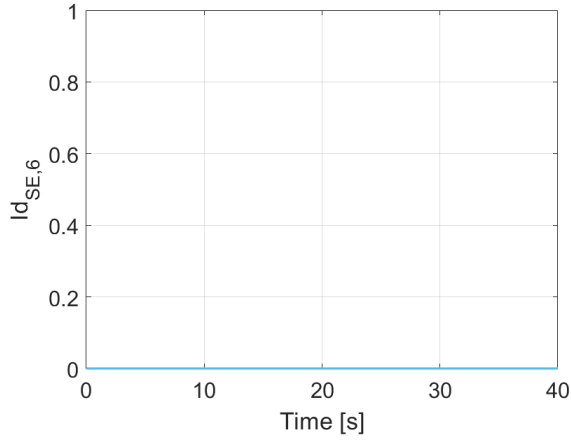
Figure 8: Temporal evolution of fault indicator $Id_{E,i}^{\tau-\tau_0+1,\tau}$ for springs 2, 4, 6 and 7.



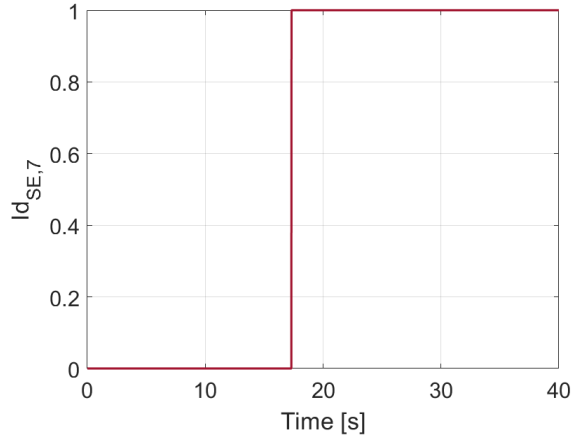
(a) Spring 2



(b) Spring 4

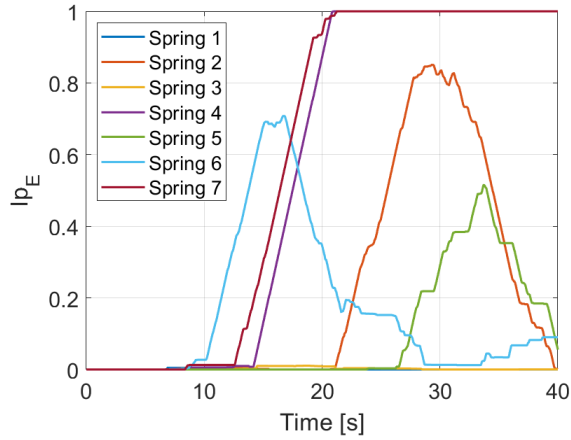


(c) Spring 6

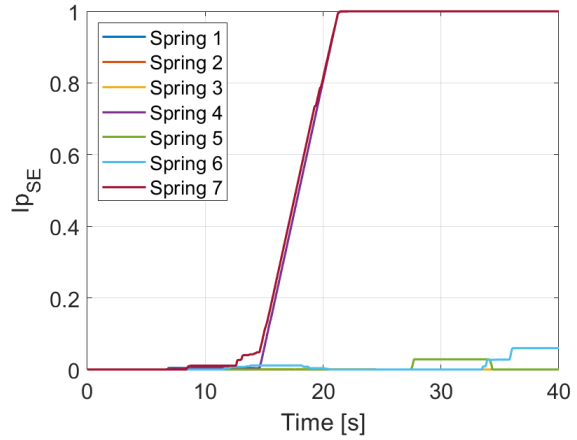


(d) Spring 7

Figure 9: Temporal evolution of fault indicator $Id_{SE,i}^{\tau-\tau_0+1,\tau}$ for springs 2, 4, 6 and 7.



(a) $I_{PE,i}^{\tau-\tau_0+1,\tau}$



(b) $I_{PSE,i}^{\tau-\tau_0+1,\tau}$

Figure 10: Temporal evolution of the probabilistic fault indicators $I_{PE,i}^{\tau-\tau_0+1,\tau}$ and $I_{PSE,i}^{\tau-\tau_0+1,\tau}$.

Neutralization of temperature effects in damage diagnosis of MDOF systems by combinations of autoencoders and particle filters

Francesco Cadini^{*1}; Luca Lomazzi¹; Marc Ferrater Roca¹; Claudio Sbarufatti¹; Marco Giglio¹

March 9, 2021

¹Politecnico di Milano, Dipartimento di Meccanica, Via La Masa 1, I-20156 Milano, Italy

**Corresponding author: francesco.cadini@polimi.it*

Abstract

In the last years, scientific and industrial communities have put a lot of efforts into the development of a new framework for the assessment of structural integrity, generally known as Structural Health Monitoring (SHM), which should allow real-time, automatic evaluations of the state of the structures based on a network of permanently installed sensors. In the context of mechanical, aerospace and civil structures, several approaches have been proposed to address the SHM problem, yet, it remains often difficult to diagnose damages and estimate the structural health when dealing with varying operating and environmental conditions. Particle Filters have already been proposed as a time-domain-based method in the field of SHM, showing promising results as estimators of hidden, not directly observable states, such as those typically related to damages. At the same time, neural networks-based autoencoders have been proposed for structural damage detection, demonstrating to be capable of capturing damage-related features from vibration measurements. This work aims at exploiting the individual advantages offered by the two approaches by combining them in a novel algorithm for structural damage detection and localization, robust with respect to changing environmental conditions. The algorithm is further equipped with a fault indicator module stemming from the introduction of an automatic threshold and both deterministic and probabilistic fault indicators, thus offering a complete, valuable tool for supporting decision making with limited human intervention. [The method is demonstrated with reference to a numerical MDOF system whose parameters are taken from a literature benchmark case study.](#)

Keywords: Structural health monitoring; changing environmental conditions; diagnosis; damage localization; particle filter; autoencoder.

1 Introduction

Structural systems exposed to long service times, changing environmental and operating conditions and occasional loads may suffer from damage within their lifespan. For example, civil infrastructures, including buildings and bridges, crucial for a well-functioning society, face serious safety problems due to ageing [1]. In general, increasing the expected lifetime of a structure would be appealing, especially in case of very large infrastructures, because it can significantly increase the return on investment of the existing assets [2]. In this context, updating of maintenance policies plays a fundamental role for the economic and safe management of mechanical and structural systems. In fact, corrective and preventive maintenance strategies are gradually being replaced by condition-based and predictive maintenance techniques, relying on automatic evaluations of the state of the structures based on a network of permanently installed sensors, so-called Structural Health Monitoring (SHM), leading to large operative cost reductions and to the improvement of safety margins.

Several approaches have been proposed in the literature to correlate any deviation of suitably defined damage sensitive features (extracted from measured data) with the presence of a damage, possibly also identifying damage parameters, such as position, type, extent, and finally enabling damage prognosis. A typical categorization is made according to whether they operate in the frequency or time domain. As for the frequency domain feature extraction methods, it is worth mentioning the envelope spectrum [3], cepstrum [4], high-order spectrum and coherence function [5]. In particular, it has been thoroughly shown that damage detection may be successfully performed in the frequency domain by means of the transmissibility functions (TFs) [6–13], defined as the ratio of two response spectra of like-variables at two different locations (or nodes of the structural model) for a given excitation [14]. Among time domain features, time-waveform indices, orbits, probability density functions and probability density moments are commonly used. Applying time domain methods, little to no data is lost before processing the signal, allowing for detailed analyses, yet with the possibility of incurring into the risk of making diagnosis more burdensome due to the often required accumulation of available data [5]. For the sake of completeness, it is worth mentioning that mixed time-frequency analysis may also be adopted. These hybrid approaches are particularly useful for revealing the inherent information of non-stationary signals, which may be contained in the measures taken from the damaged structure [15]. For a thorough discussion of such a class of analysis techniques, the reader is referred to [15], where the benefits and limitations of these methods are discussed.

However, a general problem of any feature extraction method is that they are sensitive to any change in the environmental and operating conditions, including temperature, pressure, humidity and operative loads, which act as confounding influences, thus hampering the damage identification process potentially increasing the false alarm rate, as widely discussed in [16], [17], [18] and [19]. In this context, several approaches have been proposed to magnify the effect of damage over the monitored features and suppress the influence of confounding factors, usually referred to as data

1
2
3
4
5 39 normalization [16]. Some methods rely on regression and interpolation techniques to “learn” the
6 40 dependence of any measured feature from the varying boundary condition [20–23]. Other methods
7 41 leverage on a feature’s shift, induced by damage, “orthogonal” with respect to the reference normal
8 42 condition space. These include, for example, singular-value decomposition [24], principal component
9 43 analysis [25], factor analysis [26], cointegration [27, 28] and auto-associative neural networks [29].
10 44 However, most of these approaches can often only detect the presence of damages in structures,
11 45 not being able to locate and quantify them. So far, no general method provides fault isolation for
12 46 a wide range of systems while accounting for possible variations of operational and environmental
13 47 conditions. In most cases, these methods appear to be, in fact, case-specific, hence no extension of
14 48 such algorithms to generic problems seems to be able to provide reliable results. An exception seems
15 49 the work in [30], where an approach is proposed based on the quantification of stiffness variation
16 50 of all the elements in a structure due to temperature and damage effects, followed by suppression
17 51 of temperature effects to estimate the actual damage location and extent. That method works in
18 52 the frequency-domain, in fact the procedure needs a harmonic force to be applied to the structure
19 53 under examination, in order to determine the actual frequency response function, which is further
20 54 processed for detecting, localizing and quantifying the damage.
21
22
23
24
25
26
27

28 55 Recently, particle filters (PFs) and other Bayesian methods have been used as time-domain tools
29 56 for structural parameters identification [31] and fault diagnosis [32, 33]. For example, some works
30 57 used PFs for identifying the stiffnesses of a multiple-degree of freedom (MDOF) system subject to a
31 58 seismic-like acceleration forcing function [34]. Moreover, the PF estimation capabilities in presence
32 59 of non-linear dynamics for the spring components have also been investigated, albeit restricting
33 60 the attention to the problem of system identification, without delving into the potentiality of
34 61 the method as a damage diagnosis tool. To the best of the authors knowledge, the effects of
35 62 environmental conditions have not been taken into account yet in damage diagnosis methods based
36 63 on the use of PFs in the time domain.
37
38
39
40
41

42 64 Furthermore, machine learning approaches, specifically neural networks, have been widely im-
43 65 plemented for damage diagnosis [35, 36], due to their performance in capturing the behavior of
44 66 relevant damage features even in presence of very complex dynamics, whose detailed physics-based
45 67 modeling would often require extraordinary computational efforts. In particular, neural network-
46 68 based autoencoders have been quite extensively used for performing damage detection [35, 37, 38].
47 69 For example, some early work [39] proposed the use of autoencoders for extracting damage-related
48 70 features from vibration measurements in the frequency domain, thus being able to perform novelty
49 71 detection in MDOF-modeled systems. However, that procedure relied on the information extracted
50 72 from the transmissibility function, which, as already mentioned, may not always provide reliable
51 73 results in damage localization [14].
52
53
54
55
56

57 74 In this work, we propose an original time-domain approach to perform fault identification
58 75 in structural components subject to degradation, under changing operating and environmental
59 76 conditions. Exploiting the complementarity of PFs and autoencoders outlined above, in this paper
60
61
62
63
64
65

1
2
3
4 77 it is proposed to combine them to derive a robust and flexible algorithm, offering the possibility
5
6 78 to automatically perform damage detection and identification in a unique, coherent and simple
7
8 79 framework. More specifically, the PF estimates some not directly observable structural parameters
9
10 80 on the basis of commonly available vibration measurements (e.g., accelerations, positions, etc.). PF
11
12 81 posterior estimation is then combined with temperature measurements using autoencoders, which
13
14 82 suppress confounding influences over the estimated structural parameters. Finally, for an effective
15
16 83 use of the algorithm as a decision support, a novel detection strategy is also proposed, based on
17
18 84 the introduction of automatic thresholds, thus delivering a result less dependent from external,
19
20 85 i.e., human, interpretation. The method is demonstrated with reference to a MDOF system whose
21
22 86 parameters are taken from a literature benchmark case study [39].

23
24 87 The paper is organized as follows. In Section 2 the generic methodological approach is presented,
25
26 88 focusing on the specific design of the PF and of the autoencoder, tailored to the specific application
27
28 89 to the MDOF system model. Section 3 introduces a case study, which consists of a 6-DOF system
29
30 90 affected by temperature variations. The Section first presents a brief sensitivity analysis aimed
31
32 91 at tuning the performances of the PF algorithm, and then demonstrates the performances of the
33
34 92 proposed methodology. In Section 4 the conclusions of this work are provided, along with a critical
35
36 93 discussion of the main results achieved and possible future work.

31 94 **2 Methodology**

37
38 95 The methodology is proposed with reference to a modeling strategy commonly used to represent
39
40 96 the dynamic behavior of many mechanical, aeronautical and civil structural systems, such as rotary
41
42 97 machines, multi-storey buildings and multi-span bridges, i.e., the one-dimensional MDOF systems
43
44 98 [40–42]. MDOF structural systems are also known as periodic structures, which basically consist
45
46 99 of several structural components of the same type, i.e., springs, masses, dampers, joined together
47
48 100 [41, 43]. These models are particularly useful for describing the vibration of a structure when it
49
50 101 experiences significant motions in one preferential direction. However, the proposed methodology
51
52 102 is generic and not bounded to the specific model employed for simulating the structure under mon-
53
54 103 itoring. Hence, any other modelling technique different from the MDOF system can in principle
55
56 104 be considered, with no compatibility issues with the proposed framework, as long as a model of
57
58 105 the structure is provided. For instance, the Finite Element modelling strategy may represent a
59
60 106 promising alternative to the MDOF technique, yet more complicated, which would also open up
61
62 107 the chance to deal with non-periodic structures. In fact, a combination of Particle Filter as dynamic
63
64 108 state estimation tool and Finite Element model of different types of structures, e.g., rubber sheet
65
66 109 with a hole, single span beam and multi-span masonry arch bridge, was employed in the work in [44]
67
68 110 with satisfactory performances. Similarly, nonlinear Finite Element method and extended Kalman
69
70 111 filter were successfully combined in a unique framework to estimate some non-linear material pa-
71
72 112 rameters of a structural system [45]. In this context, according to the common practice in the SHM
73
74 113 field, structural damage is modeled as a stiffness reduction of one or more springs in the system



Figure 1: MDOF mass-spring-damper system.

[30, 37, 39]. Since the stiffness values are not directly observable parameters, a PF algorithm is derived for the estimation of the hidden stiffnesses on the basis of the most commonly available vibration measurements, i.e., the accelerations of the MDOF system masses, although the filter could in principle be generalized to process also other types of possible measurements (positions and velocities).

Then, within the PF framework, the differential equations describing the dynamic evolution of each degree of freedom of the MDOF system are discretized in time and used to create the state-space for the PF-based state estimation process. At each time step, the acceleration of each degree of freedom of the system is measured. Simultaneously, a sufficiently large number of possible system dynamic evolutions (particles) are sampled and are assigned some importance weights based on the observation likelihood. The weights are then used to provide an estimate of the MDOF model structural stiffnesses within an augmented state parameter estimation framework. This process allows to obtain temporal estimates of the system stiffnesses, which can be used to evaluate the structure health state.

As shown in previous works of literature (e.g., [32]) and also later in this paper, if no external operating and/or environmental conditions are modifying the values of the system stiffnesses, in principle PF would allow not only to detect the presence of damage, but, at the same time, to locate and, somehow, quantify it. When, on the other hand, the effects of external conditions on the stiffnesses are superposed to those of damages, then even the simple damage detection task by PF is severely hampered. We here propose to address this issue by processing the PF estimates of the stiffnesses through a neural network autoencoder, previously trained with a healthy, but temperature-dependent baseline, so as to be able to capture the physical relationship between the external conditions and the stiffnesses. During the operational phase, the error between the input and the reconstructed data serves, upon the introduction of an automatic threshold, for the damage diagnosis purpose. By so doing, the autoencoder will be able to generate signals sensitive to the presence of damages only, which will be further processed to obtain an automatic alarm system.

In what follows, some details of PF algorithms and of autoencoders are provided, with a focus on how they are combined to perform damage diagnosis. For further mathematical details on the individual methods, the interested reader is referred to the vast literature available.

2.1 State-space model and particle filter

Consider a generic MDOF mass-spring-damper system as the one shown in Figure 1. According to common practice in this kind of SHM applications, the consolidated assumption of viscous damping is made in this work, which represents a velocity-dependent damping formulation allowing not to introduce non-linearities in the system, while still guaranteeing a quite satisfactory description of the damping effects [46]. In particular, the widely adopted proportional damping, or Rayleigh damping, assumption is made [47]. Some issues may arise adopting this model, e.g., (i) proportional damping does not allow for satisfactory representation of eventual non-linear damping behaviors or (ii) it provides not very accurate results when the structure undergoes yielding, buckling or when the local behavior around the tip of an eventual crack has to be investigated, to cite some. However, being these particular scenarios not relevant in this work, proportional damping is considered to be a valid and accurate enough damping modelling technique. Moreover, a relevant property of Rayleigh damping is that it can be applied both to structures made of homogeneous materials and to those made of non-homogeneous materials, without any difference in the specific formulation, which allows not limiting to analyze structures made of isotropic materials, but also more complex systems including non-isotropic materials [48]. In this work, damping is assumed to be proportional to stiffness only through a coefficient β , assumed identical for all the dampers in the MDOF system [49]. In order to be able to perform stiffness parameters estimation, an augmented state space representation of the system is introduced, which includes four types of variables: position and speed of each mass of the system, stiffness value of the springs of the structure and proportionality constant of damping. Hence, the state vector for n degrees of freedom becomes:

$$\mathbf{x}^\tau = \left[x_1^\tau \quad \dots \quad x_n^\tau \quad y_1^\tau \quad \dots \quad y_n^\tau \quad k_1^\tau \quad \dots \quad k_{n+1}^\tau \quad \beta \right]^\top \quad (1)$$

where x_i^τ is the position of mass i at time step τ , y_i^τ is the speed of mass i at the generic, discrete time step τ , k_i^τ is the i -th spring stiffness at time step τ and β is the proportionality constant of damping, according to the relationship $c_i^\tau = \beta k_i^\tau$. Within the PF framework, the state-space model describing the system evolution at the discrete time step τ must be a hidden Markov process of the form:

$$\mathbf{x}^\tau = g(\mathbf{x}^{\tau-1}, \mathbf{w}^{\tau-1}) \quad (2)$$

where $g(\cdot)$ represents a generic function, which may be non-linear, and $\mathbf{w}^{\tau-1}$ is the process noise vector value at time step $\tau-1$, here assumed to be distributed according to a Gaussian multivariate distribution $N(0, \Sigma_w)$, $\Sigma_w = \text{diag}(\sigma_{x_1}, \dots, \sigma_\beta)$. In the specific system considered in this study, i.e., a MDOF mass-spring-damper system, four state evolution equations are considered, one for each type of state included in the state vector of equation 1. The dynamic evolution of each individual mass position is then governed by:

$$x_i^{\tau+1} = y_i^\tau dt + x_i^\tau + w_{\text{position}}^\tau; \quad \forall i = 1, \dots, n \quad (3)$$

1
2
3
4
5
6
7
8
9
10
11
12
13
14
15
16
17
18
19
20
21
22
23
24
25
26
27
28
29
30
31
32
33
34
35
36
37
38
39
40
41
42
43
44
45
46
47
48
49
50
51
52
53
54
55
56
57
58
59
60
61
62
63
64
65

175 which is obtained from the discretization of the system of differential equations of motion with the
176 addition of the position process noise $w_{position}^\tau$. The state-space equation for the velocity of each
177 degree of freedom (mass) is given by:

$$y_i^{\tau+1} = \frac{F_i^\tau}{m_i} dt + y_i^\tau \left(1 - \frac{dt}{m_i} (c_i + c_{i+1})\right) + y_{i-1}^\tau \frac{dt}{m_i} c_i + y_{i+1}^\tau \frac{dt}{m_i} c_{i+1} - x_i^\tau \frac{dt}{m_i} (k_i^\tau + k_{i+1}^\tau) + x_{i-1}^\tau \frac{dt}{m_i} k_i^\tau + x_{i+1}^\tau \frac{dt}{m_i} k_{i+1}^\tau + w_{speed}^\tau; \quad \forall i = 1, \dots, n \quad (4)$$

178 where F_i^τ represents the forcing load applied to mass m_i , c_i is the damping coefficient value of
179 the i -th damper and w_{speed}^τ is the speed process noise. Equation 4 is again obtained from the
180 discretization of the system of differential equations of motion with the addition of the speed process
181 noise w_{speed}^τ . Note that for the side masses equation 4 must be updated deleting some terms, in
182 particular those including x_{i-1}^τ and y_{i-1}^τ for $i = 1$, and those with x_{i+1}^τ and y_{i+1}^τ for $i = n$. Spring
183 stiffness values are assumed to be invariant over time in a healthy structure without any variations
184 of operating and/or environmental conditions, such as temperature. Therefore, in agreement with
185 the common parameter identification practice, each parameter k_i is modeled as an augmented state
186 characterized by a value constant in time, only slightly perturbed by some unmodeled dynamics,
187 here represented by the process noise w_{spring}^τ :

$$k_i^{\tau+1} = k_i^\tau + w_{spring}^\tau; \quad \forall i = 1, \dots, n + 1 \quad (5)$$

188 In case temperature variations occur, we assume that the stiffness values evolve according to the
189 following relationship:

$$k_i(T) = 0.1 (T)^2 - 18T + k_i(0^\circ C); \quad \forall i = 1, \dots, n + 1 \quad (6)$$

190 where T identifies the external temperature measured in $^\circ C$. Equation 6 is obtained from [30] by
191 rescaling the coefficients of the original equation describing the elastic modulus as a function of
192 the temperature [50, 51] to have a stiffness value of $10^4 \frac{N}{m}$ at $0^\circ C$ in correspondence of an elastic
193 modulus of $203.07 GPa$. The proportionality constant of damping is assumed to be invariant over
194 time. Therefore, as typically done in the parameter identification practice, the parameter β is
195 modeled as an augmented state characterized by a value constant in time, only slightly perturbed
196 by some unmodeled dynamics, here represented by the process noise $w_{damping}^\tau$:

$$\beta^{\tau+1} = \beta^\tau + w_{damping}^\tau \quad (7)$$

197 hence, in case temperature variations occur, the i -th damping value changes accordingly to the
198 change of the related stiffness value, i.e., k_i , according to the equation $c_i^\tau = \beta^\tau k_i^\tau$.

199 In the PF framework, the hidden Markov states whose evolution is described in equations 3, 4,
200 5 and 7 are assumed to be indirectly observed by collecting some measurements z . The relationship

201 between the hidden states and the measurement \mathbf{z}^τ is assumed to be known and to take the following
 202 form:

$$\mathbf{z}^\tau = h(\mathbf{x}^\tau, \mathbf{v}^\tau) \quad (8)$$

203 where $h(\cdot)$ is a generic function, which may be non-linear, and \mathbf{v}^τ is the measurement noise vector
 204 at time step τ , here assumed to be distributed according to a Gaussian multivariate distribution
 205 $N(0, \Sigma_v)$, $\Sigma_v = \text{diag}(\sigma_{z_1} \dots \sigma_{z_n})$. In this study, without any loss of generality, we restrict our
 206 attention to the case in which only acceleration measurements are available for each degree of
 207 freedom (mass). The measurement equation relating the acceleration value of mass m_i to the state
 208 vector at time step τ is:

$$z_i^\tau = \frac{F_i^\tau}{m_i} - \frac{y_i^\tau}{m_i}(c_i + c_{i+1}) + \frac{y_{i-1}^\tau}{m_i}c_i + \frac{y_{i+1}^\tau}{m_i}c_{i+1} - \frac{x_i^\tau}{m_i}(k_i^\tau + k_{i+1}^\tau) + \frac{x_{i-1}^\tau}{m_i}k_i^\tau + \frac{x_{i+1}^\tau}{m_i}k_{i+1}^\tau + v_i^\tau; \quad \forall i = 1, \dots, n \quad (9)$$

209 where v_i^τ represents the acceleration measurement noise at time step τ . Note that for the side
 210 masses equation 9 must be updated deleting some terms, in particular those including x_{i-1}^τ and
 211 y_{i-1}^τ for $i = 1$, and those with x_{i+1}^τ and y_{i+1}^τ for $i = n$.

212 Then, in the PF framework it is possible to divide the filtering process in two stages, whose
 213 final objective is the on-line, recursive estimation of the posterior probability density function (pdf)
 214 $p(\mathbf{x}^\tau | \mathbf{z}^{1:\tau})$ of the hidden state vector \mathbf{x}^τ conditioned on the sequence of data observed up to time
 215 step τ , i.e., $\mathbf{z}^{1:\tau}$.

216 In the first step (also called transition or prediction stage), the pdf of the hidden states \mathbf{x}^τ at
 217 time step τ , i.e., $p(\mathbf{x}^\tau | \mathbf{z}^{1:\tau})$, is predicted based on prior information available at time step $\tau - 1$.
 218 Operatively, the process equations 3, 4, 5 and 7 are used for the random generation of N_s possible
 219 state trajectories (particles) \mathbf{x}_s^τ , $s = 1, \dots, N_s$, at time step τ , which is equivalent to sampling the
 220 importance density function (the prior) $p(\mathbf{x}^\tau | \mathbf{x}^{\tau-1})$.

221 Then, in the second stage (also called update stage), as soon as a new observation \mathbf{z}^τ is acquired
 222 at time step τ , according to the Bayes' theorem, the measurement equation 9 is used to assign a
 223 weight w_s^τ to each of the N_s particles, recursively calculated as:

$$w_s^\tau = w_s^{\tau-1} \cdot \prod_{i=1}^n \frac{1}{\sqrt{2\pi}\sigma_{z_i}} e^{-0.5 \left(\frac{z_{s,i}^\tau - a_i^\tau}{\sigma_{z_i}} \right)^2} \quad (10)$$

224 where $z_{s,i}^\tau = h(\mathbf{x}_s^\tau, \sigma_{z_i})$ is the acceleration virtual measurement of mass m_i , associated to the
 225 particle \mathbf{x}_s^τ at time τ and computed according to measurement equation 9, $\sigma_{z_i}^2$ the variance of the
 226 i -th measurement and $z_i^\tau = a_i^\tau$ is the acceleration observation of the i -th DOF at time step
 227 τ . Equation 10 is formulated under the hypothesis of Gaussian measurement noise \mathbf{v}^τ equal for all
 228 the acceleration measurements available.

Upon the normalization of the importance weights, the posterior pdf can then be approximated by the ordered set $\{\mathbf{x}_s^\tau, \tilde{w}_s^\tau\}_{s=1}^{N_s}$ [52, 53], or, using the Monte Carlo formalism:

$$p(\mathbf{x}^\tau | \mathbf{z}^{1:\tau}) \approx \sum_{s=1}^{N_s} \tilde{w}_s^\tau \delta_{\mathbf{x}_s^\tau, \mathbf{x}^\tau} \quad (11)$$

where \tilde{w}_s^τ represents the normalized weight assigned to the s -th particle. Note that, to avoid the problem of degeneracy, bootstrap resampling is applied at each time step τ , which implies re-setting the importance weights of the particles to $w_j^\tau = \frac{1}{N_s}$. Hence, the state estimate $\hat{\mathbf{x}}^\tau$ is computed as the mean value of the posterior distribution of the state vector \mathbf{x}^τ estimated by the particle filter. For a more detailed discussion on particle filtering and Monte Carlo methods, the reader is referred to the seminal works [54] and [52].

Indeed, in this context, the problem of the identifiability of the parameters becomes very important. Thus, identifiability assessment should always be performed before the application of the method. This activity is out of the scope of the present work, in which identifiability is heuristically assessed by trial-and-error procedure. In case more complex systems are involved, the heuristic approach should possibly consist of increasing the number of forcing terms and, in case applying more loads is hard in the specific real application (e.g., on large civil infrastructures), diversification of the type of observations could prove a good strategy, e.g., considering displacement, velocity and acceleration measurements together. The interested reader is referred to [55] for further details about the identifiability problem.

2.2 Combination of PF with neural network-based auto-encoders

Neural networks are computational models aimed at fitting any linear and/or non-linear relationship $\mathbf{y} = f(\mathbf{x})$ between some input and output vectors \mathbf{x} and \mathbf{y} . A network is a collection of connected elements, called *nodes* or *neurons*, arranged in layers. In general, the architecture of a neural network includes one input layer, some hidden layers and the output layer. Considering a simplified case with one hidden layer only, each node $i = 1, \dots, N_i$ of the input layer receives one input signal x_i and is fully connected to each node $j = 1, \dots, N_h$ of the hidden layer through a path to which a weight w_{ij} is associated. All the input signals x_i feeding a node j and a bias parameter b_j are summed up to give the excitation $\sum_{i=1}^{N_i} (w_{ij} \cdot x_i) + b_j$ of that specific hidden neuron. The excitation signal is further processed by a generally non-linear *activation function*, thus giving rise to the j -th hidden node output $z_j = g(\sum_{i=1}^{N_i} (w_{ij} \cdot x_i) + b_j)$. Note that the activation function $g(\cdot)$ is a monotonically increasing, continuous function with output range $(0, 1)$, and that the bias has the purpose of giving a constant offset to the excitation level of the hidden nodes, or, equivalently, to set different activation thresholds. Each node $j = 1, \dots, N_h$ of the hidden layer is then fully connected to each output node $k = 1, \dots, N_o$ through a weight w_{jk} . All the signals z_j feeding an output node k are summed up to give the excitation $\sum_{j=1}^{N_h} (w_{jk} \cdot z_j)$ of that specific output neuron. The excitation signal is further processed by a usually linear activation function $h(\cdot)$, thus giving

rise to the k -th node output $y_k = h(\sum_{j=1}^{N_h}(w_{jk} \cdot z_j))$. The equation describing the input-output relationship can then be written in a compact form:

$$y_k = h\left(\sum_{j=1}^{N_h}(w_{jk} \cdot (g(\sum_{i=1}^{N_i}(w_{ij} \cdot x_i) + b_j)))\right) \quad (12)$$

Under some assumptions, the Cybenko theorem [56] guarantees that expressions as that in equation 12 are universal approximators, provided the proper architecture and suitable values of the weights are used. However, the theorem does not provide any strategy to build an effective network. While the architecture is often left to the designer experience, several methods have been proposed to identify optimal sets of weights, through procedures generally known as “training” or “learning”, the most popular of which is probably the error back-propagation algorithm with gradient descent. The training algorithm requires that a set of input-output examples be available from the observed process to be approximated. The inputs are fed to the network, which produces some outputs. The outputs are then compared with the actual ones and the error is then used to back-updating the weights by a weight gradient-descent approach. The procedure ends when satisfactory generalization capabilities and reconstruction errors are achieved (see [57]).

In this framework, the *autoencoders* (or *auto-associative neural networks*), are deep neural models (i.e., containing more than three layers, including input and output) including a dimensionality reduction side and a reconstructing side, exploited for learning data properties in an unsupervised manner [58]. In particular, the dimensionality reduction side reduces the dimensionality of the input data fed to the network, while the reconstructing side is aimed at reconstructing in the output layer the same values fed in input to the network. In this work, the auto-associative neural network architecture considered is described by a symmetric structure, consisting of two mirrored multilayer perceptrons (MLPs), with one input layer, three hidden layers (typically called mapping, bottleneck and demapping layers) and an output layer (Figure 2). Indeed, the input and output vectors have the same dimension, which is typically larger than the bottleneck size. The mapping and demapping layers usually have the same number of nodes, which is greater than that of the input vector. During the mapping phase, which involves input, mapping and bottleneck layers, if the bottleneck has less nodes than input and output layers, then the autoencoder reduces the input dimensionality through the following general relationship:

$$\mathbf{y} = H_{map}(\mathbf{x}) \quad (13)$$

where $H_{map}(\cdot)$ is the vector of generic models implemented by the first MLP of the autoencoder (see equation 12). The subsequent demapping phase aims at reconstructing the input variables in the output nodes via the demapping layer, which is an “inverted” version of the first MLP, according

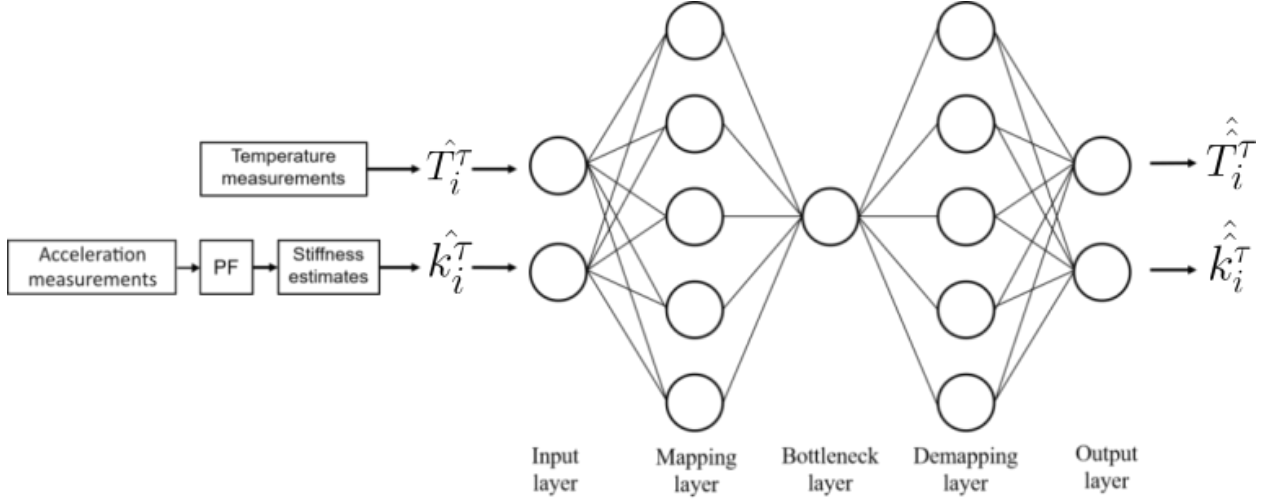


Figure 2: Proposed autoencoder structure.

to the following relationship:

$$\hat{\mathbf{x}} = H_{demap}(\mathbf{y}) \quad (14)$$

where $H_{demap}(\cdot)$ is the vector of generic models implemented by the second MLP of the autoencoder and $\hat{\mathbf{x}}$ is the reconstructed input vector in the output layer.

In this work, different autoencoders are associated to each spring of the MDOF model. Each autoencoder is then structured with two input nodes, characterized by linear functions, one receiving the temperature observed at the location of the associated spring and one receiving the PF-based estimate of the stiffness for each spring, i.e., as illustrated above, the mean of the PF-based sample posterior pdfs of the stiffnesses. The two input values are then processed by the autoencoder mapping layer, combined into a single signal within the single bottleneck node and then further reconstructed in the output vector of size two. The choice of one single node in the bottleneck layer (activated by a sigmoid function) is inspired by a similar strategy followed in the work in [37] and, at the same time, it is also intuitively sound. In fact, only one variable, i.e., the temperature, can give rise to variations in the structural stiffnesses in healthy conditions. The mapping and demapping layers are made up of 5 nodes, identified upon a trial and error procedure, each characterized by a sigmoid activation function. This architecture allows the autoencoder to extract relevant information about the nature of the spring stiffness change during the operational phase, eventually leading to the detection and the localization of the structural damage, as it will be shown in Section 3. In fact, autoencoders are able to reconstruct the input variables in the output layer according to the baseline they have been trained with. Thus, if any change occurs in the correlation between the input parameters (i.e., in our case temperatures and estimated stiffnesses), since the autoencoder tends to provide in output the correlations it has been trained to recognize, it should give rise to some discrepancies between the input and the output data. Then, by processing some properly defined reconstruction error (or distance) between the input and the output signals, it is possible, in

1
2
3
4
5
6
7
8
9
10
11
12
13
14
15
16
17
18
19
20
21
22
23
24
25
26
27
28
29
30
31
32
33
34
35
36
37
38
39
40
41
42
43
44
45
46
47
48
49
50
51
52
53
54
55
56
57
58
59
60
61
62
63
64
65

principle, to detect any anomaly in the input signals which disrupt their healthy baseline correlation. In order to further localize the anomalies, as anticipated above, for the general case of a n -degrees of freedom MDOF model, $n + 1$ autoencoders must be associated to the $n + 1$ spring stiffnesses in the system. Indeed, only the outputs of the autoencoders associated to a damaged spring would then be affected by the presence of the anomaly, thus consequently allowing for their localization.

Here, according to several works of literature [37, 58, 59], the squared error is used to measure the differences between the inputs and the reconstructed outputs of the autoencoders, upon proper normalization of their values:

$$SE_i^\tau = (\hat{T}_i^\tau - \hat{\hat{T}}_i^\tau)^2 + (\hat{k}_i^\tau - \hat{\hat{k}}_i^\tau)^2 \tag{15}$$

where SE_i^τ is the squared error between the input variables (\hat{T}_i^τ and \hat{k}_i^τ) and the output variables ($\hat{\hat{T}}_i^\tau$ and $\hat{\hat{k}}_i^\tau$) recorded at time step τ on the i -th spring of the system. Additionally, it is here proposed to also use the simple error:

$$E_i^\tau = (\hat{T}_i^\tau - \hat{\hat{T}}_i^\tau) + (\hat{k}_i^\tau - \hat{\hat{k}}_i^\tau) \tag{16}$$

Note that, for a proper functioning of neural networks, the normalization of all the training data is a common practice, which becomes basically mandatory when the inputs are quantities characterized by different units of measures (as it is the case in the present work). Here, the input data are normalized according to the following linear transformations:

$$\frac{\hat{T}_i^\tau - (-50^\circ C)}{120^\circ C - (-50^\circ C)} \tag{17}$$

$$\frac{\hat{k}_i^\tau}{1.1 \cdot 10^4 \frac{N}{m}} \tag{18}$$

so that the errors defined above can vary in the ranges $E_i^\tau \in [-2, 2]$ and $SE_i^\tau \in [0, 2]$. From here on, the values \hat{T}_i^τ and \hat{k}_i^τ directly refer to the already normalized input data.

In practical applications, the healthy baseline to be used for training the $n + 1$ autoencoders can be acquired during the early life of the system, when it is reasonable to assume that no damages are present. Then, upon proper excitation of the structure, the PF algorithm described above can be turned on, so as to provide estimates of the model stiffnesses. At the same time, the temperature at each spring location must be recorded. Indeed, for a correct functioning of the algorithm, a rather wide range of temperatures should be explored, either artificially applied or, for certain types of structures, only expected to occur in the environment, during the recording of the baseline.

2.3 Definition of the diagnostic indicators

For the definition of suitable diagnostic indicators, to be used for timely triggering diagnostic alarms, in principle one could set proper thresholds for the errors described in the previous Section, as also suggested in [39] for SE_i^τ . Unfortunately, as it shall be shown in the next Section, the choice of the proper threshold values is somewhat arbitrary and, if not properly set, may easily lead to unreliable results, either too conservative (too many false alarms) or too risky (too many missed alarms). The problem is further exacerbated by the fact that both the autoencoder inputs are affected by noises, the temperature measurement noise and the whole uncertainty affecting the PF-based stiffness estimates, due to a combination of acceleration measurement noise, process noises (unmodeled dynamics) and Monte Carlo errors. Indeed, this is one of those “eternal” dilemmas ever characterizing any diagnostic task, for which no definitive answers exist. Nevertheless, in this work an attempt is made to address this issue, which will be proven to be effective at least within the scope of the application presented here. The proposed approach consists of combining an automatic threshold definition module with the construction of both a deterministic and a probabilistic indicator. More specifically, two automatic thresholds for each spring $i = 1, \dots, n + 1$ are introduced as:

$$ATE_i^1 = p1(E_i^{1:\tau_0}) \quad (19a)$$

$$ATE_i^{99} = p99(E_i^{1:\tau_0}) \quad (19b)$$

where $p1(E_i^{1:\tau_0})$ and $p99(E_i^{1:\tau_0})$ are the 1th and the 99th percentiles of the probability density function of the error defined in equation 16, respectively, computed over a fixed time window of width τ_0 time steps taken at the beginning of the operational life of the structure, when the system is assumed to be in healthy conditions. In a similar fashion, an automatic threshold for each spring i can also be defined for the squared error as:

$$ATSE_i^{99} = p99(SE_i^{1:\tau_0}) \quad (20)$$

where $p99(SE_i^{1:\tau_0})$ is the 99th percentile of the probability density function of the squared error defined in equation 15 taken over the same time window of width τ_0 time steps defined above.

Then, in order to operatively trigger the diagnostic alarm, a binary, deterministic fault indicator is introduced for each spring i , which compares the threshold value with the error value computed as the moving average of the errors for each spring i . The moving average is computed over a sliding window of width τ_0 time steps, equal to that used for the definition of the automatic threshold:

$$Id_{E,i}^{\tau-\tau_0+1,\tau} = \begin{cases} 1 & \text{if } \mu_{E_i^{\tau-\tau_0+1,\tau}} < ATE_i^1 \vee \mu_{E_i^{\tau-\tau_0+1,\tau}} > ATE_i^{99} \\ 0 & \text{otherwise} \end{cases} \quad (21)$$

1
2
3
4
5
6
7
8
9
10
11
12
13
14
15
16
17
18
19
20
21
22
23
24
25
26
27
28
29
30
31
32
33
34
35
36
37
38
39
40
41
42
43
44
45
46
47
48
49
50
51
52
53
54
55
56
57
58
59
60
61
62
63
64
65

369 where $\mu_{E_i^{\tau-\tau_0+1,\tau}}$ indicates the moving average of the errors for each spring i computed over the
370 sliding window $[\tau - \tau_0 + 1, \tau]$. Thus, when the error value E_i^τ at time step τ , for spring i , exits
371 the healthy region defined by the thresholds ATE_i^1 and ATE_i^{99} , the fault indicator value is set to
372 1, indicating a possible damage is occurring in spring i . By so doing, alarms should be triggered
373 only in presence of persistent variations of the signal $\mu_{E_i^{\tau-\tau_0+1,\tau}}$, as those induced by damages,
374 filtering out random fluctuations due to noises and disturbances. Indeed, the choice of the width
375 of the window of the moving average-based filter is again another of those long-standing diagnostic
376 problems: here, in order to reduce the number of parameters to be tuned and to make the algorithm
377 as automatic as possible, the width of the window is taken equal to that used for the definition of
378 the error thresholds, i.e., τ_0 . Besides the convenience associated to the reduction of the tunable
379 algorithm parameters, the choice also intuitively makes sense, in that the use of different widths
380 for the definition of the automatic thresholds and for its operative use might, perhaps, introduce
381 biases caused by different samples size considered in each window, thus leading to a less robust
382 monitoring performance. Note that, due to the well-known properties of a moving average, the
383 wider the window is, the more robust the algorithm is with respect to false alarms due to spurious
384 fluctuations of the error, at the price though of being slower in detecting anomalies. On the other
385 hand, the narrower the window is, the faster the algorithm is, at the price of a potentially high
386 false alarm rate.

387 Following the same procedure described above, a binary, deterministic fault indicator for each
388 spring i is defined also with respect to the squared error:

$$Id_{SE,i}^{\tau-\tau_0+1,\tau} = \begin{cases} 1 & \text{if } \mu_{SE_i^{\tau-\tau_0+1,\tau}} > ATSE_i^{99} \\ 0 & \text{otherwise} \end{cases} \quad (22)$$

389 The introduction of the moving average-based filter renders the algorithm less sensitive to
390 random fluctuations. However, as it will be shown in Section 3, false alarms might still be present
391 and even missed alarms, if the algorithm is too slow and no detection is achieved within a reasonable
392 time horizon, before the damage evolves to catastrophic levels. Thus, an alternative indicator based
393 on a different perspective is here proposed to further support any decision making process based
394 on this algorithm. In particular, in order to be able to account for the uncertainties arising from
395 the employment of the deterministic indicators, two probabilistic fault indicators are introduced:

$$Ip_{E,i}^{\tau-\tau_0+1,\tau} = \frac{\sum_{j=\tau-\tau_0+1}^{\tau} Id_{E,i}^j}{\tau_0} \quad (23)$$

$$Ip_{SE,i}^{\tau-\tau_0+1,\tau} = \frac{\sum_{j=\tau-\tau_0+1}^{\tau} Id_{SE,i}^j}{\tau_0} \quad (24)$$

1
2
3
4
5
6
7
8
9
10
11
12
13
14
15
16
17
18
19
20
21
22
23
24
25
26
27
28
29
30
31
32
33
34
35
36
37
38
39
40
41
42
43
44
45
46
47
48
49
50
51
52
53
54
55
56
57
58
59
60
61
62
63
64
65

396 where the fault indicators $Id_{E,i}^\tau$ and $Id_{SE,i}^\tau$ are the instantaneous counterparts of the previously
397 introduced $Id_{E,i}^{\tau-\tau_0+1,\tau}$ and $Id_{SE,i}^{\tau-\tau_0+1,\tau}$, evaluated at time step τ :

$$Id_{E,i}^\tau = \begin{cases} 1 & \text{if } E_i^\tau < ATE_i^1 \vee E_i^\tau > ATE_i^{99} \\ 0 & \text{otherwise} \end{cases} \quad (25)$$

$$Id_{SE,i}^\tau = \begin{cases} 1 & \text{if } SE_i^\tau > ATSE_i^{99} \\ 0 & \text{otherwise} \end{cases} \quad (26)$$

399 At a first sight, the definition of the indicators $Ip_{E,i}^{\tau-\tau_0+1,\tau}$ and $Ip_{SE,i}^{\tau-\tau_0+1,\tau}$ apparently just shifts
400 the application of the moving average from the instantaneous errors $E_i^{1:\tau_0}$ and $SE_i^{1:\tau_0}$ to the de-
401 terministic instantaneous indicators $Id_{E,i}^\tau$ and $Id_{SE,i}^\tau$, respectively. However, this simple operation
402 allows a probabilistic interpretation of the results, which, as it shall be shown in the next Section,
403 enriches the information conveyed by the diagnostic module, since it accounts for the uncertainties
404 involved in the estimation process.

405 3 Case Study

406 The structure considered in this case study is modelled on the basis of the MDOF system shown
407 in Figure 1, considering six degrees of freedom. The structural parameter values characterizing
408 the 6-DOF model are taken from the work in [39], i.e., $m_i = 1kg \forall i = 1, \dots, n$, $k_j = 10^4 \frac{N}{m}$ and
409 $c_j = 20 \frac{N \cdot s}{m}$ (i.e., $\beta = 2 \cdot 10^{-3}$) $\forall j = 1, \dots, n + 1$. The process noises are described by normal
410 distributions with zero mean and variances $\sigma_{w,position}^2 = 10^{-16}m^2$, $\sigma_{w,speed}^2 = 10^{-16} \frac{m^2}{s^2}$, $\sigma_{w,spring}^2 =$
411 $20 \frac{N^2}{m^2}$ and $\sigma_{w,damping}^2 = 8 \cdot 10^{-13}$ for position, velocity, stiffness and damping proportionality constant
412 states, respectively, whereas the acceleration measurement noise variance is taken $\sigma_v^2 = 20 \frac{m^2}{s^4}$. Note
413 that the variance of the process noise related to the damping proportionality constant is set so that
414 the same standard deviation to nominal value ratio is achieved for damping and stiffness values.

415 First, the performances of the PF algorithm will be analyzed for the case the 6-DOF system
416 is not affected by damages and it operates with all the elements at a constant temperature. The
417 reference state evolution x_{ref}^τ is syntetically generated according to equations 3 and 4, using the
418 stiffness values of the healthy baseline (i.e., $k_j = 10^4 \frac{N}{m} \forall j = 1, \dots, n + 1$) and the related damping
419 values obtained through the proportionality constant β . The synthetic acceleration measurements
420 a_i^τ of each mass m_i are then calculated on the basis of the reference state evolution x_{ref}^τ by using
421 equation 9. Then, damages will be artificially introduced and, at the same time, the temperature
422 will be varied in time. A new reference state evolution x_{ref}^τ will be generated and, accordingly, a
423 new set of synthetic acceleration measurements will be computed.

3.1 Undamaged structure with constant temperature

The structural elements are assumed to be in equilibrium with the external temperature, constant and equal to $T = 0^\circ C$. The time horizon of the analysis is $T_{hor} = 8s$, discretized in $N_t = 1.2 \cdot 10^4$ time intervals of width $dt = 0.667ms$ each. The 6-DOF system is excited by an external sinusoidal load $F_1 = 40 \sin(25 \cdot 2\pi t) N$ applied to mass m_1 . Note that applying external forces for monitoring the health state of structures is typical in the SHM field. For instance, bridges may be excited by means of servo-hydraulic vibration generators [60] or electrodynamic shakers [61], to cite some, which are tools that can excite structures with prescribed force patterns, such as sinusoidal forces or random vibrations. The sampling frequency is $f_s = 1/dt = 1500Hz$, which turns out to be sufficiently larger than the forcing function frequency $f_{force} = 25Hz$, thus satisfying the Shannon sampling theorem. The particles values are initialized as follows:

- the position and velocity states estimates are initialized according to a normal distribution with zero mean and variance $\sigma_{w,position}^2 = 10^{-16}m^2$ and $\sigma_{w,speed}^2 = 10^{-16}\frac{m^2}{s^2}$, respectively;
- the stiffnesses and damping coefficient values are initialized to a random number between the 90% and the 110% of the actual state value to be estimated.

The objective of this first case study is that of testing the behavior of the PF in estimating the model stiffnesses. It is worth reminding that the state estimator proposed here is the mean of the posterior pdf of equation 11. To this aim, a particle filter with 10^4 particles is used for estimating the whole state vector \mathbf{x}^τ at each time step τ , according to the procedure outlined in Section 2.1. Figure 3 shows the state estimates (coloured lines) for only the spring stiffnesses k_2, k_4, k_6 and k_7 , i.e., the mean value of the respective marginal state posterior pdf. The estimates of the other stiffnesses (k_1, k_3 and k_5) show very similar behaviors, so they are not shown here for brevity's sake. It can be seen that all the stiffnesses are satisfactorily estimated, after a fast transient needed to pass from the initial value to the actual one. It is however important to further delve into the performance of the PF, since the estimated stiffnesses will then be fed to the autoencoders, so that any estimation error will propagate and affect the diagnostic module outputs.

Thus, in order to quantify the quality of the stiffness estimates, the root mean square error (RMSE) is calculated over T_{hor} for all the stiffness estimates. The results are compared in Table 1, column 2. Spring 1 is the one characterized by the maximum RMSE value, followed by springs 6 and 7. No increasing trend seems to characterize the RMSE as the springs move away from the point of application of the excitation. In order to improve the statistics of the estimates, a new simulation with $3 \cdot 10^4$ particles is then run. Figure 4 shows the PF-based estimates, which, on a first visual inspection, seems to be better than before, as confirmed by the RMSEs reported in Table 1, column 3. Moreover, the RMSE values obtained with $3 \cdot 10^4$ particles seem not to exhibit the same trend observed before among the different springs, with spring 1 still being the one characterized by the maximum RMSE, followed now by spring 2. Unfortunately, due to the non-linearity of the state space in equations 3 and 4, it is not an easy task to draw any conclusions on this analysis,

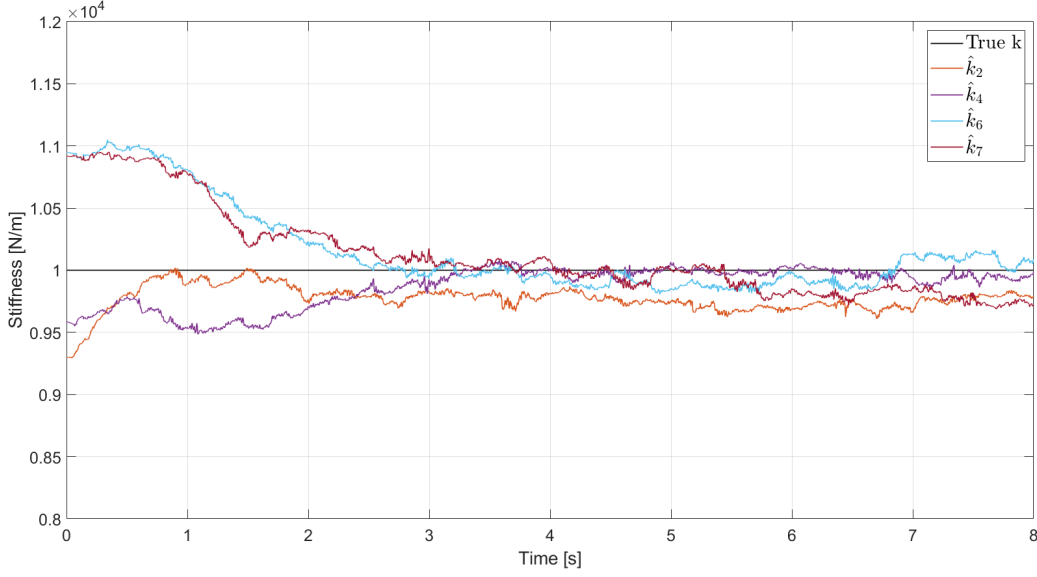


Figure 3: Temporal evolution of the particle filter stiffness estimates and reference stiffness values (black) of springs $i = 2$, $i = 4$, $i = 6$ and $i = 7$ - undamaged scenario with excitation force applied at mass m_1 and 10^4 particles.

Component	RMSE @ 10k particles $\left[\frac{N}{m}\right]$	RMSE @ 30k particles $\left[\frac{N}{m}\right]$
Spring 1	450.0	452.0
Spring 2	250.0	228.0
Spring 3	143.2	90.1
Spring 4	211.2	62.5
Spring 5	201.8	132.9
Spring 6	388.2	102.2
Spring 7	373.7	153.8

Table 1: PF estimates of k_2 , k_4 , k_6 and k_7 in the undamaged scenario, with excitation applied at mass m_1 .

which is also out of the scope of this work. In any case, it has been verified that an increase in the number of particles used in the PF improves the performances.

The simulations are performed using a laptop with 16GB RAM and six physical Intel Core i7-9750H CPUs. The mean time required by the PF for estimating the 8s time history with $3 \cdot 10^4$ particles is approximately four times the mean time required using 10^4 particles. The computational times are slightly higher than the expected linear increase with the number of particles. That is due to the fact that some background processes always run in the computer and that the code is not completely computationally efficient, since the main goal of this work is to test a new SHM algorithm.

For completeness, some simulations have been carried out where the position and also the

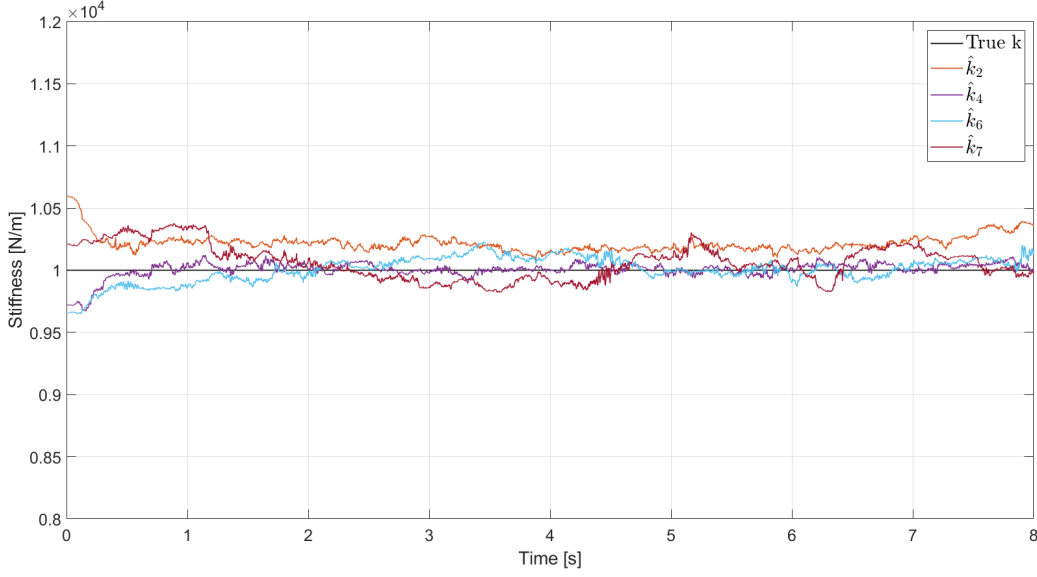


Figure 4: Temporal evolution of the particle filter stiffness estimates and reference stiffness values (black) of springs $i = 2$, $i = 4$, $i = 6$ and $i = 7$ - undamaged scenario with excitation force applied at mass m_1 and $3 \cdot 10^4$ particles.

number of exciting loads was varied, obtaining different behaviors, but it was not possible to identify any clear scheme, so they are not reported here for brevity's sake. In what follows, the algorithm will be always demonstrated with respect to the springs 2, 4, 6 and 7, keeping in mind that an increase in the number of particles can always reduce the fluctuations and, consequently, improve the results, provided enough computational resources are available.

3.2 Damaged structure with temperature variation in time

The same model of Section 3.1 is here considered. Before running the estimation simulation, the healthy baseline for the autoencoders training is acquired by simulating the system with no damages and by simultaneously running the PF for estimating the model stiffnesses over $N_t = 1.2 \cdot 10^4$ time steps of width $dt = 0.667ms$ each, corresponding to a baseline time horizon of $T_{hor}^{baseline} = 8s$, during which the temperatures of all the structural elements are assumed to be in equilibrium with an external temperature linearly varying from $-30^\circ C$ to $100^\circ C$ with step $0.1^\circ C$. The range of temperature variation has been chosen wide enough to guarantee the autoencoders are trained over an input space which almost surely contains examples of temperatures that will be encountered during operation. Indeed, this is possible only in artificially generated case studies, as in the present work, or in all those applications where a temperature-controlled environment can be created; in real applications this is not generally possible, and a long baseline should be acquired in order to ensure the temperature range is sufficiently represented.

Note that, for simplicity and with no loss of generality, all the springs are subjected to the

490 same temperature. As verified by the authors, but not reported here for the sake of brevity, the
491 algorithm can effectively cope with the effects of a spatial temperature gradient, i.e., temperatures
492 varying across the elements of the structure. In fact, the spring stiffness-temperature relationship
493 is independently “encoded” spring by spring, so that a spatially non-uniform temperature varia-
494 tion can only affect the dynamics of the system, which is fully captured by the PF, similarly to
495 considering different stiffness values amongst the degrees of freedom.

496 The baseline is then constructed by associating the temperature observations, either generated
497 at time step τ using $\hat{T}^\tau = T^\tau + w_T^\tau$, where w_T^τ is the temperature observation noise, which in the
498 present work is $w_T^\tau \sim N(0, 0.1)^\circ C$, or directly acquired in the field, to the PF-based estimates of the
499 model stiffnesses. A total of $N_t = 1.2 \cdot 10^4$ examples per spring are thus generated, which are used for
500 training seven autoencoders, each associated to a different spring of the model and characterized by
501 the architecture described in Section 2.2. The construction of the autoencoders and their training
502 have been performed resorting to the MATLAB Deep Learning ToolboxTM. Once the autoencoders
503 are properly trained, it is possible to put them on-line according to the scheme illustrated in Section
504 2.2. In order to test the diagnostic module over a time span larger than in the undamaged case,
505 the time horizon of the analysis is now extended to $T_{hor} = 40s$, discretized into $N_t = 6 \cdot 10^4$
506 time steps of $0.667ms$ each. By so doing, we let the algorithm settle after damages are artificially
507 introduced in the system. Again, the structural elements are assumed to be in equilibrium with
508 the external temperature, which is let decrease linearly from $40^\circ C$ to $10^\circ C$ within the time horizon
509 T_{hor} . Two different damages are assumed that can occur in the structure, i.e., a sudden drop in
510 the structural stiffness value of a spring and a progressive degradation. We consider the cases of
511 (i) a sudden damage consisting of a 10% reduction of the stiffness value associated to spring 7 (the
512 most critical one), occurring at time $t = 10.0s$, and (ii) a progressive, linear decrease of the stiffness
513 value associated to spring 4, occurring at time $t = 13.3s$ and leading to a final stiffness value (at
514 T_{hor}) equal to the 43% of the corresponding healthy one at the same temperature, i.e., at $10^\circ C$.
515 Those damage values are typical in the SHM field and are different enough to allow testing the
516 proposed methodology both with minor stiffness degradations, i.e., 10%, and with more significant
517 ones, i.e., the 57% stiffness reduction modelled on spring 4 [62, 63].

518 The system dynamics is simulated, according to the equations presented in Section 2.1, starting
519 from the following initial state vector values:

$$50 \quad x_i^0 = 0 \text{ m} \quad \forall i = 1, \dots, n \quad (27a)$$

$$52 \quad y_i^0 = 0 \frac{\text{m}}{\text{s}} \quad \forall i = 1, \dots, n \quad (27b)$$

$$54 \quad k_j^0 = 9440 \frac{\text{N}}{\text{m}} \quad \forall j = 1, \dots, n + 1 \quad (27c)$$

$$58 \quad \beta^0 = 2 \cdot 10^{-3} \quad (27d)$$

523 where k_j^0 represents the j -th spring stiffness at the initial temperature $T^0 = 40^\circ C$. A PF with

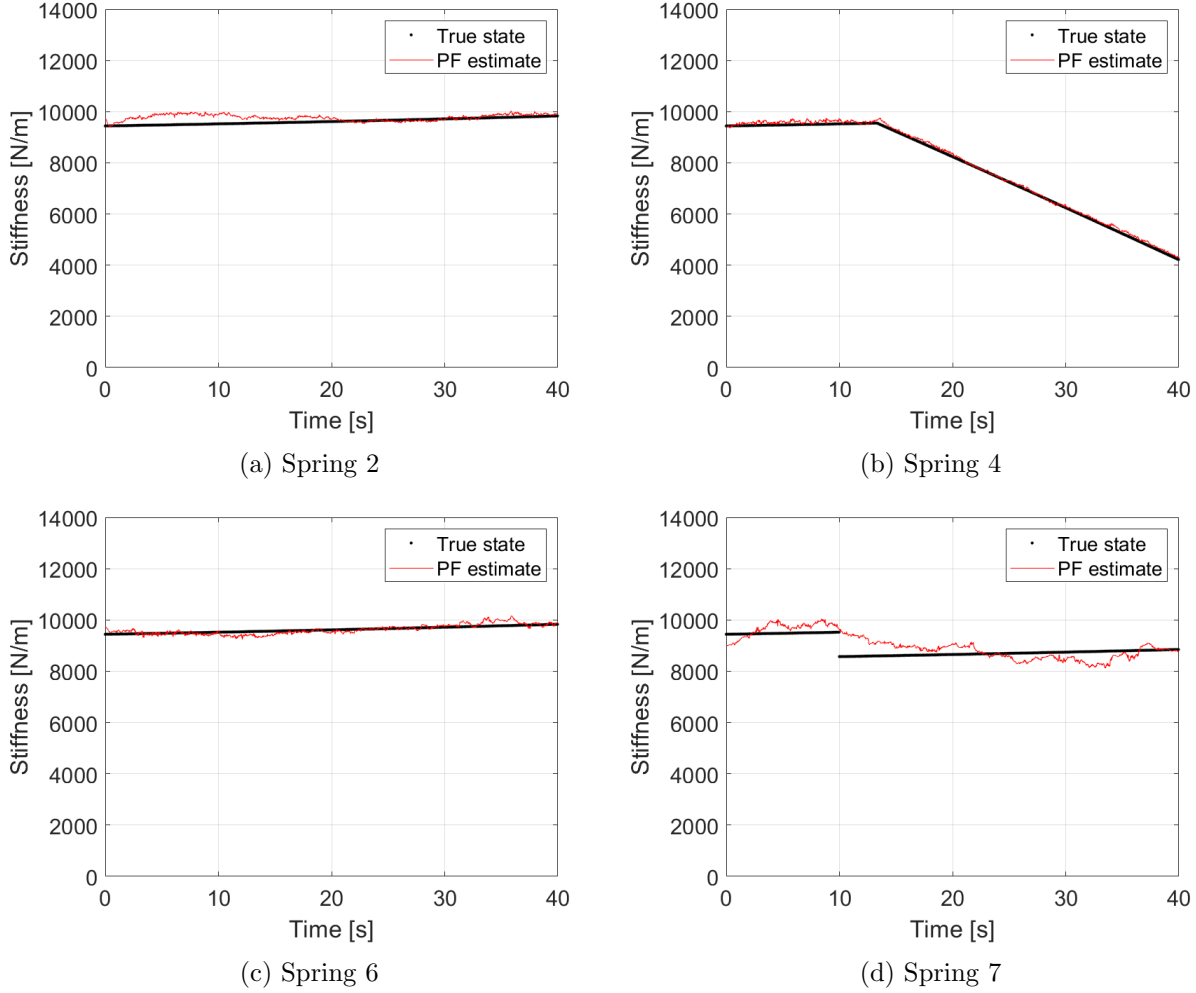


Figure 5: Temporal evolution of the particle filter stiffness estimates (red) and true stiffness values (black) of spring $i = 2$ (a), $i = 4$ (b), $i = 6$ (c) and $i = 7$ (d).

3 · 10⁴ particles is used for estimating the whole state vector \mathbf{x}^τ at each time step τ , according to the procedure outlined in Section 2.1. Figure 5 shows the state estimates (red lines) and the corresponding reference values (black) of the spring stiffnesses $k = 2$ (a), $k = 4$ (b), $k = 6$ (c) and $k = 7$ (d). As expected, the PF performances appear to be satisfactory, even in presence of the damages, with quite fast settling times. Indeed, while sudden changes might probably be detected just by processing the PF estimates, the slower, progressive damages may not easily be distinguished from the temperature effects. That is the case of slow progressive degradations, with characteristic time close to the one driving the stiffness change due to temperature effects. However, that is not the case of the present study, in which the progressive degradation damage is clearly visible just by looking at the PF estimate (Figure 5b).

The PF-estimated stiffness values and the temperature measurements, corrupted with noise according to the same procedure aimed at building the healthy baseline illustrated in this Section,

1
2
3
4
5
6
7
8
9
10
11
12
13
14
15
16
17
18
19
20
21
22
23
24
25
26
27
28
29
30
31
32
33
34
35
36
37
38
39
40
41
42
43
44
45
46
47
48
49
50
51
52
53
54
55
56
57
58
59
60
61
62
63
64
65

are then fed, in real time at each time step τ , to the seven autoencoders. Figure 6 shows the time evolution of the error E_i^τ between the input and output values of the autoencoder (solid lines), calculated according to equation 16, its average over the time window of width τ_0 time steps, i.e., $\mu_{E_i^{\tau-\tau_0+1,\tau}}$ (black, dashed lines), and the corresponding automatic thresholds ATE_i^1 and ATE_i^{99} (red, dashed and dotted lines), for the stiffnesses k_2 , k_4 , k_6 and k_7 . The first τ_0 time steps of the analysis are used to automatically set the error thresholds for each stiffness in the system, implicitly assuming the system is in its healthy state at early times. Accordingly, the thresholds are reported in the Figure only after the healthy baseline processing is completed. At the same time, Figure 7 is built following the same procedure, but using the squared error SE_i^τ between the input and output values of the autoencoder (see equation 15), its average over the time window of width τ_0 time steps, i.e., $\mu_{SE_i^{\tau-\tau_0+1,\tau}}$, and the associated automatic threshold $ATSE_i^{99}$, for the stiffnesses k_2 , k_4 , k_6 and k_7 . Note that different scales have been used for each sub-Figure due to the fact that, at the end of the simulation, the error E_4^τ and squared error SE_4^τ related to spring number 4 are much greater than those associated to k_2 , k_6 and k_7 . The corresponding deterministic fault indicators $Id_{E,i}^{\tau-\tau_0+1,\tau}$ and $Id_{SE,i}^{\tau-\tau_0+1,\tau}$ are shown in Figures 8 and 9, respectively, whereas their probabilistic counterparts $Ip_{E,i}^{\tau-\tau_0+1,\tau}$ and $Ip_{SE,i}^{\tau-\tau_0+1,\tau}$ are shown in Figures 10a and 10b, respectively, for the stiffnesses k_2 , k_4 , k_6 and k_7 . Although no damages are introduced on spring $i = 2$, the mean error associated to stiffness k_2 (Figure 6a) exits the healthy region in a brief time window centred at $t = 30s$, re-entering it by the end of the simulation. Differently, the mean squared error associated to stiffness k_2 never exceeds the automatic threshold $ATSE_2^{99}$ (Figure 7a). Accordingly, the deterministic damage indicator $Id_{E,2}^{\tau-\tau_0+1,\tau}$ is triggered at time $t = 26.1s$ and deactivated after 8.6s (Figure 8a), while $Id_{SE,2}^{\tau-\tau_0+1,\tau}$ is always equal to zero (Figure 9a), not triggering any diagnostic alarm. The probabilistic indicator, or probability of damage occurrence, $Ip_{E,2}^{\tau-\tau_0+1,\tau}$ reaches a peak value of 85% within the mission time, while $Ip_{SE,2}^{\tau-\tau_0+1,\tau}$ always remains null. Instead, both the mean error and the mean squared error associated to stiffness k_4 exceed the automatic thresholds $\{ATE_4^1, ATE_4^{99}\}$ and $ATSE_4^{99}$ (Figures 6b and 7b, respectively). That is coherent with the fact that a progressive degradation damage is introduced in that spring starting from time $t = 13.3s$. In particular, the error mean value $\mu_{E_4^{\tau-\tau_0+1,\tau}}$ exceeds the one of the related threshold with a time delay from the time instant in which the damage is introduced evaluated in $T_{4,E} = 3.0s$. Similarly, the squared error mean value $\mu_{SE_4^{\tau-\tau_0+1,\tau}}$ exceeds the one of the related threshold with a time delay evaluated in $T_{4,SE} = 3.0s$. Accordingly, the deterministic damage indicators $Id_{E,4}^{\tau-\tau_0+1,\tau}$ and $Id_{SE,4}^{\tau-\tau_0+1,\tau}$ (Figures 8b and 9b, respectively) are raised at the time the related mean error and mean squared error values exit the healthy region. The probabilistic indicators $Ip_{E,4}^{\tau-\tau_0+1,\tau}$ and $Ip_{SE,4}^{\tau-\tau_0+1,\tau}$ clearly identify the damage on spring $i = 4$, reaching, after a brief transient phase, the unit value, which is kept constant until the end of the analysis. Coherently with the fact that no damages are introduced on spring $i = 6$, the mean squared error associated to stiffness k_6 (Figure 7c) never exceeds the automatic threshold $ATSE_6^{99}$. However, the same consideration is not true for the mean error value. In fact, according to Figure 6c, the $\mu_{E_6^{\tau-\tau_0+1,\tau}}$ value exits the healthy region at time $t = 14.0s$, re-entering it after 4.6s. That behaviour is reflected on the deterministic fault indicators. In fact, while the

575 indicator $Id_{SE,6}^{\tau-\tau_0+1,\tau}$ (Figure 9c) is always equal to zero, not triggering any diagnostic alarm, the
 576 one related to the non-squared error (Figure 8c) is raised at time $t = 14.0s$, and is turned off at time
 577 $t = 18.6s$. Accordingly, also the probabilistic indicators $Ip_{E,6}^{\tau-\tau_0+1,\tau}$ and $Ip_{SE,6}^{\tau-\tau_0+1,\tau}$ have a slightly
 578 different behaviour. In fact, the squared error based probability of damage occurrence outperforms
 579 the error based one, determining a maximum value $max(Ip_{SE,6}^{\tau-\tau_0+1,\tau}) = 6\%$, while according to
 580 $Ip_{E,6}^{\tau-\tau_0+1,\tau}$ a maximum damage probability of 71% is estimated. Finally, both the mean error
 581 and the mean squared error associated to stiffness k_7 exceed the respective automatic thresholds
 582 (Figures 6d and 7d, respectively). That is coherent with the fact that a step damage is introduced
 583 in that spring starting from time $t = 10s$. In particular, the error mean value $\mu_{E_7}^{\tau-\tau_0+1,\tau}$ exceeds
 584 the one of the related threshold with a time delay from the time instant in which the damage is
 585 introduced evaluated in $T_{7,E} = 7.2s$. Similarly, the squared error mean value $\mu_{SE_7}^{\tau-\tau_0+1,\tau}$ exceeds
 586 the one of the related threshold with a time delay evaluated in $T_{7,SE} = 7.3s$. Accordingly, the
 587 deterministic damage indicators $Id_{E,7}^{\tau-\tau_0+1,\tau}$ and $Id_{SE,7}^{\tau-\tau_0+1,\tau}$ (Figures 8d and 9d, respectively) are
 588 raised at the time the related mean error and mean squared error values exit the healthy region.
 589 The probabilistic indicators $Ip_{E,7}^{\tau-\tau_0+1,\tau}$ and $Ip_{SE,7}^{\tau-\tau_0+1,\tau}$ clearly identify the damage on spring $i = 7$,
 590 reaching, after a brief transient phase, the unit value, which is kept constant until the end of the
 591 analysis. [All the results presented above are summarized in table 2.](#)

Damage indicator	Performace
$Id_{E,2}$	X - Short false alarm
$Id_{E,4}$	✓ - Damage identified
$Id_{E,6}$	X - Short false alarm
$Id_{E,7}$	✓ - Damage identified
$Id_{SE,2}$	✓ - Correctly classified as healthy
$Id_{SE,4}$	✓ - Damage identified
$Id_{SE,6}$	✓ - Correctly classified as healthy
$Id_{SE,7}$	✓ - Damage identified
$Ip_{E,2}$	X - False damage probability > 50%
$Ip_{E,4}$	✓ - Damage identified
$Ip_{E,6}$	X - False damage probability > 50%
$Ip_{E,7}$	✓ - Damage identified
$Ip_{SE,2}$	✓ - Damage identified
$Ip_{SE,4}$	✓ - Correctly classified as healthy
$Ip_{SE,6}$	✓ - Correctly classified as healthy
$Ip_{SE,7}$	✓ - Damage identified

Table 2: Summary table of the damage indicators for springs 2, 4, 6 and 7.

4 Discussion

The model-based framework presented in this work offers the advantage that, in real applications, most algorithm parameters can be set up by trial-and-error procedures during a preliminary, purely numerical phase, where the dynamic behavior of the system and the associated acceleration measurements are synthetically generated using the process and the measurement equations. The calibrated parameters are probably not “optimal” for the real application, due to the model errors, but would certainly guarantee satisfactory performances of the algorithm. For instance, the performance of the whole framework significantly depends on the performance of the PF, which, in turn, is quite sensitive to both the measurement and the process noise. While the measurement noise is related to the precision of the sensors (although there might also be some calibration margin), the process noise is well-known to be mainly a filter calibration factor, not easily identifiable a-priori. The suggestion is then to calibrate the process noise by means of a trial-and-error approach, also according to common practice in the literature [64, 65]. Another example is represented by the detection thresholds, which are set according to specific percentiles of the pdfs of the squared error and the error defined by equations 15 and 16, respectively, the calibration of which is again suggested via a trial-and-error procedure, with the ultimate goal of establishing a trade-off between false alarms rate and raising time for damage alarms. The usual percentiles considered in statistics may be adopted, e.g., 95th, 99th and 99.9th percentile. The greater the percentile, the smaller the false alarms rate, albeit at the price of an increase in the raising time for damage detection. As far as the autoencoders are concerned, the healthy baseline acquisition should be performed over a temperature range sufficiently wide to cover most of the temperatures the structure will experience during its operational life. Since this may be a lengthy process, it is suggested to start acquiring the baseline right after the structure installation, i.e., when the structure is reasonably still healthy, start using the diagnostic tool and keep re-training the autoencoders as new temperature ranges are experienced. Another possible strategy may be that of numerically generating the missing examples of the relationship between temperature and stiffness by using some sufficiently accurate material model, which would provide a hybrid experimental-numeric baseline for training the autoencoders. This procedure has the advantage of potentially covering any temperature range, at the risk of introducing modelling errors that would certainly affect the diagnostic performances.

5 Conclusions

This study proposes a novel combination of particle filter and neural network-based autoencoder to identify the structural parameters of mechanical and/or civil structures modelled as mono-dimensional MDOF systems, and to perform damage diagnosis (both detection and localization) in presence of changing environmental conditions. The case study reported in Section 3 demonstrates that the developed framework is capable of providing a real-time temporal estimation of the stiffness of each spring in the MDOF system, by means of accelerations measurements only, and of assessing the health status of the structure under analysis, successfully detecting and localizing eventual

1
2
3
4
5 630 damages.

6
7 631 The particle filter stiffness estimation process is able to detect any change in the stiffness value
8 632 of the components of the system, however it cannot provide by itself any information about the
9 633 cause of that variation. In fact, structural properties may vary both in case of damage and in
10 634 presence of changing external conditions. Note that, in this study, only temperature is considered
11 635 amongst the external conditions capable of changing the stiffness properties in the healthy condi-
12 636 tion of the system. Thus, a properly trained auto-associative neural network has to be coupled
13
14 637 with the PF in order to offset the effects of temperature variations on structural dynamics. A
15 638 healthy baseline covering the whole range of operating conditions is first acquired with the purpose
16 639 of performing the learning phase of the autoencoder. In the operational phase, the mean values
17 640 of the error and of the squared error between input and output variables of the neural networks,
18 641 determined over a moving time window which considers the last τ_0 time steps before the actual
19 642 one, are compared to the respective automatic thresholds, thus eventually triggering the related
20 643 automatic fault indicator, $Id_{E,i}^{\tau-\tau_0+1,\tau}$ and $Id_{SE,i}^{\tau-\tau_0+1,\tau}$, respectively, for the detection and localization
21 644 of structural damages. However, occasional false alarms are also triggered due to oscillations in the
22 645 particle filter estimates, hence a probabilistic, more robust fault indicator is introduced with the
23 646 purpose of mitigating this problem, i.e., $Ip_{E,i}^{\tau-\tau_0+1,\tau}$ and $Ip_{SE,i}^{\tau-\tau_0+1,\tau}$, respectively for the error and
24 647 the squared error between the input and the output of the autoencoder. The probabilistic fault
25 648 indicators provide satisfactory results in terms of detection and localization of structural damages,
26 649 however their robustness should be further investigated testing more complex systems. Moreover,
27 650 the failure probability of undamaged springs may be further decreased by better estimating the
28 651 structural characteristics, thus damping out the eventual oscillations of the particle filter estimates.
29 652 Indeed, as discussed in Section 3.1, increasing the number of particles may be beneficial to that
30 653 purpose. However, since the computational time required is more than proportional to the num-
31 654 ber of particles considered in the analysis, this strategy may severely compromise the algorithm
32 655 real-time capabilities. Overall, the squared error-based deterministic fault indicator outperforms
33 656 the error-based one, in that the former does not present any false alarm, while the latter may
34 657 erroneously identify damage in healthy springs, as already discussed in Section 3.2. The same
35 658 consideration also holds for the probabilistic indicators, with the squared error-based one providing
36 659 lower damage probability of the healthy springs with respect to the error-based one. Moreover,
37 660 the fault indicators relying on the error value and the ones relying on the squared error value raise
38 661 alarms with comparable time delays from the actual damage instants.

39
40
41
42
43
44
45
46
47
48
49
50
51
52 662 The proposed method is believed to be ready to be employed to real structures, provided that
53 663 some key points are considered: (i) the autoencoders database may be built by installing sensors
54 664 on the structure, acquiring the baseline in its early life, confidently assuming that the structure is
55 665 healthy right after being installed or built; (ii) the baseline acquisition process should be long enough
56 666 to capture the whole expected temperature variability during the operational life of the monitored
57 667 structure, in order to allow the autoencoders working in the learnt space during the diagnostic

1
2
3
4
5 668 phase; (iii) the temperatures may be acquired using at least one sensor per degree of freedom, to
6 669 consider temperature variability in time and space and (iv) at least one accelerometer per DOF
7 670 should be installed on the structure. However, more sensors may be installed on the structure
8
9 671 both for redundancy and for collecting more information about the single DOF, which may not be
10 672 a concentrated entity in the real world, in order to determine the corresponding acceleration and
11
12 673 temperature values.

13
14 674 Not all the open issues have been properly addressed. Further work is required to test the ro-
15 675 bustness of the damage detection and localization procedure with respect to different environmen-
16 676 tal/operating conditions (other than temperature). For instance, in case of structures significantly
17
18 677 affected by traffic and/or wind loads, a typical SHM problem in large infrastructures, these could
19 678 be considered as different/additional forcing terms, as they do not directly influence the stiffness
20
21 679 properties of the structure. In this regard, performing the diagnostic task only on the basis of
22 680 vibration signals induced by environmental/operative loads (wind, traffic, etc.) would be more
23
24 681 practical in realistic scenarios, yet more challenging, mainly due to the random nature of this kind
25 682 of excitations. Finally, the effectiveness of the proposed methodology with non-linear behaviours
26
27 683 and non-Gaussian noise could be also investigated, with the aim of increasing its generality.

30 684 **References**

- 31
32 685 [1] Dan M. Frangopol and Min Liu. Maintenance and management of civil infrastructure based on
33
34 686 condition, safety, optimization, and life-cycle cost. *Structure and Infrastructure Engineering*,
35 687 3(1):29–41, 2007.
- 36
37 688 [2] Lisa Ziegler, Elena Gonzalez, Tim Rubert, Ursula Smolka, and Julio J. Melero. Lifetime
38
39 689 extension of onshore wind turbines: A review covering germany, spain, denmark, and the uk.
40 690 *Renewable and Sustainable Energy Reviews*, 82:1261 – 1271, 2018.
- 41
42 691 [3] J. Courrech and M. Gaudet. Envelope analysis - the key to rolling-element
43
44 692 bearing diagnosis. *Bruel & Kjaer internal document*. available online at
45 693 <https://www.bksv.com/media/doc/BO0187.pdf>.
- 46
47 694 [4] U. Dackermann, W. A. Smith, R. B. Randall. Damage identification based on response-
48
49 695 only measurements using cepstrum analysis and artificial neural networks. *Structural Health*
50 696 *Monitoring*, 13(4):430–444, 2014.
- 51
52 697 [5] Chris Mechefske. Machine condition monitoring and fault diagnostics. In Clarence W. de Silva,
53 698 editor, *Vibration and Shock Handbook*, chapter 25. CRC Press, Taylor and Francis Group, Boca
54
55 699 Raton, FL, 2005.
- 56
57 700 [6] Timothy J. Johnson and Douglas E. Adams. Transmissibility as a differential indicator of
58
59 701 structural damage. *Journal of Vibration and Acoustics*, 124, 10 2002.

1
2
3
4
5
6
7
8
9
10
11
12
13
14
15
16
17
18
19
20
21
22
23
24
25
26
27
28
29
30
31
32
33
34
35
36
37
38
39
40
41
42
43
44
45
46
47
48
49
50
51
52
53
54
55
56
57
58
59
60
61
62
63
64
65

[7] Nuno M.M. Maia, Raquel A.B. Almeida, Antonio P.V. Urgueira, and Rui P.C. Sampaio. Damage detection and quantification using transmissibility. *Mechanical Systems and Signal Processing*, 25(7):2475–2483, 2011.

[8] G. Manson and K. Worden. Experimental validation of a structural health monitoring methodology: Part iii. damage location on an aircraft wing. *Journal of Sound and Vibration*, 259(2):365–385, 2003.

[9] M.J. Schulz, A.S. Abdelnaser, P.F. Pai, M.S. Linville and J. Chung. Detecting structural damage using transmittance functions. In *International Modal Analysis Conference, Orlando, Florida*, pages 638–644, 1997.

[10] M.J. Schulz, P.F. Pai and D.J. Inman. Health monitoring and active control of composite structures using piezoceramic patches. *Compos.: Part B*, 30(7):713–725, 1999.

[11] H. Zhang, M.J. Schulz, F. Ferguson and P.F. Pai. Structural health monitoring using transmittance functions. *Mech. Syst. Signal Process.*, 13(5):765–787, 1999.

[12] A. Ghoshal, M.J. Sundaresan, M.J. Schulz and P.F. Pai. Structural health monitoring techniques for wind turbine blades. *J. Wind Eng. Ind. Aerodyn.*, 85(3):309–324, 2000.

[13] V. Caccese. Detection of bolt load loss in hybrid composite/metal bolted connections. *Eng. Struct.*, 26(7):895–906, 2004.

[14] Simon Chesne and Arnaud Deraemaeker. Damage localization using transmissibility functions: A critical review. *Mechanical Systems and Signal Processing*, 38(2):569 – 584, 2013.

[15] Z.K. Peng and F.L. Chu. Application of the wavelet transform in machine condition monitoring and fault diagnostics: a review with bibliography. *Mechanical Systems and Signal Processing*, 18(2):199 – 221, 2004.

[16] H. Sohn. Effects of environmental and operational variability on structural health monitoring. *Philos. Trans. R. Soc. London A Math. Phys. Eng. Sci.*, 365(1851):539–560, 2007.

[17] C.R. Farrar, W.E. Baker, T.M. Bell, K.M. Cone, T.W. Darling, T.A. Duffey, A. Eklund, and A. Migliori. Dynamic characterization and damage detection in the i-40 bridge over the rio grande. *Technical Report*, 6 1994.

[18] M.P. Limongelli. Frequency response function interpolation for damage detection under changing environment. *Mechanical Systems and Signal Processing*, 24(8):2898 – 2913, 2010.

[19] Charles Farrar, S. W. Doebling, Phillip Cornwell, and Erik Straser. Variability of modal parameters measured on the alamosa canyon bridge. *Proceedings of International Modal Analysis Conference*, 1, 01 1997.

1
2
3
4
5
6
7
8
9
10
11
12
13
14
15
16
17
18
19
20
21
22
23
24
25
26
27
28
29
30
31
32
33
34
35
36
37
38
39
40
41
42
43
44
45
46
47
48
49
50
51
52
53
54
55
56
57
58
59
60
61
62
63
64
65

[20] B. Peeters and G. De Roeck. One-year monitoring of the z24-bridge: environmental effects versus damage events. *Earthq. Eng. Struct. Dyn.*, 30(2):149–171, 2001.

[21] K. Worden, H. Sohn, and C. R. Farrar. Novelty detection in a changing environment: regression and interpolation approaches. *J. Sound Vib.*, 258(4):741–761, 2002.

[22] C. P. Fritzen, G. Mengelkamp, and A. Guemes. Elimination of temperature effects on damage detection within a smart structure concept. *Struct. Heal. Monit.*, 10:15–17, 2003.

[23] K. Worden and E. J. Cross. On switching response surface models, with applications to the structural health monitoring of bridges. *Mech. Syst. Signal Process.*, 98:139–156, 2018.

[24] R. Ruotolo and C. Surace. Damage detection using singular value decomposition. *DAMAS 97*, 1997.

[25] A. M. Yan, G. Kerschen, P. De Boe, and J. C. Golinval. Structural damage diagnosis under varying environmental conditions - part ii: Local pca for non-linear cases. *Mech. Syst. Signal Process.*, 19(4):865–880, 2005.

[26] J. Kullaa. Is temperature measurement essential in structural health monitoring? *Proc. 4th Int. Workshop on Structural Health Monitoring*, pages 717–724, 2003.

[27] E. J. Cross, K. Worden, and Q. Chen. Cointegration: a novel approach for the removal of environmental trends in structural health monitoring data. *Proceedings of the Royal Society of London A: Mathematical, Physical and Engineering Sciences*, 467(2133):2712–2732, 2011.

[28] H. Shi, K. Worden, and E. J. Cross. A regime-switching cointegration approach for removing environmental and operational variations in structural health monitoring. *Mech. Syst. Signal Process.*, 103:381–397, 2018.

[29] H. Sohn, K. Worden, and C. R. Farrar. Statistical damage classification under changing environmental and operational conditions. *J. Intell. Mater. Syst. Struct.*, 13(9):561–574, 2002.

[30] William Soo Lon Wah, Yung-Tsang Chen. A new approach toward damage localization and quantification of structures under changing temperature condition. *Journal of Low Frequency Noise, Vibration and Active Control*, 2018.

[31] Anis Ben Abdesslem, Nikolaos Dervilis, David Wagg, and Keith Worden. Model selection and parameter estimation in structural dynamics using approximate bayesian computation. *Mechanical Systems and Signal Processing*, 99:306 – 325, 2018.

[32] Chunfeng Wan, Rui Huang, Liyuan Huang, Bo Wen, and Tadanobu Sato. Damage identification using particle filters. *Procedia Engineering*, 188:41 – 47, 2017. Structural Health Monitoring - From Sensing to Diagnosis and Prognosis.

1
2
3
4
5
6
7
8
9
10
11
12
13
14
15
16
17
18
19
20
21
22
23
24
25
26
27
28
29
30
31
32
33
34
35
36
37
38
39
40
41
42
43
44
45
46
47
48
49
50
51
52
53
54
55
56
57
58
59
60
61
62
63
64
65

[33] F. Cadini, E. Zio and G. Pelsoni. Particle filtering for the detection of fault onset time in hybrid dynamic systems with autonomous transitions. *IEEE Transactions on Reliability*, 61(1):130–139, 2012.

[34] Eleni Chatzi and Andrew Smyth. The unscented kalman filter and particle filter methods for nonlinear structural system identification with non-located heterogeneous sensing. *Structural Control and Health Monitoring*, 16:99 – 123, 02 2009.

[35] Chathurdara Sri Nadith Pathirage, Jun Li, Ling Li, Hong Hao, Wanquan Liu, and Pinghe Ni. Structural damage identification based on autoencoder neural networks and deep learning. *Engineering Structures*, 172:13 – 28, 2018.

[36] L.H. Yam, Y.J. Yan, and J.S. Jiang. Vibration-based damage detection for composite structures using wavelet transform and neural network identification. *Composite Structures*, 60(4):403 – 412, 2003.

[37] H. Sohn, K. Worden, and C. R. Farrar. Novelty detection using auto-associative neural network. *ASME International Mechanical Engineering Congress and Exposition, Proceedings*, 2:1525–1532, 2001.

[38] Chia-Ming Chang, Tzu-Kang Lin, and Chih-Wei Chang. Applications of neural network models for structural health monitoring based on derived modal properties. *Measurement*, 129:457 – 470, 2018.

[39] K. Worden. Structural fault detection using a novelty measure. *Journal of Sound and Vibration*, 201(1):85 – 101, 1997.

[40] I. S. Cade, P. S. Keogh, and M. N. Sahinkaya. Fault identification in rotor/magnetic bearing systems using discrete time wavelet coefficients. *IEEE/ASME Transactions on Mechatronics*, 10(6):648–657, Dec 2005.

[41] J.S. Sakellariou and S.D. Fassois. Stochastic output error vibration-based damage detection and assessment in structures under earthquake excitation. *Journal of Sound and Vibration*, 297(3):1048 – 1067, 2006.

[42] S. Marchesiello, A. Fasana, L. Garibaldi, and B.A.D. Piombo. Dynamics of multi-span continuous straight bridges subject to multi-degrees of freedom moving vehicle excitation. *Journal of Sound and Vibration*, 224(3):541 – 561, 1999.

[43] G.P. Cimellaro, S. Marasco. M dof systems. In *Introduction to Dynamics of Structures and Earthquake Engineering. Geotechnical, Geological and Earthquake Engineering, vol 45*. Springer, Cham, 2018.

[44] H.A. Nasrellah and C.S. Manohar. Finite element method based monte carlo filters for structural system identification. *Probabilistic Engineering Mechanics*, 26(2):294–307, 2011.

1
2
3
4
5
6
7
8
9
10
11
12
13
14
15
16
17
18
19
20
21
22
23
24
25
26
27
28
29
30
31
32
33
34
35
36
37
38
39
40
41
42
43
44
45
46
47
48
49
50
51
52
53
54
55
56
57
58
59
60
61
62
63
64
65

[45] H. Ebrahimian, R. Astroza and J.P. Conte. Extended kalman filter for material parameter estimation in nonlinear structural finite element models using direct differentiation method. *Earthquake Engineering & Structural Dynamics*, 44(10):1495–1522, 2015.

[46] J. F. Hall. Problems encountered from the use (or misuse) of rayleigh damping. *Earthquake Engng Struct. Dyn.*, 35:525–545, 2006.

[47] John William Strutt Baron Rayleigh. *The theory of sound*. Macmillan, 1896.

[48] C. Kyriazoglou, F.J. Guild. Finite element prediction of damping of composite gfrp and cfrp laminates – a hybrid formulation – vibration damping experiments and rayleigh damping. *Composites Science and Technology*, 67(11):2643–2654, 2007.

[49] Liangliang Cheng and Alfredo Cigada. An analytical perspective about structural damage identification based on transmissibility function. *Structural Health Monitoring*, 19(1):142–155, 2020.

[50] O. Hubert, X. Milhet, P. Gadaud, M. Tatat, P. Renault and C. Coupeau. Modeling of young’s modulus variations with temperature of ni and oxidized ni using a magneto-mechanical approach. *Materials Science and Engineering: A*, 633:76–91, 2015.

[51] W. Wang, B. Liu and V. Kodur. Effect of temperature on strength and elastic modulus of high-strength steel. *J. Mater. Civ. Eng.*, 25(2):174–182, 2013.

[52] Arnaud Doucet, Simon Godsill, and Christophe Andrieu. On sequential monte carlo sampling methods for bayesian filtering. *Statistics and Computing*, 10(3):197–208, Jul 2000.

[53] Joao FG de Freitas, Mahesan Niranjana, Andrew H. Gee, and Arnaud Doucet. Sequential monte carlo methods to train neural network models. *Neural computation*, 12(4):955 – 993, 2000.

[54] M. S. Arulampalam, S. Maskell, N. Gordon, and T. Clapp. A tutorial on particle filters for online nonlinear/non-gaussian bayesian tracking. *IEEE Transactions on Signal Processing*, 50(2):174–188, Feb 2002.

[55] M.N. Chatzis, E.N. Chatzi and A.W. Smyth. On the observability and identifiability of nonlinear structural and mechanical systems. *Structural Control and Health Monitoring*, 22(3):574–593, 2015.

[56] G. Cybenko. Approximation by superpositions of a sigmoidal function. *Mathematics of Control, Signals and Systems*, 2:303 – 314, 1989.

[57] Christopher M. Bishop. *Neural Networks for Pattern Recognition*. Oxford university press, 1995.

1
2
3
4
5
6
7
8
9
10
11
12
13
14
15
16
17
18
19
20
21
22
23
24
25
26
27
28
29
30
31
32
33
34
35
36
37
38
39
40
41
42
43
44
45
46
47
48
49
50
51
52
53
54
55
56
57
58
59
60
61
62
63
64
65

832 [58] Mark A Kramer. Nonlinear principal component analysis using autoassociative neural net-
833 works. *AIChE journal*, 37(2):233–243, 1991.

834 [59] Mohamed-Faouzi Harkat, Salah Djelal, Nouredine Doghmane, and Mohamed Benouaret. Sen-
835 sor fault detection, isolation and reconstruction using nonlinear principal component analysis.
836 *International Journal of Automation and Computing*, 4(2):149–155, 2007.

837 [60] Y. Deger, R. Cantieni and S. Pietrzko. Modal analysis of an arch bridge: experiment, finite
838 element analysis and link. *Proceedings of the 12th International Modal Analysis Conference*
839 (*IMAC*), pages 425–432, 1994.

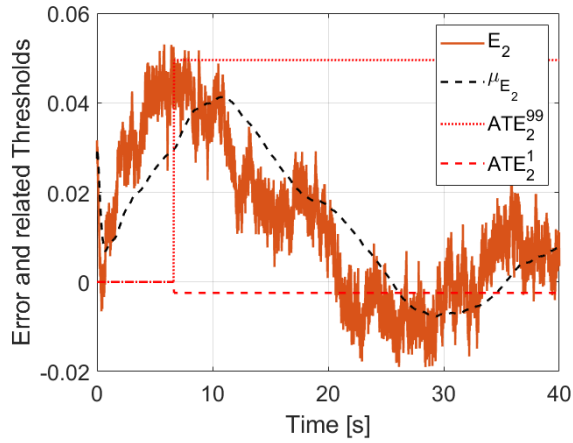
840 [61] P. Fanning, P. Healy, A. Pavic, P. Reynolds and J. Brownjohn. Sean o’casey bridge: comparison
841 of operational and traditional modal analysis test results. *Proceedings of the 2nd International*
842 *Operational Modal Analysis Conference*, pages 293–298, 2007.

843 [62] S. Cofre-Martel, P. Kobrich, E. Lopez Droguett and V. Meruane. Deep convolutional neural
844 network-based structural damage localization and quantification using transmissibility data.
845 *Shock Vib.*, 2019.

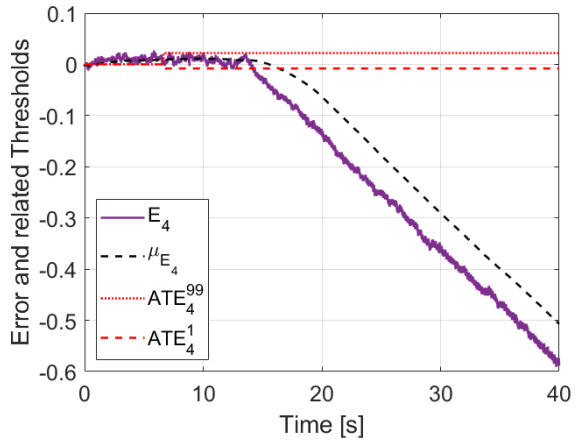
846 [63] A. Deraemaeker, E. Reynders, G. De Roeck and J. Kullaa. Vibration-based structural health
847 monitoring using output-only measurements under changing environment. *Mechanical Systems*
848 *and Signal Processing*, 22(1):34–56, 2008.

849 [64] M. Corbetta, C. Sbarufatti, M. Giglio and M.D. Todd. Optimization of nonlinear, non-gaussian
850 bayesian filtering for diagnosis and prognosis of monotonic degradation processes. *Mechanical*
851 *Systems and Signal Processing*, 142:305–322, 2018.

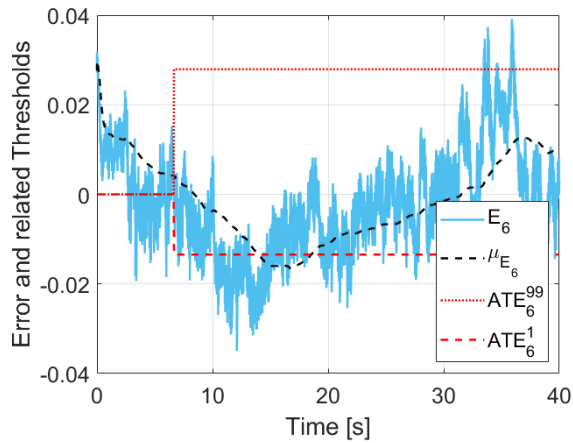
852 [65] M. Corbetta, C. Sbarufatti and M. Giglio. Optimal tuning of particle filtering random noise for
853 monotonic degradation processes. *European Conference of the PHM Society 2016 Proceedings*,
854 2016.



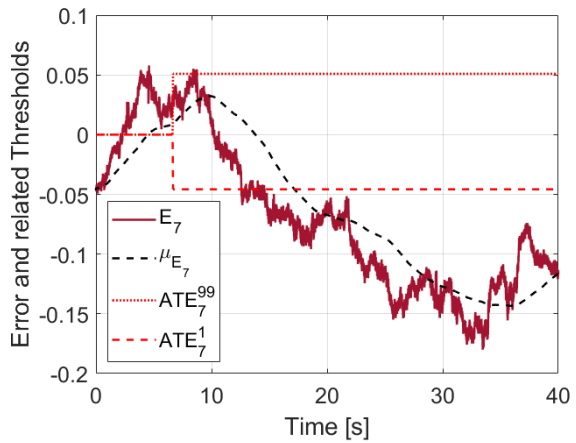
(a) Spring 2



(b) Spring 4



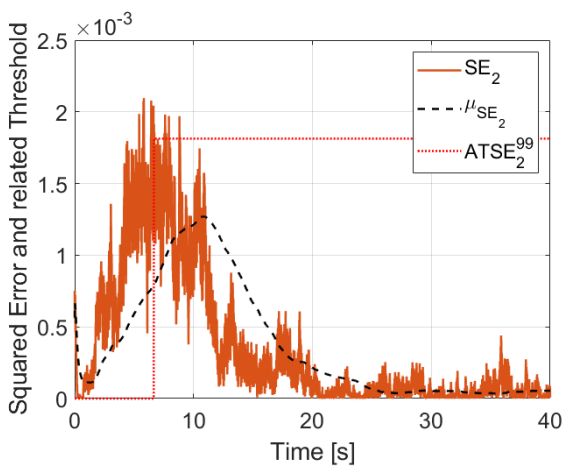
(c) Spring 6



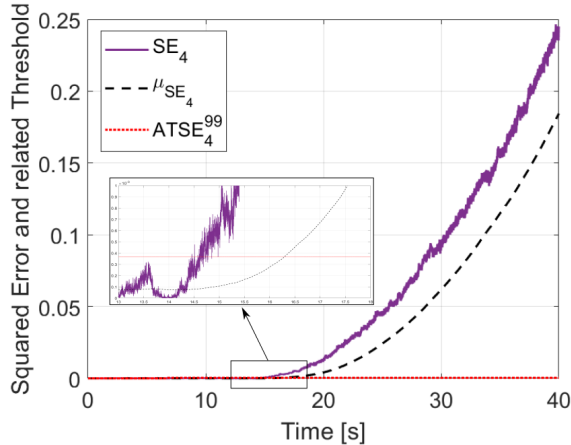
(d) Spring 7

Figure 6: Temporal evolution of the error E_i^T between the input and the output layers of the autoencoder (solid lines) for k_2 , k_4 , k_6 and k_7 , the colored dashed and dotted lines indicate the corresponding automatic thresholds and the black dashed ones the moving average.

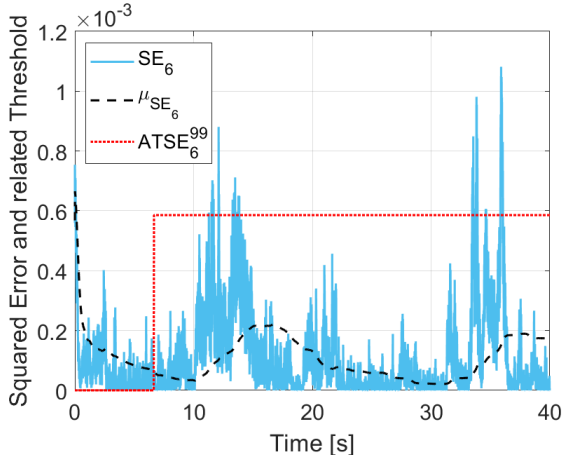
1
2
3
4
5
6
7
8
9
10
11
12
13
14
15
16
17
18
19
20
21
22
23
24
25
26
27
28
29
30
31
32
33
34
35
36
37
38
39
40
41
42
43
44
45
46
47
48
49
50
51
52
53
54
55
56
57
58
59
60
61
62
63
64
65



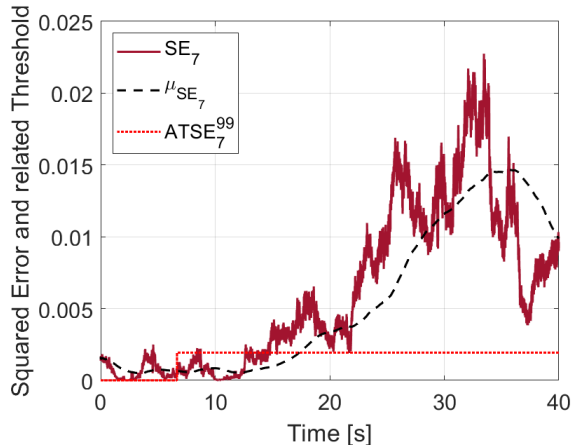
(a) Spring 2



(b) Spring 4



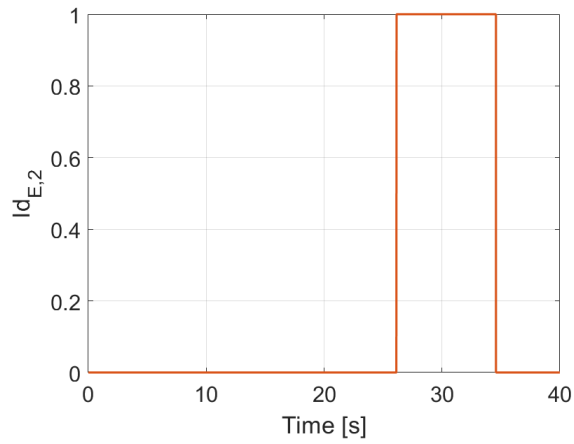
(c) Spring 6



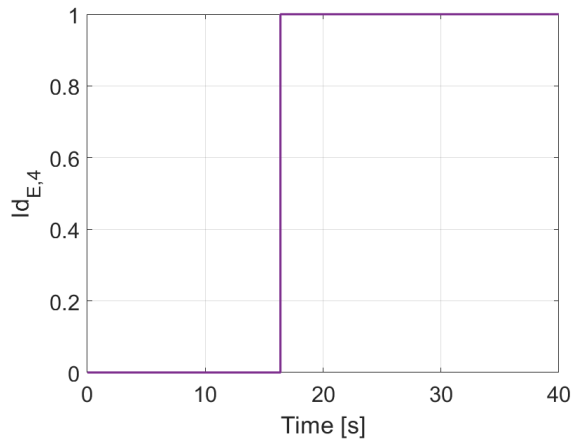
(d) Spring 7

Figure 7: Temporal evolution of the squared error SE_i^T between the input and the output layers of the autoencoder (solid lines) for k_2 , k_4 , k_6 and k_7 , the colored dotted lines indicate the corresponding automatic thresholds and the black dashed ones the moving average.

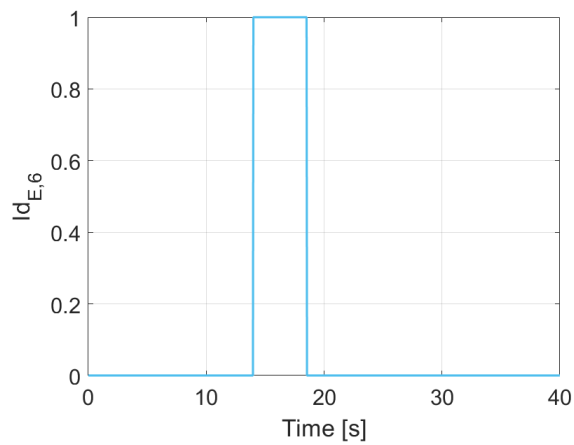
1
2
3
4
5
6
7
8
9
10
11
12
13
14
15
16
17
18
19
20
21
22
23
24
25
26
27
28
29
30
31
32
33
34
35
36
37
38
39
40
41
42
43
44
45
46
47
48
49
50
51
52
53
54
55
56
57
58
59
60
61
62
63
64
65



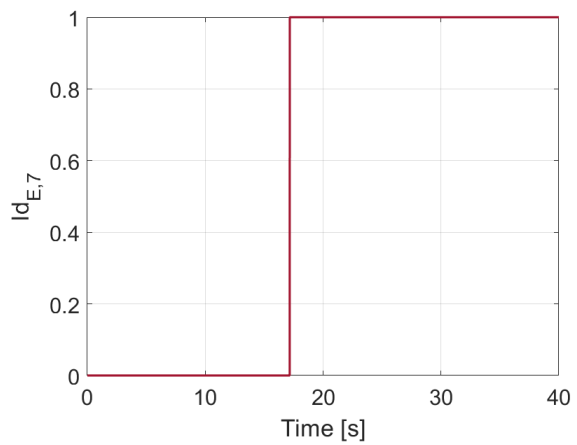
(a) Spring 2



(b) Spring 4

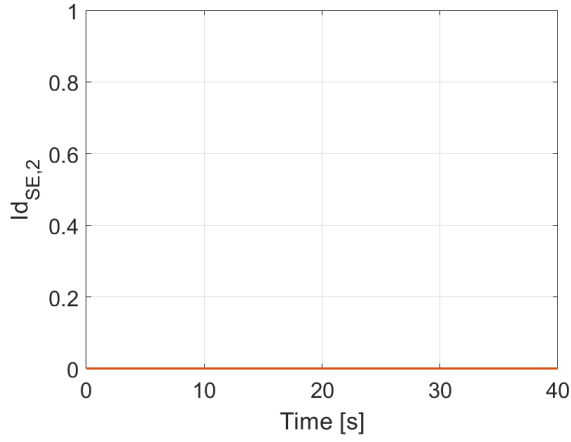


(c) Spring 6

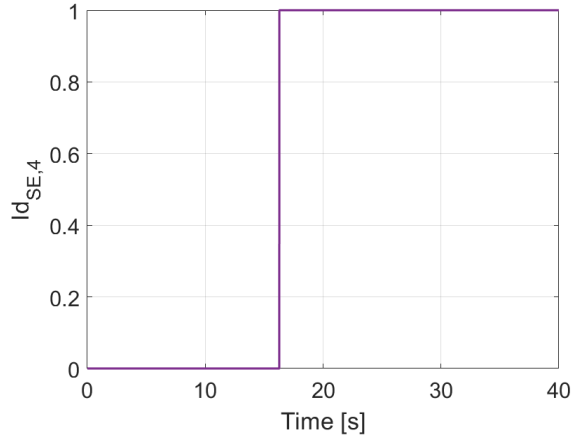


(d) Spring 7

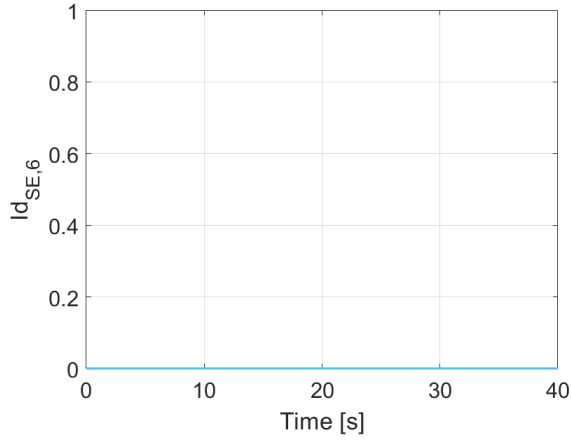
Figure 8: Temporal evolution of fault indicator $Id_{E,i}^{\tau-\tau_0+1,\tau}$ for springs 2, 4, 6 and 7.



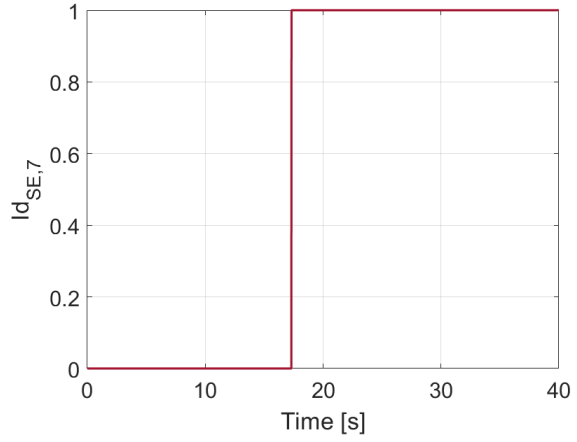
(a) Spring 2



(b) Spring 4

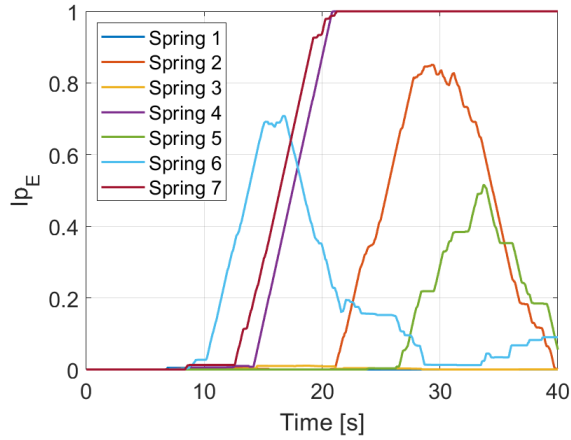


(c) Spring 6

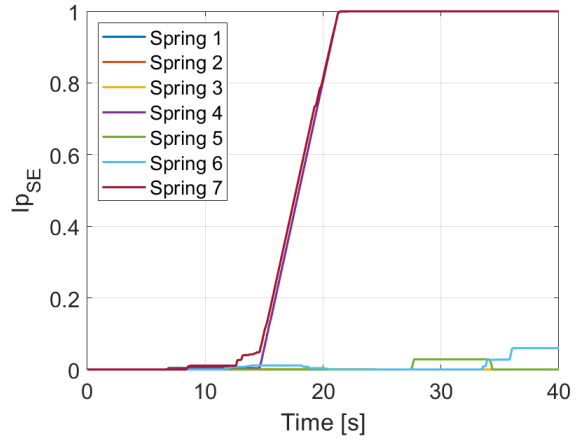


(d) Spring 7

Figure 9: Temporal evolution of fault indicator $Id_{SE,i}^{\tau-\tau_0+1,\tau}$ for springs 2, 4, 6 and 7.



(a) $I_{PE,i}^{\tau-\tau_0+1,\tau}$



(b) $I_{PSE,i}^{\tau-\tau_0+1,\tau}$

Figure 10: Temporal evolution of the probabilistic fault indicators $I_{PE,i}^{\tau-\tau_0+1,\tau}$ and $I_{PSE,i}^{\tau-\tau_0+1,\tau}$.

Francesco Cadini: Conceptualization, Methodology, Investigation, Formal analysis, Validation, Writing - review & editing, Supervision. **Luca Lomazzi:** Investigation, Formal analysis, Software, Writing - reviewing & editing. **Marc Ferrater Roca:** Formal analysis, Software, Writing - original draft preparation. **Claudio Sbarufatti:** Validation, Writing - reviewing & editing. **Marco Giglio:** Resources, Supervision.

Declaration of interests

The authors declare that they have no known competing financial interests or personal relationships that could have appeared to influence the work reported in this paper.

The authors declare the following financial interests/personal relationships which may be considered as potential competing interests: